THE UNIVERSITY
of EDINBURGH

GENERATION of SYNTHETIC SPINDLE CHECKPOINT SIGNALS

Ivan Yuan

Thesis presented for the Degree of Doctor of Philosophy

Wellcome Trust Centre for Cell Biology
University of Edinburgh

2015

Declaration

I declare that this thesis was composed by myself and that the work presented herein is my own except where indicated otherwise.

Ivan Yuan
June 2015

Acknowledgements

A PhD is hard work. One is never certain what obstacles may lie on the path to scientific achievement. What is certain, however, is that one could never get there alone. Without the expertise and encouragement of colleagues, without the critical feedback of supervisors, without the sympathy of friends and family, no-one would ever complete a PhD.

With this in mind, I wish to express my sincere gratitude to Kevin, my supervisor, for devising a genuinely interesting project and for always keeping the door open to discussions and complaints alike. Karen – your never-ending patience and cheerful optimism in the lab kept me going half the time, even if you didn't know it, and I'm sure you'll be glad that I will no longer be encroaching on your lab space or standing in front of your drawers mid-way through a time-course experiment. Never have I met someone who was so ready to give away their hard-earned expertise and time soley for the benefit of others. Onur – it was great to have someone so upbeat and ready to help like you in the lab, you truly are one of the reasons that our lab has such a welcoming and friendly reputation in the Centre, unlike some of the cold, emotion-less pits of scientific slavery that I can think of. Ioanna – you've been a tremendous help, especially during these last few weeks of thesis-writing, and I wish you the very best with Bub1 and the rest of your PhD. Sadhbh and Priya – I hope you will enjoy your time in the Hardwick lab as much as I did!

I also wish to thank the other members of the Hardwick, Marston, Ohkura, Allshire and Sawin labs that have assisted me technically or morally, or both, over the last four years. In particular, Kitty, Kostas, Rachael, Stefan and Vasso – I shall miss you all very much. Dave – I suspect that you will never read this, but I want to say anyway how much I appreciated your technical assistance and the banter we had in COIL. Dr (Mrs) Claudia Schaffner – I hope you realise how important you have been to my pending level-up to LVL: PhD! For my parents, without whose encouragement and support I would never have undertaken my PhD – you know I will be forever grateful for this opportunity.

Last but certainly not least – Anne: you've been a much bigger help to me in the last three years than I can express in words here, especially since you had to first suffer through your PhD and then mine, but I just want to say: *danke schoen*!

Lay summary

How do cells ensure that they have correct amount of DNA (chromosomes) when they divide? Cells with an incorrect amount of DNA have catastrophic fates – in humans, Down's syndrome is caused by sperm or egg cells with improper amounts of DNA (an extra copy of chromosome 21). Cancer cells also often contain improper amounts of DNA.

When a cell divides to form two identical new (daughter) cells, it first duplicates its DNA and then partitions this DNA equally between the two daughter cells. If this DNA is not partitioned equally, then the daughter cells will contain either too much or too little DNA.

Cells have a mechanism called the spindle checkpoint that checks if their DNA going to be evenly partitioned; if it looks like there's going to be a problem with doing this, then the spindle checkpoint will not allow cells to divide before the problem is fixed.

The spindle checkpoint is a complex piece of cellular mechanism that is difficult to understand. To simplify this problem, we have engineered an artificial, stripped-down version of it that uses as few components of the mechanism as possible. This approach allows us to better understand the contribution of each individual component to the overall workings of the mechanism.

Importantly, we have discovered that we can make an artificial yet fully functional version of the spindle checkpoint by combining only two components togther, one called Spc7 and one called Mph1. This shows that these two components of the spindle checkpoint can directly the assembly of all the other pieces to make a functional spindle checkpoint.

Abstract

The spindle checkpoint ensures proper chromosome segregation by monitoring kinetochore-microtubule interactions: unattached kinetochores recruit checkpoint proteins that combine to form a diffusible inhibitor which delays anaphase, thus buying cells time to fix attachment errors.

Although the major checkpoint proteins were identified some 25 years ago, we have only just begun to understand how they assemble at unattached kinetochores to generate the crucial checkpoint signal. Much of this can be attributed to the difficulty associated with studying these proteins at the kinetochores, which are highly complex and thus often make clean dissection of function impossible.

To circumvent this problem, a synthetic version of the spindle checkpoint was engineered on an ectopic location on a chromosome arm away from kinetochores in *S. pombe*. This work describes how the co-targeting of only two checkpoint components, the outer kinetochore protein Spc7 and the checkpoint kinase Mph1, was found to be sufficient to successfully generate a checkpoint-dependent metaphase arrest and how this paves the way for a clearer, more joined-up understanding of how the checkpoint works.

List of abbreviations

APC/C	Anaphase promoting complex/cyclosome
Bub	Budding uninhibited by benzimidazoles
CENP	Centromere protein
CDC	Cell division cycle
CDK	Cyclin-dependent kinase
DMSO	Dimethyl sulfoxide
FRAP	Fluorescence recovery after photobleaching
GFP	Green fluorescent protein
KMN	KNL1-Mis12-Ndc80 complex
KT	Kinetochore
NPC	Nuclear pore complex
Mad	Mitotic arrest deficient
MCC	Mitotic checkpoint complex
nmt/ P_{nmt}	No message in thiamine (promoter)
P_{adh}	Alcohol dehydrogenase (promoter)
PCR	Polymerase chain/Pure chance reaction
PMG	*Pombe* minimal medium
PTM	Post-translational modification
tTA/rtTA	(Reverse) transcriptional transactivator
RZZ	Rod1-Zwilch-ZW10 complex
SPB	Spindle pole body
TetR/rTetR	(Reverse) tetracycline repressor
tetO	Tet operator
tdT	tdTomato
TPR	Tetratricopeptide repeat
WT	Wild type
YES	Yeast extract supplemented

Table of contents

Abstract

Acknowledgements

List of abbreviations

List of figures

CHAPTER 1
Introduction

1.1 A unified view of the cell cycle 1
1.2 The spindle checkpoint: summary 2
1.3 Chapter layout 2
1.4 APC/C inhibitory signals 2
1.4.1 Mad2-Cdc20 2
1.4.2 BUBR1/Mad3 and the Mitotic Checkpoint Complex (MCC) 3
1.5 Assembly of checkpoint signalling scaffolds 5
1.5.1 Role of Mps1 in the assembly of the KNL1-Spc7-Bub3-Bub1 scaffold 8
1.5.2 Role of Mps1 in the assembly of the Mad1-Mad2 scaffold 9
1.5.3 Mutual dependencies between Spc7/KNL1-Bub3-Bub1 and Mad1-C-Mad2 11
1.5.4 Are checkpoint components needed at kinetochores? 11
1.6 Tension sensing with Aurora B kinase 12
1.7 Checkpoint silencing 14
1.7.1 Silencing inactivates the spindle checkpoint 14
1.7.2 Silencing mechanisms 14
1.8 Aims of this work 15

CHAPTER 2
Materials & Methods

2.1 DNA methods 17
2.1.1 Polymerase chain reaction 17
2.1.2 Gateway® cloning 17
2.1.3 Site directed mutagenesis 17
2.1.4 Sequencing 17
2.1.5 Restriction endonuclease digestion 17
2.1.6 De-Phosphorylation 17
2.1.7 Ligation 17
2.1.8 Bacterial transformation 17
2.1.9 Yeast transformation 18
2.1.10 Yeast genomic DNA extraction 18
2.1.11 Ethanol precipitation of DNA 18
2.2 Protein methods 19
2.2.1 Yeast protein lysis buffer 19
2.2.2 Yeast protein extracts 19
2.2.3 Co-immunoprecipitation with GFP-Trap® 19

CHAPTER 2
Materials & Methods (contd.)

2.2 Protein methods (contd.) 19
2.2.4 SDS-PAGE 19
2.2.5 Immunoblot 20
2.2.6 Protein visualisation 20
2.2.7 Antibodies used in this work 20
2.3 Yeast methods
2.3.1 Anhydrotetracycline 21
2.3.2 Wide-field epi-fluorescence microscopy 21
2.3.3 Fluorescence recovery after photobleaching (FRAP) 21
2.3.4 Tethering assay 23
2.3.5 Synthetic arrest assay 23
2.4 Reaction kits 23
2.5 Yeast media 24
2.5.1 Yeast Extract Supplemented (YES) 24
2.5.2 Pombe minimal medium (PMG)/clear PMG medium 24
2.5.3 Supplements mix (20x) 24
2.5.4 Minerals mix (1000x) 25
2.5.5 Vitamins mix (1000x) 25
2.6 List of primers used in this work 26
2.7 List of plasmids used in this work 28
2.8 List of fission yeast strains used in this work 29
2.9 Plasmid construction 31
2.9.1 *pIY01 (pDUAL-P_{nmt81}-2xFLAG-rTetR-mCherry-Gateway®)* 31
2.9.2 *pIY02 (pDUAL-P_{nmt81}-2xFLAG-rTetR-Gateway®)* 31
2.9.3 *pIY03 (pLYS1U-Padh15-NLS-2xFLAG-rTetR-Gateway®)* 31

CHAPTER 3
Phosphorylation of a C-terminal Mad1 fragment is sufficient for C-Mad2 recruitment

3.1 Introduction: the usefulness of ectopic tethering systems 33
3.2 Designing an ectopic tethering system in S. pombe 34
3.3 Using ectopic tethering to examine Mad1-Mad2 interaction 35
3.4 Mad1 coiled coils 1-3 not required for stably associated Mad2 binding 37
3.5 Ectopically recruited Mad2 is more dynamic than tethered $Mad1_{\Delta 1\text{-}148}$ 39
3.6 Phosphorylation of Mad1 C-terminus crucial for C-Mad2 binding 42
3.7 Conclusions and perspectives 44

CHAPTER 4
Phosphomimetic Spc71-666-9TE is sufficient to recruit Bub1, Bub3 and Mad3 in a manner comparable to that at endogenous kinetochores

4.1 Introduction 46
4.2 Interplay between Bub3, Bub1, Mad3/BUBR1 and Spc7/KNL1 46
4.3 Selecting the right fragment of Spc7 to tether 46
4.2 Re-engineering the tethering construct 47

CHAPTER 4
Phosphomimetic Spc71-666-9TE is sufficient to recruit Bub1, Bub3 and Mad3 in a manner comparable to that at endogenous kinetochores (contd.)

4.5 Ectopically tethered $Spc7_{1-666}$-9TE is sufficient to recruit a stably associated form of Mad3 independently of Mph1 kinase. 48

4.6 Ectopically tethered $Spc7_{1-666}$-9TE recruits Mad3 in a manner similar to that at unattached kinetochores 51

4.7 The role of the Mad3 HIG motif in checkpoint signalling 54

4.8 Ectopically co-tethered Mad1 and $Spc7_{1-666}$-9TE insufficient to generate checkpoint arrest 56

4.9 Summary and perspectives 57

CHAPTER 5
Co-localisation of $Spc7_{1-666}$-9TE and $Mph1_{\Delta1-302}$ kinase is sufficient to ectopically activate the spindle checkpoint away from kinetochores

5.1 Introduction 58

5.2 Co-tethered $Mph1_{\Delta1-303}$ and $Spc7_{1-666}$-9TE are sufficient to generate a *tetO* array dependent metaphase arrest 58

5.3 $Spc7_{1-666}$-9TE and $Mph1_{\Delta1-302}$ induced metaphase arrest is spindle checkpoint -dependent 62

5.4 Summary and perspectives 66

5.4.1 Concentration of checkpoint components key for signalling activation 66

5.4.2 Mapping the synthetic signalling pathway 66

5.4.3 The role of the SPBs in tethering-induced checkpoint signalling 68

Final Discussion 69

Bibliography 71

List of figures

CHAPTER 1
Introduction

1.1 Structures of Mad1 and Mad2 reveals their mode of interaction
1.2 Structure of a partial *S. pombe* MCC structure reveals two modes of Mad3-mediated APC/C inhibition
1.3 Checkpoint scaffolds at unattached kinetochores
1.4 Interplay between Bub3, Bub1 and Spc7/KNL1 in checkpoint scaffold assembly

CHAPTER 2
Materials & Methods

2.1 Engineering an improved tethering vector, pIY03

CHAPTER 3
Phosphorylation of a C-terminal Mad1 fragment is sufficient for C-Mad2 recruitment

3.1 Ectopic tethering of Mad1 fragments
3.2 N-terminal coiled coils of Mad1 are dispensable for C-Mad2 recruitment
3.3 C-Mad2 more dynamic than tethered $Mad1_{\Delta 1\text{-}148}$ at ectopic array
3.4 Phosphorylation of Mad1 C-terminus crucial for C-Mad2 binding

CHAPTER 4
Phosphomimetic $Spc7_{1\text{-}666}$-9TE is sufficient to recruit Bub1, Bub3 and Mad3 in a manner comparable to that at endogenous kinetochores

4.1 $Spc7_{1\text{-}666}$-9TE as an ectopic anchor for Bub3, Bub3 and Mad3
4.2 Ectopically tethered $Spc7_{1\text{-}666}$-9TE is sufficient to recruit Bub3, Bub1 and Mad3 independently of Mph1 kinase
4.3 Ectopic recruitment of Mad3 by $Spc7_{1\text{-}666}$-9TE is Bub1 and Bub3 dependent
4.4 Bub1 and Mad3 dynamics at ectopic array mirrors those at unattached kinetochores
4.5 The role of the Mad3 HIG motif in checkpoint signalling

CHAPTER 5
Co-localisation of $Spc7_{1\text{-}666}$-9TE and $Mph1_{\Delta 1\text{-}302}$ kinase is sufficient to ectopically activate the spindle checkpoint away from kinetochores

5.1 Ectopic tethering of a Mph1 fragment that is unable to localise to kinetochores
5.2 Co-tethered $Mph1_{\Delta 1\text{-}302}$ and $Spc7_{1\text{-}666}$-9TE sufficient to generate a metaphase arrest
5.3 Tethering induced metaphase arrest requires both tethered $Mph1_{\Delta 1\text{-}302}$ and $Spc7_{1\text{-}666}$-9TE
5.4 Mad2 localises to SPBs during tethering induced metaphase arrest
5.5 Tethering induced metaphase arrest is spindle checkpoint dependent

CHAPTER 1
Introduction

1.1 A unified view of checkpoints in the cell cycle

The cell cycle can be defined as the series of events that cells must undergo in order to reproduce. The concept of checkpoints in the cell cycle, where progression to the next step in the cycle is dependent on the fulfilment of certain conditions, was first introduced in 1988 by Weinert & Hartwell (Weinert and Hartwell, 1988). The description of the DNA damage checkpoint in their study encapsulates the checkpoint concept: upon detection of a specific cellular event (DNA damage), a negative feedback signal is generated that prevents cell cycle progression (G2 arrest) until the checkpoint trigger is removed (DNA damage repaired).

The discovery of the DNA damage checkpoint came at a time of debate in cell cycle research, when two seemingly incompatible views of the cell cycle had emerged. On the one hand, yeast genetics groups suggested that the cell cycle was a set of dependent events where later events were conditional on the successful completion of preceding events (Lee and Nurse, 1988). In this respect the cell cycle was likened to a linear metabolic pathway, with each stage of the cycle producing a component that was required for the next stage. This model was thus referred to as the 'product-substrate' model.

On the other hand, evidence from embryological studies using eggs and oocytes was used to argue that the cell cycle oscillates between mitosis and DNA synthesis irrespective of whether either process had been completed. This view came from observations in early embryonic cells that the cell cycle continued to progress even though key events such as DNA synthesis were inhibited (Dasso and Newport, 1990). Later work showed that neither view was entirely correct (Lucchini et al., 1990; McCarroll and Fangman, 1988), and it was not until the discovery of checkpoints that the genetic and embryonic evidence was reconciled to produce a unified view of the cell cycle. It was later realised that the continued cell cycle progression observed in early embryonic cells with incomplete DNA synthesis was not due a lack of checkpoint-enforced dependencies, but rather because the checkpoint signals being generated in those cells were too weak to prevent progression (Murray and Kirschner, 1989).

Since the discovery of the DNA damage checkpoint, several other checkpoints have been described, including the intra-S checkpoint, triggered by unreplicated DNA, and the spindle assembly checkpoint (also known as the mitotic checkpoint, spindle checkpoint or SAC; hereafter referred to as the spindle checkpoint), triggered by defects in spindle attachment to chromosomes. This latter checkpoint forms the subject of this work. The existence of the spindle checkpoint was first hinted at in 1969 by the work of Nicklas and Koch, which showed that insect cells possessed an intrinsic ability to correct experimentally-induced errors in chromosome alignment (Nicklas and Koch, 1969). This work was the first to observe that chromosomes can

somehow sense the level of tension applied to them, and that this was linked to the activation of the spindle checkpoint. However, it was not until 1990 that the major components of the spindle were identified using genetic screens in yeast (Hoyt et al., 1991; Li and Murray, 1991). Since then, work on the spindle checkpoint has focussed on understanding what activates the checkpoint, its signal transduction pathways and how it is de-activated ('silenced').

1.2 The spindle checkpoint: summary

The spindle checkpoint is a conserved eukaryotic mechanism that prevents aneuploidy during mitotic and meiotic division. The spindle checkpoint achieves this by monitoring chromosome attachments to the spindle microtubules; erroneous attachments or the absence of attachment activates the checkpoint and delays entry into anaphase. Once proper attachments have been made, the spindle checkpoint is satisfied and subsequently turned off ('silenced'), allowing cells to proceed to anaphase.

The spindle checkpoint delays anaphase by inhibiting Cdc20 (Hwang et al., 1998) (*S. pombe*: Slp1 (Kim et al., 1998)), an essential activator of the anaphase promoting complex/cyclosome (APC/C). The APC/C is the E3 ubiquitin ligase that signals anaphase entry by targeting securin and cyclin B for degradation. In all model organisms the spindle checkpoint proteins involved in generating this APC/C inhibitory signal consist of the **m**itotic **a**rrest **d**efective (Mad) and **b**udding **u**ninhibited by **b**enzimidazoles (Bub) proteins (Mad1, Mad2, BUBR1/Mad3, Bub1, Bub3), as well as the Mps1 (*S. pombe*: Mph1) and Aurora B (*S. pombe*: Ark1) kinases.

Until recently the checkpoint signal was held to originate exclusively from unattached kinetochores (Rieder et al., 1995), where the various Mad and Bub protein assemble into inhibitory complexes before diffusing away to inhibit the APC/C. More recent work shows that inhibitory complexes can also be generated at other locations, such as the nuclear pore complexes (NPCs) (Rodriguez-Bravo et al., 2014) (see Section 1.5.4).

1.3 Chapter layout

This chapter begins by describing how the APC/C is inhibited by the effectors of the spindle checkpoint, in particular the MCC. How these effectors are assembled from their constituent components will then be described, and the role of Mps1/Mph1 and Aurora B/Ark1 kinases on this assembly will be highlighted. The chapter ends with a discussion of how the checkpoint is silenced.

1.4 APC/C inhibitory signals

The first APC/C inhibitory signal to be described was an 'activated' form of Mad2, which was found to form a stable complex with Cdc20 (De Antoni et al., 2005). BUBR1 (Mad3 in yeast) was subsequently discovered to also exhibit APC/C inhibition (Tang et al., 2001), and it is now clear that Mad2 and Mad3/BUBR1 act together as part of a larger inhibitory complex termed the **m**itotic **c**heckpoint **c**omplex (MCC). The MCC is comprised of Mad2-Mad3/BUBR1-Bub3-

Cdc20 in all model organisms except for *S. pombe*, in which the MCC lacks Bub3. The MCC is a far more potent APC/C inhibitor *in vitro* than either Mad2 or Mad3/BUBR1 alone (Fang, 2002).

1.4.1 Mad2-Cdc20

The inhibitory Mad2-Cdc20 complex is formed through what is termed the 'Mad2 template model'. This model arose from the discovery that Mad2 exists in two structurally distinct forms, termed open (O-Mad2) and closed (C-Mad2) (De Antoni et al., 2005; Luo et al., 2002). Throughout the cell cycle, Mad2 remains bound to its upstream partner Mad1 as part of a highly stable, tetrametric $(Mad1\text{-}C\text{-}Mad2)_2$ complex (hereafter referred to as Mad1-C-Mad2). Upon activation of the spindle checkpoint, this Mad1-C-Mad2 complex is directed to unattached kinetochores, whereupon the Mad1-bound C-Mad2 becomes capable of dimerising with molecules of cytosolic O-Mad2. This dimerisation induces the structural conversation of O-Mad2 to C-Mad2, which can then bind Cdc20 to form Mad2-C-Cdc20 (Fang et al., 1998; Luo et al., 2002).

Unlike Mad1-bound C-Mad2, which is stably associated, O-Mad2 dimerisation with C-Mad2 is highly transient, leading to high turnover/cycling of O-Mad2 at unattached kinetochores. This difference in the dynamic s of C-Mad2 and O-Mad2 provided key experimental evidence for the 'Mad2-template' model; studies initially using *in vivo* (Howell et al., 2004; Shah et al., 2004) and later *in vitro* (Vink et al., 2006) **F**luorescence **R**ecovery **A**fter **P**hoto-bleaching (FRAP) techniques revealed two distinct pools of Mad2: one immobile (Mad1-C-Mad2) and one highly dynamic (cycling O-Mad2). At the same time, crystallisation of the Mad1-C-Mad2 complex (Musacchio et al., 2002) and the O-Mad2-C-Mad2 dimer (Mapelli et al., 2007) provided structural evidence for the model. The C-terminal tail of O-Mad2 was found to undergo a major conformational change upon binding of Mad1 or Cdc20, lowering itself over the bound molecule to lock it in place. This feature of Mad2 forms the structural basis for the observed stability of the Mad1-C-Mad2 and Mad2-C-Cdc20 complexes, and is referred to as the 'safety-belt' mechanism (Fig. 1.1B, C).

Although now universally accepted, open questions remain about the 'Mad2-template' model. First, it has never been clear whether a newly formed molecule of C-Mad2 binds Cdc20 immediately following dimerisation, or whether it dissociates from the kinetochore-bound Mad1-C-Mad2 complex and diffuses away to bind Cdc20 elsewhere. If the latter case is true, it would require the existence of a diffusible, transiently un-bound C-Mad2 molecule that is capable of binding Cdc20. This hypothetical molecule has never been identified, and is referred to in the literature as intermediate Mad2 (I-Mad2) or Mad2*.

1.4.2 BUBR1/Mad3 and the Mitotic Checkpoint Complex (MCC)

As noted above, the binding of BUBR1/Mad3 and Mad2 to Cdc20 together produces more potent APC/C inhibition *in vitro* than either does alone (Tang et al., 2001). As its name suggests, BUBR1 (Bub-related kinase 1) and its yeast homologue Mad3 both share common features with the checkpoint protein Bub1, and all three proteins are believed to have evolved from a common

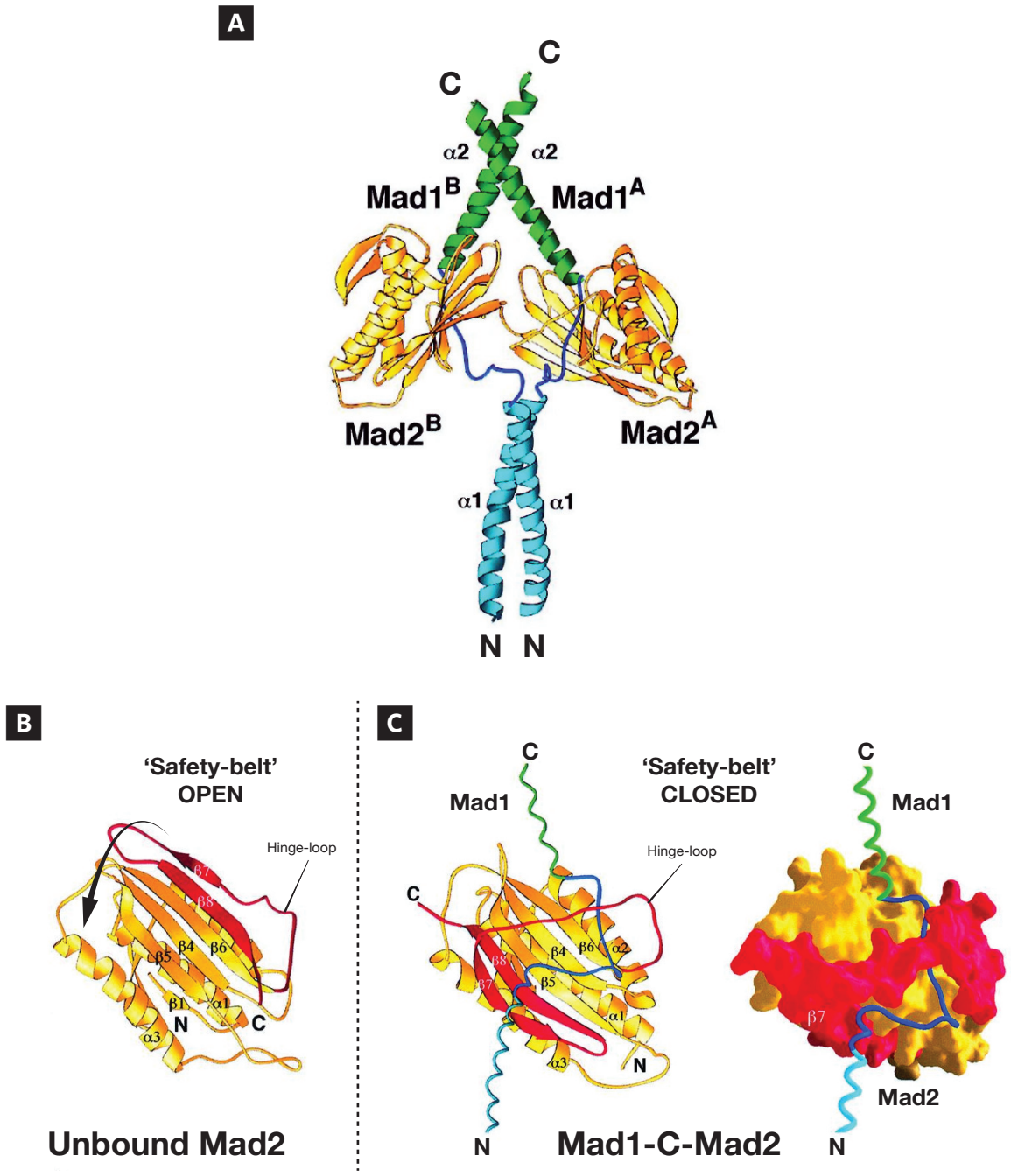

Fig. 1.1 – Structures of Mad1 and Mad2 reveals their mode of interaction. (A) Schematic of a Mad1-C-Mad2 tetrameric complex. The complex comprises of a Mad1 homodimer with two bound molecules of Mad2. The N-terminal coiled coils of Mad1 (cyan) mediate Mad1 dimerisation, whilst the C-terminal coiled coils (green) are required for kinetochore localisation. The Mad2 binding site of Mad1 lies between these two regions (dark blue). Note the contrast between the long, elongated coiled coil structure of Mad1 and the compact globular structure of Mad2. **(B, C)** 'Safety-belt' mechanism of Mad2 underlies the stability of the Mad1-C-Mad2 complex. **(B)** Unbound Mad2 molecule showing the 'safety-belt' (red) and flexible hinge-loop region. Arrow indicates conformation change of the 'safety-belt' upon Mad1 binding. **(C)** Mad1-bound Mad2 showing 'safety-belt' closed through conformational change in the flexible hinge-loop induced by Mad1 binding. This locks Mad1 and Mad2 together and explains why Mad1-C-Mad2 exists as a highly stable, constitutively bound complex *in vivo.* Diagrams adapted from (Sironi *et al.*, 2002).

ancestor (Vleugel et al., 2012). Features of BUBR1/Mad3 include an N-terminal **t**etra**t**ricopeptide **r**epeat (TPR) domain, a Bub3-binding domain (also known as the GLEBS domain), and a C-terminal kinase domain that is absent in Mad3. Curiously, BUBR1/Mad3 contains a number of conserved APC/C^{Cdc20} binding motifs that are normally found on APC/C^{Cdc20} substrates. These D(estruction) (RxxLxxxx [EDNQ]) and KEN boxes (KEN) usually mark their bearer for ubiquitin-mediated proteolysis, and yet Mad3 is not destroyed in this way. Instead, it has long been suspected that the purpose of these APC/C^{Cdc20} binding motifs is to enable BUBR1/Mad3 to act as a competitive inhibitor or 'pseudo-substrate' for Cdc20 (DeLuca et al., 2011). Indeed, our lab was the first to demonstrate that Mad3 requires both of its KEN boxes for checkpoint function, and that KEN1 but not KEN2 is required for the incorporation of Mad3 into the MCC (King et al., 2007; Sczaniecka et al., 2008).

Confirmation of the 'pseudo-substrate' model arrived with the crystal structure of a partial *S. pombe* MCC comprising of C-Mad2, Cdc20 and a C-terminally truncated Mad3 that lacks KEN2 (Chao et al., 2012). This structure revealed that Mad3 binds directly to the substrate recognition domain of Cdc20 (mediating D- and KEN-box recognition), thus blocking Cdc20 access to APC/C substrates (Fig. 1.2A). This mode of binding places Mad3 KEN1 directly on top of the KEN-box binding site of Cdc20, thus confirming the finding of our lab that KEN1 is required for MCC assembly. Docking of the partial MCC structure into a cryo-electron microscopy model of human APC/C (Herzog et al., 2009) revealed a second, previously unknown method of Mad3-mediated APC/C^{Cdc20} inhibition: MCC-APC/C binding positions Mad3 in such a way that it prevents a neighbouring Cdc20 from forming a bi-partite D-box receptor with an APC/C subunit (Apc10) (Fig. 1.2B).

Although revealing, the partial MCC structure left unaddressed the question of Mad3 KEN2 function, as this was omitted from the structure. Since Mad3 KEN2 is required for checkpoint function but not MCC formation, it was speculated (Primorac and Musacchio, 2013) that KEN2 may be required for the binding of a second molecule of Cdc20. Recent evidence supports this idea (Izawa and Pines, 2014). By using a Cdc20 D-box receptor mutant (ΔDR) that allows it to form MCC but unable to bind a second Cdc20 molecule, Izawa and colleagues showed that together with the D-box, KEN2 of hsBUBR1 mediates the interaction between the MCC and the second copy of Cdc20. Moreover, this ΔDR mutant was checkpoint defective, suggesting that MCC binding of a second Cdc20 may be required for full checkpoint function.

1.5 Assembly of checkpoint signalling scaffolds

Key to our understanding of the spindle checkpoint is how the checkpoint signal is activated and propagated in space and time. Over the past decade it has become clear that MCC formation involves the assembly of two major complexes or 'scaffolds': Mad1-C-Mad2 and KNL1/Spc7/Spc105-Bub3-Bub1 (Fig. 1.3). Common to both of these checkpoint scaffolds is the importance of checkpoint kinases in their assembly and function. This section thus reviews the

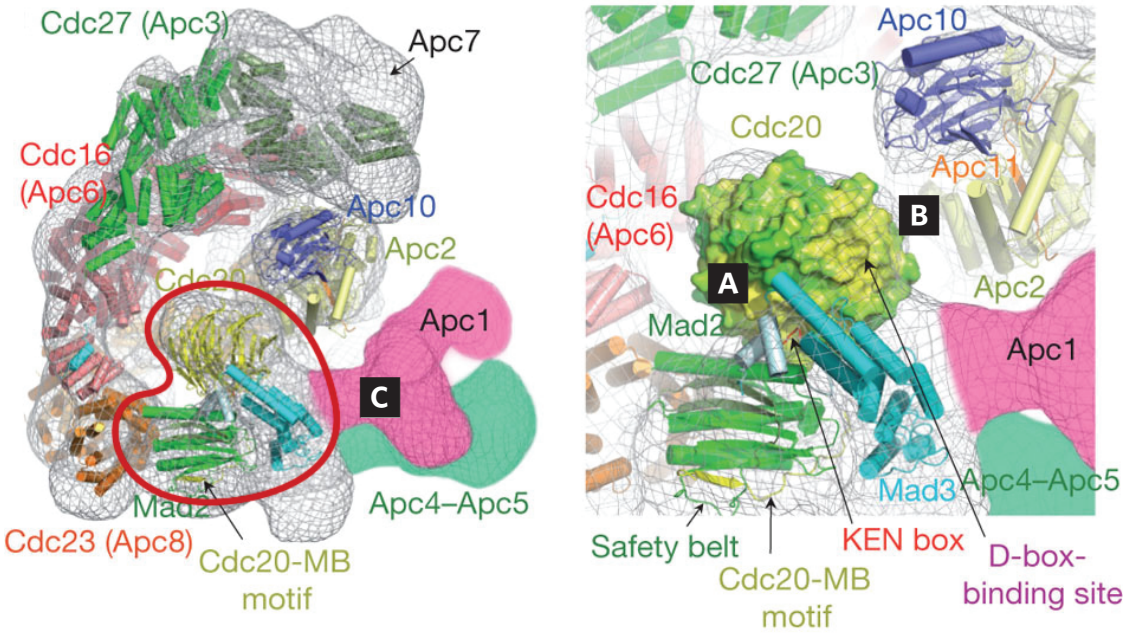

Fig. 1.2 – Structure of a partial *S. pombe* MCC structure reveals two modes of Mad3-mediated APC/C inhibition. (A) Mad3 acts as a pseudo-substrate inhibitor of APC/C. Binding of Mad3 (cyan) to Cdc20 (yellow-green) positions the first Mad3 KEN box (KEN1) directly over the substrate recognisition domain of Cdc20, thus denying Cdc20 access to APC/C^{Cdc20} substrates. This explains why KEN1 is required for both Mad3 incorporation into the MCC as well as APC/C inhibition. **(B)** Docking of the partial MCC structure into a cryo-electron microscopy model of human APC/C (Herzog *et al.* 2009) reveals a second, indirect method of Mad3-mediated APC/C^{Cdc20} inhibition. The Mad3 of a neighbouring MCC (not shown) binds to the D-box binding site (purple), changing the positioning of Cdc20 relative to the various APC/C subunits. This change in position leaves Cdc20 unable to form a D-box receptor with the APC/C subunit, Apc10. **(C)** Positioning of partial MCC (circled) within the human APC/C model. Diagrams adapted from (Chao *et al.* 2012). Cdc20 structure is colour-coded from yellow (invariant) to green (less conserved).

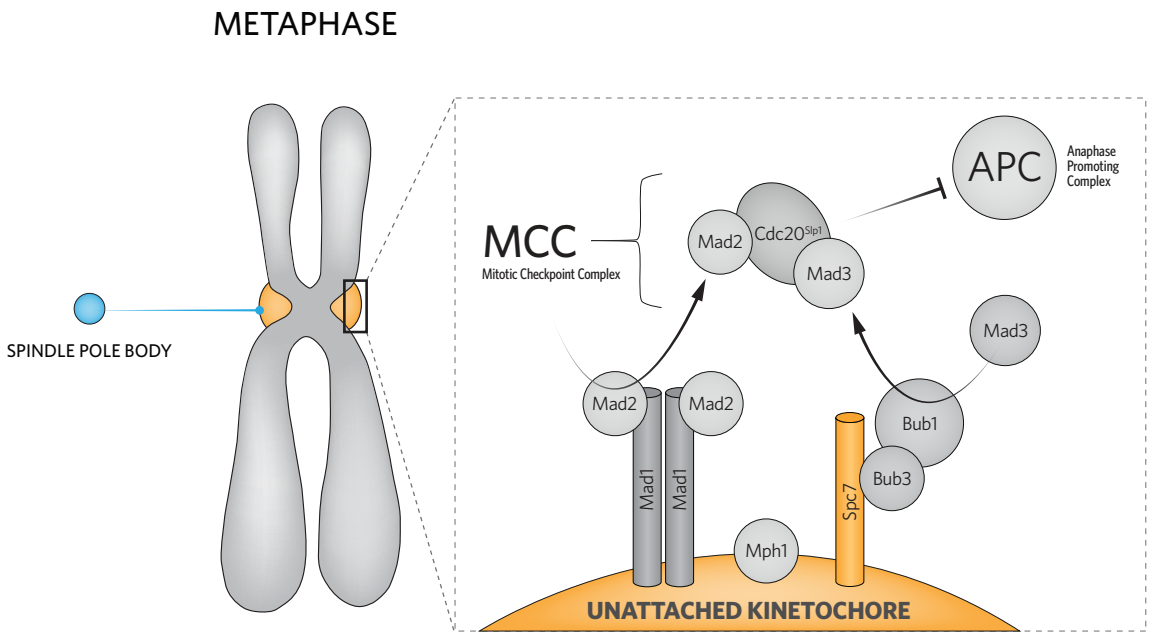

Fig. 1.3 – Checkpoint scaffolds at unattached kinetochores. For description see text.

current models for checkpoint scaffold assembly with a particular emphasis on their regulation by the Mps1/Mph1 and Aurora B/Ark1 checkpoint kinases.

1.5.1 Role of Mps1 in the assembly of the KNL1-Spc7-Bub3-Bub1 scaffold

Mps1 (**m**ono-**p**olar **s**pindle 1) is an essential checkpoint kinase that is found in all model organisms except *C. elegans*, where no homologues have been identified. Mph1 (**M**ps1 **p**ombe **h**omologue 1) differs from Mps1 in that its functions are more limited; whereas Mps1 is involved in spindle pole body (SPB) duplication, bi-orientation and the spindle checkpoint, the role of Mph1 is largely confined to bi-orientation and the spindle checkpoint (He et al., 1998; Zich and Hardwick, 2010). Overexpression of Mps1/Mph1 induces checkpoint-mediated metaphase arrest (Hardwick et al., 1996; He et al., 1998; Ito et al., 2012), whilst inhibition of Mps1 abolishes both the kinetochore localisation of all other checkpoint components as well as checkpoint function (Maciejowski et al., 2010; Sliedrecht et al., 2010; Vigneron et al., 2004).

Recent work shows that together with Aurora B/Ark1, Mps1/Mph1 is the most upstream component of the checkpoint signalling pathway. In *S. pombe*, the removal of almost all other checkpoint components from the kinetochores does not abolish checkpoint function, as long as Mph1 remains at the kinetochores (Vanoosthuyse et al., 2009). Forced targeting of Mps1/Mph1 to the kinetochores of Ptk2 (rat-kangaroo epithelial kidney) cells (Jelluma et al., 2010) and *S. pombe* (Ito et al., 2012) results in constitutive checkpoint activation (for caveats, see Chapter 3). Lastly, it has been demonstrated that in human-derived cells, Mps1 acts as a key activation trigger for the checkpoint by competing with microtubules at kinetochores (Hiruma et al., 2015; Ji et al., 2015). In light of its central role in checkpoint activation, it is perhaps not surprising that Mps1/Mph1 is involved in the assembly of both Mad1-C-Mad2 as well as KNL1/Spc7/Spc105-Bub3-Bub1 scaffolds.

Mps1/Mph1 activity is required for the localisation of Bub1 to unattached kinetochores, but only recently has the underlying mechanism become clear. Together with the Biggins lab, our lab in collaboration with J. Millar was the first to identify an outer kinetochore component, Spc7 (*S. cerevisiae*: Spc105; vertebrates: KNL1), as the key Mph1 target that enables Bub1 localisation to unattached kinetochores (London et al., 2012; Shepperd et al., 2012). KNL1 (**k**inetochore **n**u**l**l **1**) was originally identified as an essential kinetochore assembly component in *C. elegans* (Desai et al., 2003), and has since been recognised as a component of the conserved microtubule (MT)-binding KMN (**K**NL1/**M**is12/**N**dc80) outer kinetochore complex (Varma and Salmon, 2012). The function of KNL1 and its homologues is now known to extend beyond microtubule binding and include serving as a binding platform for spindle checkpoint components and protein phosphatases. Using *in vitro* kinase assays and *in vivo* imaging, our lab showed that the Mph1-dependent phosphorylation of Spc7 along a series of conserved MELT motifs ([**M**/I][**E**/D/N][I/**L**/M][S/**T**]) enables it to bind Bub1 in a Bub3-dependent manner (Shepperd et al., 2012). The Watanabe lab shortly afterwards reported similar findings which, despite some disagreement over the exact number of phosphorylated MELTs required for Bub1 recruitment,

confirmed the importance of our findings as well as their conservation in human-derived cells (Yamagishi et al., 2012) (Fig. 1.4A).

Nevertheless how Bub1 localised to kinetochores via phosphorylated KNL1/Spc7 remained unclear: did it directly interact with phospho-MELTs, or did it do so via Bub3? Attention initially focussed on the conserved N-terminal TPR domain of Bub1, as this domain interacts directly with KNL1 via the latter's KI motifs, a feature that is not present in KNL1's homologues in yeast (Kiyomitsu et al., 2007, 2011). These studies demonstrated that mutations in the hsBub1 TPR domain not only abolished its interaction with KNL1 but also interfered with downstream checkpoint signalling. Taken together with the finding that KNL1 depletion abolishes both hsBub1 kinetochore localisation and checkpoint function, these results lead Kiyomitsu and colleagues to conclude that Bub1 localises to kinetochores via interaction between its TPR domain and KNL1. This propensity of KNL1 to bind Bub proteins lead these authors to propose that hsKNL1 be renamed Blinkin (**B**ub-**l**inking **k**inetochore protein).

This hypothesis was refuted when the crystal structures of the Bub1-KNL1 and BUBR1-KNL1 complexes were solved, revealing residues that when mutated would abolish Bub1/BUBR1 interaction with KNL1 whilst leaving their kinetochore localisation intact (Krenn et al., 2012). In contrast, mutation of the Bub3-binding site of Bub1/BubR1 abolished kinetochore localisation, thus demonstrating that Bub1 localisation to the kinetochores occurs indirectly via Bub3-KNL1 interaction (Fig. 1.4B). Once Bub3 is bound to phosphorylated KNL1, Bub1 serves to stabilise the Bub3-KNL1 interaction (Krenn et al., 2012; Primorac et al., 2013).

This leaves the question of how Mad3/BUBR1 is localised to kinetochores. As previously mentioned, BUBR1 exhibits significant homology with Bub1 and contains an N-terminal TPR domain that interacts with KNL1. As with Bub1, this interaction was found to be largely dispensable for the kinetochore localisation of BUBR1 (Krenn et al., 2012), leading to suggestions that BUBR1 might localise to the kinetochores indirectly via Bub3, since both Bub1 and BUBR1 form constitutive complexes with Bub3. Surprisingly however, BUBR1 was found to be unable to stabilise the Bub3-KNL1 interaction (Krenn et al., 2012; Primorac et al., 2013), thus detracting from the Bub3-mediated model. Instead, recent evidence suggests that at least in humans, BUBR1 localises to kinetochores directly via Bub1 binding (Overlack et al., 2015); whether this model involves dynamically cycling BUBR1, and whether it extends to yeast Mad3/Bub1 recruitment remain to be seen.

1.5.2 Role of Mps1 in the assembly of the Mad1-Mad2 scaffold

Mps1/Mph1 has been implicated in regulating both Mad1-C-Mad2 complex formation at the kinetochores as well as the subsequent catalysis of O-Mad2 dimerisation. Much of the current evidence for this regulation is indirect, however, making this key process poorly understood. In human-derived cells, it has been suggested that Mps1 has multiple roles in mediating Mad1-Mad2 recruitment to the kinetochores, and that Mad1 is a possible substrate for these roles (Hewitt et al., 2010). Through the use of small-molecule Mps1 inhibitors, Hewitt and colleagues

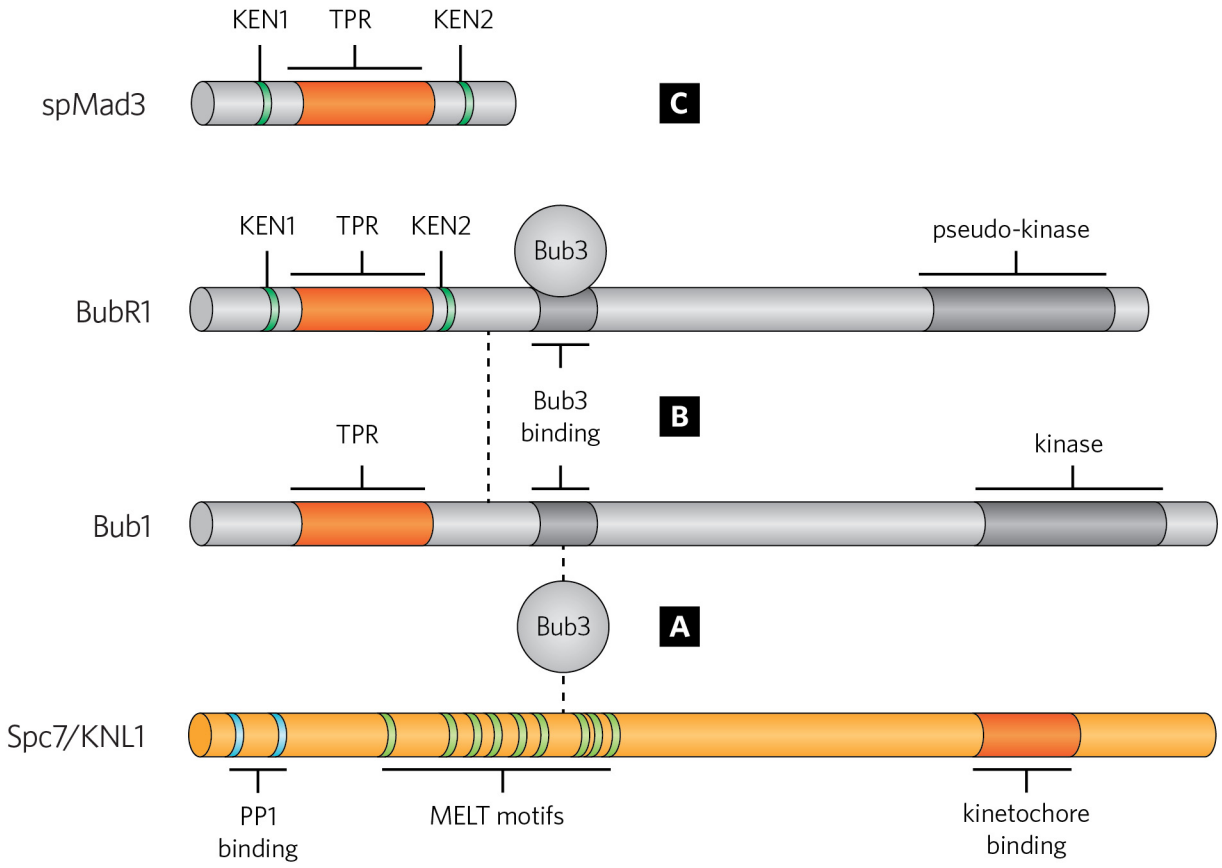

Fig. 1.4 – Interplay between Bub3, Bub1 and Spc7/KNL1 in checkpoint scaffold assembly. (A) The kinetochore localisation of Bub1 is mediated by Spc7/KNL1 containing phosphorylated MELT motifs. Previously it was believed that Spc7/KNL1 bound Bub1 directly via Bub1's TPR domain. **(B)** Unlike Bub1, human BubR1 does not localise to kinetochores via Bub3 interaction and relies instead on direct Bub1-BubR1 interaction. **(C)** Unlike Bub1 and BubR1, fission yeast Mad3 does not contain a Bub3 binding domain (B3BD), also referred to as the GLEBS domain. TPR: Tetratricopeptide repeat. PP1: Protein Phosphatase 1. Diagrams not to scale.

observed that inhibition of Mps1 prior to mitotic entry abolishes kinetochore recruitment of Mad1-C-Mad2, whereas Mps1 inhibition after mitotic entry does not evict Mad1-C-Mad2 from kinetochores but instead prevents O-Mad2 dimerisation. These results were interpreted to suggest that Mps1 activity is first required for the initial localisation of Mad1-C-Mad2 to the kinetochore, after which it is required to maintain recruitment of O-Mad2 to Mad1-C-Mad2. Although this model is attractive, it remains speculative because Mad1 has not been confirmed as an Mps1 target, and Mad1 phosphorylation sites have yet to be mutated and studied.

Similarly indirect evidence for Mps1-mediated phospho-regulation of Mad1 exists in yeast. In *S. cerevisiae*, Ndc80 has been implicated as an Mps1 target *in vitro* (Kemmler et al., 2009). Phospho-analysis by Kemmler and colleagues showed that a non-phosphorylable (alanine) form of Ndc80 rendered the checkpoint inactive, whilst a phosphomimetic mutant restored some, but not all, checkpoint function to a strain depleted of Mps1. This latter result is important as it implies that Mps1-mediated phosphorylation of other substrates is required for full checkpoint function. Again, Mad1 is a strong candidate for this role, and phospho-analysis of Mad1 will likely yield important information on Mad1-C-Mad2 interaction. It is however important to note here that the Biggins lab were unable to reproduce the results of Kemmler and colleagues .

Unlike the case for Mad1, evidence for Mps1/Mph1-mediated phospho-regulation of Mad2 has been more direct. In *S. pombe*, our lab has identified several *in vitro* phosphorylation sites on Mad2 that are important for regulating MCC-APC/C interaction, as well as possibly Mad1-C-Mad2 complex formation (Zich et al., 2012). Whereas current evidence suggests that Mps1 phosphorylation of Mad1 positively regulates checkpoint function, Zich and colleagues found that a phosphomimetic form of a Mph1 target on Mad2 actually negatively regulates checkpoint function, a surprising result that mirrors those previously obtained in human-derived cells (Wassmann et al., 2003). These results imply a novel checkpoint silencing function for Mps1 that is seemingly at odds with the current consensus that Mps1 is a positive checkpoint regulator, and further work is required to confirm these findings and reconcile them with the currently available Mps1 evidence.

1.5.3 The mutual dependencies between Spc7/KNL1-Bub3-Bub1 and Mad1-C-Mad2

Although the previous two sections have described the assembly of the Spc7/KNL1-Bub3-Bub1 and Mad1-C-Mad2 scaffolds as independent processes, recent evidence suggests that they may directly interact through Mad1-Bub1 interaction. This interaction was first hinted at by the finding of our lab that in *S. cerevisae*, Mad1 can co-immunoprecipitate with the Bub1-Bub3 complex during mitosis (Brady and Hardwick, 2000). This co-immunoprecipitation was also observed in nocodazole treated (checkpoint arrested) but not in interphasic cells, suggesting that the Mad1-Bub1-Bub3 interaction is checkpoint-specific. A direct Mad1-Bub1 interaction was recently confirmed by London and colleagues (London and Biggins, 2014a), demonstrating that in *S. cerevisae*, a central fragment of Bub1 is capable of recruiting Mad1 to kinetochores upon phosphorylation by Mps1. Moreover, by building on their earlier finding that Mps1-mediated

phosphorylation of Spc105 is sufficient for Bub1 recruitment (London et al., 2012), the authors demonstrated that Mps1 directs the assembly of a combined Spc105-Bub1-Mad1 scaffold in the following manner. First, Spc105 is phosphorylated along its MELT motifs by Mps1, which enables it to recruit the Bub3-Bub1 complex. Phosphorylation of Bub1 at specific residues identified in (London and Biggins, 2014a) then enables it to bind Mad1 and therefore Mad2. By showing that Mps1 regulates both Bub1-Mad1 interaction as well as Spc105-Bub1 interaction, these results again highlight the central importance of Mps1/Mph1 in directing checkpoint activation.

Although this unified model of checkpoint scaffold assembly at kinetochores is attractive, it is unclear if it extends beyond *S. cerevisiae*. In *C. elegans*, although a Mad1-Bub1 interaction at the kinetochores has been recently reported (Moyle et al., 2014), it is likely regulated in a different manner from the Mad1-Bub1 complex of *S. cerevisae* as no Mps1 homologues are known to exist in *C. elegans*. In mammalian systems, conflicting evidence exists on Mad1-Bub1 interaction: although a previous study found that phosphorylated hsMad1 interacts with hsBub1 (Seeley et al., 1999), a more recent study was unable to reproduce this interaction despite reporting more evidence implying its existence (Kim et al., 2012). Specifically, this latter study showed that mutation of an RLK motif on hsMad1 (originally identified in *S. cerevisae* as being critical for Mad1-Bub1 interaction (Brady and Hardwick, 2000)) abolished the kinetochore localisation of hsMad1. This was taken as evidence of hsMad1-hsBub1 interaction, but as efforts to detect a physical interaction proved fruitless, the authors could at best conclude that such an interaction is likely highly transient (Kim et al., 2012). No Mad1-Bub1 interaction has yet been reported in *S. pombe*, but it remains an intriguing possibility in light of recent genetic evidence that Bub1 is required for Mad1 localisation to kinetochores (Heinrich et al., 2012).

1.5.4 Are checkpoint components needed at kinetochores?

Although the assembly of checkpoint scaffolds at the kinetochores is now better understood, how this co-localisation of the checkpoint components at the kinetochores produces rapid, global and reversible APC/C inhibition remains the sought-after 'holy grail' of checkpoint research. Is the enrichment of checkpoint components the sole function of kinetochore localisation? Related to this, do all of the checkpoint components need to localise to the kinetochores to function? Our lab has previously shown that, uniquely in *S. pombe*, deletion of *bub3* abolishes the detectable enrichment of almost all checkpoint proteins (Mad1, Mad2, Mad3, Bub1) from kinetochores, and yet the checkpoint remains functional (Tange and Niwa, 2008; Vanoosthuyse et al., 2009; Windecker et al., 2009). Similarly, depletion of Hec1 (Ndc80) in human-derived cells evicts both Mps1 and the Mad1-C-Mad2 complex from the kinetochores without impairing checkpoint function (Martin-Lluesma et al., 2002).

These results indicate that checkpoint signalling can be initiated and propagated away from the kinetochores. Strongly supporting this idea is the recent finding in human-derived cells that nuclear pore complexes (NPCs) can function as a scaffold for checkpoint signalling, and that this generates APC/C inhibitors just before mitosis (Rodriguez-Bravo et al., 2014). Although it has

long been known that Mad1-C-Mad2 localises to the nuclear periphery during interphase, by demonstrating that this can generate APC/C inhibitors the authors presented an intriguing model whereby two distinct checkpoint scaffolds are required for rapid and global APC/C inhibition. An important implication of this model that was not directly tested by the authors is that because the KNL1-Bub3-Bub1 scaffold has not been reported to associate with NPCs, checkpoint signal generation at the NPCs likely follows a different assembly process than that at kinetochores.

The idea that the kinetochore localisation of checkpoint components is somehow essential for checkpoint signal generation is further challenged by the fact that Mad3/BUBR1 localisation to kinetochores is absent in *S. cerevisiae* (Gillett et al., 2004) and *C. elegans* (Essex et al., 2008), and may also not be required for checkpoint function in human-derived cells (London and Biggins, 2014b). As mentioned above, although Mad3 does localise to *S. pombe* kinetochores upon checkpoint activation, its eviction from the kinetochores does not abolish checkpoint function (Vanoosthuyse et al., 2009) and it will be important to determine if it can be incorporated into MCC complexes away from the kinetochores.

1.6 Tension sensing with Aurora B kinase

As mentioned above, the spindle checkpoint functions by monitoring attachment between the spindle microtubules and the kinetochore. Using vertebrate cells, Rieder and colleagues showed that a single unattached kinetochore is sufficient to activate the spindle checkpoint (Rieder et al., 1995). Improper microtubule-kinetochore attachments, such as when both sister chromosomes attach to the same pole (syntelic attachment), also activates the spindle checkpoint (Watanabe, 2012).

What is not clear is the molecular mechanism by which the spindle checkpoint detects improper kinetochore attachments. The most favoured model remains the 'tension-sensing' model (for review see (Lampson and Cheeseman, 2011)), which postulates that Aurora B kinase (*S. pombe*: Ark1) functions as a 'kinetochore stretch sensor'. Aurora B is a kinase that is part of the chromosome passenger complex (CPC), consisting of Aurora B, Survivin, Borealin and the inner centromere protein (INCENP). The CPC is positioned at the centre between two sister kinetochores (also known as the inner centromere). It is believed that when proper (bi-polar) attachment occurs, the opposing forces exerted on the two sister kinetochores pulls them apart, thus moving them farther apart from Aurora B at the centre. This in turn reduces the level of phosphorylation of Aurora B substrates, including the outer kinetochore protein Ndc80. The phosphorylation of Ndc80 by Aurora B weakens and ultimately breaks kinetochore-microtubule attachments. This in turn results in unattached kinetochores, which then triggers the spindle checkpoint.

This Aurora B-dependent 'tension-sensing' model is thus a spatial model that is based on two key observations. First, it was shown that the phosphorylation levels of a given Aurora B substrate are inversely proportional to the distance between Aurora B and that substrate (Liu et

al., 2009). Second, if Aurora B is experimentally moved from the inner centromere to the outer centromere, then Aurora B substrates become constitutively phosphorylated, and it becomes impossible to stabilise kinetochore-microtubule attachments.

The 'tension-sensing' model is at present the most attractive answer to the question of how the spindle checkpoint can detect and thus respond to improper chromosome attachments; it explains how properly attached (under tension) and improperly attached (no tension) chromosomes can be distinguished. However, it is increasingly clear that the tension-sensing model requires revision to accommodate recent findings. It was recently shown in human cells that a significant pool of Aurora B kinase is found at the outer kinetochore, even after Hec1 (vertebrate homologue of Ndc80) is dephosphorylated (DeLuca et al., 2011). This suggests that the phosphorylation of Hec1 is not entirely regulated by the spatial positioning of Aurora B. One possible explanation is that there are multiple ways by which Aurora B activity is regulated, although no experimental evidence for this currently exists. It will be interesting to see if these observations are also true for Ark1 and Ndc80.

1.7 Checkpoint silencing

1.7.1 Silencing inactivates the spindle checkpoint

Once proper microtubule-kinetochore attachments have been established, the spindle checkpoint is satisfied and signalling must be inactivated in order to allow cells to proceed to anaphase. This is known as checkpoint silencing, which encompasses a range of different mechanisms with varying degrees of conservation and experimental evidence. When proper microtubule-kinetochore attachments are made and checkpoint silencing is initiated, active APC/C inhibitors are both present in the cytoplasm as well at the kinetochores where they are generated. Thus, in order to effect silencing the cell must (i) stop further APC/C inhibitor generation at the kinetochores, and (ii) quench the active APC/C inhibitors in the cytoplasm.

1.7.2 Silencing mechanisms

The most conserved silencing mechanism is mediated by PP1 phosphatase (**P**rotein **p**hosphatase **1**; *S. pombe*: Dis2). At the kinetochores, KNL1/Spc7 acts in conjunction with the kinesins Klp5/6 to mediate the recruitment of PP1/Dis2 (Liu et al., 2010). Once at the kinetochores, $PP1^{Dis2}$ phosphatase activity opposes kinetochore-localised Aurora B kinase acting to destabilise microtubule-kinetochore attachments. When the kinetochore is not under tension (stretched), Aurora B targets KNL1, rendering it unable to recruit PP1. Once proper attachments have been made, kinetochore stretch acts to distance KNL1 from Aurora B, thus relieving the inhibitory phosphorylation on KNL1 (Liu et al., 2010). This enables the recruitment of PP1 to the kinetochores, whereupon the stabilising effect of PP1 on attachments ensures further recruitment of PP1 in a positive-feedback loop. Thus, the end effect of PP1-mediated silencing is the reversal of checkpoint kinase activity at the kinetochores. Key PP1 substrates remain to be identified.

Another silencing mechanism that has been proposed to remove the APC/C inhibitors being generated at the kinetochore is dynein-dependent 'stripping' of Mad2. Unlike PP1-mediated silencing, this 'stripping' mechanism is likely neither essential nor conserved. Upon proper microtubule-kinetochore attachment, Mad1 and Mad2 are transported along the spindle fibres from unattached kinetochores to the spindle pole bodies (SPBs) by the dynein/dynactin microtubule motor complex (Gassmann et al., 2010; Howell et al., 2001). Detracting from the importance of 'stripping' however is the observation that depletion of Spindly, a kinetochore component required for the dynein binding, does not completely abolish poleward Mad1/Mad2 transport in HeLa cells (Gassmann et al., 2010). This is currently no evidence for 'stripping'-mediated silencing in yeast.

Vertebrates have a unique silencing mechanism in the form of $p31^{comet}$, a competitive inhibitor of Mad2 (no $p31^{comet}$ homologues have been reported in yeast). The structure of $p31^{comet}$ was found to closely resemble that of Mad2, enabling it to bind or 'cap' Mad2 within the Mad1-C-Mad2 complex (Xia et al., 2004; Yang et al., 2007). Thus, $p31^{comet}$ has been proposed to mediate silencing through preventing the dimerisation and subsequent activation of soluble O-Mad2. However, although it is accepted that $p31^{comet}$ is an important silencing mechanism in vertebrates because its depletion constitutively activates the checkpoint while its overexpression overrides it (Habu et al., 2002), exactly where this silencing occurs remains controversial. $p31^{comet}$ localises to kinetochores, where it was originally proposed to 'cap' kinetochore bound Mad1-C-Mad2. However, using an antibody that preferentially binds O-Mad2, Westhorpe and colleagues found that $p31^{comet}$ localisation to the kinetochore did not affect the amount of O-Mad2 localised at kinetochores, even upon $p31^{comet}$ overexpression (Westhorpe et al., 2011). This suggests that $p31^{comet}$ effects silencing downstream of kinetochores, and the authors propose a model in which $p31^{comet}$ binding to MCC via Mad2 promotes MCC disassembly. Like many such attractive models, current evidence for $p31^{comet}$-mediated MCC disassembly is largely indirect and more work will be required for its acceptance.

1.8 Aims of this work

This work aims to achieve the following two goals:

1. **A better understanding of Mad1-Mad2 interaction**. The evidence reviewed above indicate that certain aspects of the regulation of Mad1-Mad2 interaction remain poorly understood. Chapter 3 will thus first examine the role of the N-terminus of Mad1 in mediating Mad1-C-Mad2 interaction. Then, the phospho-regulation of Mad1 will be examined using a series of Mad1 phospho-mutants created based on mass spectrometry data.
2. **Determine whether the role of kinetochores in spindle checkpoint signalling is solely to enrich for checkpoint components**. Since the discovery that unattached kinetochores are one of the major sources of the spindle checkpoint signal, this is arguably one of the biggest unresolved questions of checkpoint signalling. This important issue forms the

recurring theme for this entire work, but is most directly addressed in Chapters 4 and 5 where the enrichment of checkpoint components away from the kinetochores will be tested to determine if they are able to generate a 'synthetic' checkpoint signal that is capable of delaying cells in metaphase.

CHAPTER 2

Materials & Methods

2.1 DNA methods

2.1.1 Polymerase chain reaction

For cloning work, Phusion® or Q5® High-Fidelity 2X Master Mix (New England Biolabs) was used in accordance with the manufacturer's instructions. PCR products were visualised by agarose gel electrophoresis using ethidium bromide.

2.1.2 Gateway® cloning

All Gateway®-based cloning was performed using kits (LR Clonase II Enzyme Mix, BP Clonase II Enzyme Mix) obtained from Invitrogen (Section 2.4) in accordance with the manufacturer's instructions, **except that all volumes indicated in the instructions were halved to give a final volume of 5 µl/reaction**.

2.1.3 Site directed mutagenesis

All site-directed mutagenesis was performed using the Quikchange® II or Quikchange® Lightning site-directed mutagenesis kits (Strategene) (Section 2.4) in accordance with the manufacturer's instructions, **except that all volumes indicated in the instructions were scaled-down by 5x to give a final volume of 10 µl/reaction**.

2.1.4 Sequencing

Sanger sequencing was carried out by Genepool (University of Edinburgh) on samples processed with BigDye® v3.1 Cycle Sequencing Kit (Applied Biosystems). BigDye® reactions were performed in accordance with the manufacturer's instructions.

2.1.5 Restriction endonuclease digestion

All restriction enzymes were obtained from New England Biolabs or Roche and used in accordance with the manufacturer's instructions.

2.1.6 De-Phosphorylation

Linearised vectors were treated with Antarctic Phosphatase (New England Biolabs) in accordance with the manufacturer's instructions.

2.1.7 Ligation

Ligations were performed using T4 Quick Ligase (New England Biolabs) in accordance with the manufacturer's instructions before transformation into *E. coli* (Section 2.1.8).

2.1.8 Bacterial transformation

Transforming DNA was added to de-frosted chemically-competent *E. coil* cells in a pre-chilled screw-cap tube. Following gentle mixing, the mix was incubated on wet ice for 30 min. before being subjected to heat shock at 42 °C in a water bath for 45 s. 200-900 µl of pre-warmed SOC

medium was then added and cells were allowed to recover for 1 hour at 37 °C with shaking before plating unto selective plates.

2.1.9 Yeast transformation

Both lithium acetate and electroporation were used for yeast transformation. **It should be noted that some constructs exhibited greater transformation efficiency using one method than the other, and thus the optimal method for a given construct should be determined empirically.** For **electroporation**, cells were grown to mid-exponential phase (OD_{600} = 0.5) in YES (Section 2.5.1) before harvesting (1701 x *g*, 2 min 30 s) and transferred to a pre-chilled microfuge tube and placed on wet ice. Cells were washed once with ice-cold water and once with ice-cold 1 M sorbitol. Following the sorbitol wash cells were re-suspended in ice-cold sorbitol to a final density of 1 x 10^9 cell/ml. 40 µl of the cell suspension was transferred to a pre-chilled microfuge tube containing 10 µl of transforming DNA (~1.5 µg) and mixed. The mixture was then transferred to a pre-chilled cuvette (0.2 cm gap) and incubated for 5 min. on wet ice before being electroporated at 1.8 kV, 200 Ω, 25 µF capacitance using a BioRad electroporator. After electroporation 500 µl of ice-cold sorbitol was immediately added to the cuvette before the entire mix was transferred to a clean microfuge tube. Transformed cells were harvested (1701 x *g*, 2 min) and depending on the type of selection either plated unto selective plates or being allowed to recover in YES at 30 °C with shaking overnight before plating.

For **lithium acetate** transformation (Ito et al., 1983), exponentially growing cells were obtained as described above, and after harvesting (1701 x *g*, 2 min 30 s) cells were washed once with 25 ml of water before being resuspended in 1 ml of water. 1 x 10^8 cells were then aliquoted for each transformation. After spinning (1701 x *g*, 2 min 30 s) to remove the water, cells were incubated in 100 mM lithium acetate buffer (0.1 M lithium acetate pH 4.9) at 30 °C for 30 min. before pelleting and resuspension in a transformation mix consisting of 290 µl of PEG buffer (50 % w/v polyethylene glycol 3350, 0.1 M lithium acetate pH 4.9) and ~2 µg of transforming DNA. This mix was then incubated at 30 °C for 60 min., before being subjected to heat shock at 42 °C for 15 min. Transformed cells were harvested (1701 x *g*, 2 min) and depending on the type of selection either plated unto selective plates or being allowed to recover in YES at 30 °C with shaking overnight before plating.

2.1.10 Yeast genomic DNA extraction

Yeast genomic DNA for cloning and for diagnostic PCR was obtained using the single-tube LiOAc-SDS lysis method described in (Lõoke et al., 2011).

2.1.11 Ethanol precipitation of DNA

To precipitate DNA from aqueous solutions, three volumes of ice-cold 96 % ethanol and 1/10 volume 3 M sodium acetate solution was first added to one volume of DNA solution in a microfuge tube. After incubating on wet ice for 15-30 min., tubes were centrifuged at maximum speed at 4 °C for 10 min. before the supernatant was removed and a wash of 500 µl 70 % ethanol solution applied. Without mixing, the tubes were re-spun at maximum speed at 4 °C for 5 min.

After removing the wash solution, tubes were air-dried for 5 min. before the pellet was resuspended in TE buffer.

2.2 Protein methods

2.2.1 Yeast protein lysis buffer

The 'CLAAPE' protease inhibitor mix indicated with an asterisk (*) is composed of the following protease inhibitors: chymostatin, leupeptin, aprotinin, antipain, pepstatin and E-64, all dissolved in DMSO at a final concentration of 10 mg/ml each.

Component	Final conc.
HEPES, pH 7.6	50 mM
KCl	75 mM
$MgCl_2$	1 mM
EGTA	1 mM
TX-100	0.1 %
$NaVO_4$	1 mM
CLAAPE mix*	
PMSF	1 mM

2.2.2 Yeast protein extracts

10-25 ml of cells were grown overnight in the appropriate medium (30 °C, 250 RPM) before being harvested (1701 x *g*, 2 min 30 s) and transferred to a screw-cap tube. A wash with 1 ml of ice-cold water was then applied before cell pellet sizes were normalised and mixed with 100 µl of lysis buffer (Section 2.2.1) and an equal quantity of silica beads. Cells were broken by bead-beating (2 x 20 s, 1 min. on ice in between) before 100 µl of 2x sample buffer was added. After brief vortexing, extracts were denatured at 95 °C for 5 min. before cell debris was pelleted by centrifugation (10,621 x *g*, 5 min., 4 °C). Cleared cell extracts were then immediately loaded onto SDS-PAGE gels (Section 2.2.4).

2.2.3 Co-immunoprecipitation with GFP-Trap®

For pull-down of GFP-tagged proteins, magnetic GFP-Trap®_M beads (Chromotek) was used in accordance with the manufacturer's instructions with the following modifications: 3 µl of beads were typically used per reaction; cells lysed at 4 °C using a Ribolyser (Hybaid) for 2 x 20s at force setting 4.5 with chilling on ice in between each round of lysis. Samples were then separated using SDS-PAGE.

2.2.4 SDS-PAGE

Resolving gels were made according to the following recipe:

	10.0 %	12.5 %	15.0 %

40 % acrylamide	3.7 ml	4.7 ml	5.6 ml
2 % Bis	0.98 ml	0.75 ml	0.64 ml
1.5 M Tris-HCl pH 8.8		3.75 ml	
Water		*to 15 ml*	

150 µl 10 % ammonium persulfate (APS) and 15 µl TEMED was added immediately prior to use. Resolving gels were overlaid with butan-1-ol and allowed to set before the alcohol was removed and stacking gel added:

40 % acrylamide	6.25 ml
2 % Bis	3.33 ml
1.0 M Tris-HCl pH 6.8	6.25 ml
Water	*to 50 ml*

Proteins were typically resolved on 10 cm x 20 cm SDS-PAGE gels for 90 min at a constant voltage of 120-160 V in SDS-PAGE buffer (50 mM Tris, 384 mM glycine, 2 % SDS).

Following resolution, proteins were transferred unto nitrocellulose membranes (GE Healthcare) using a TE77 semi-dry transfer unit (Hoefer) at 125 mA for 90 min in semi-dry transfer buffer (25 mM Tris, 130 mM glycine, 20 % methanol).

2.2.5 Immunoblot

Membranes were blocked in blocking solution (1x PBS, 0.04 % Tween 20, 4 % w/v dried skimmed milk (Marvel)) for 40 min. at room temperature before incubation overnight in primary antibody at 4 °C. Membranes were then washed with PBS + 0.04 % Tween 4 times for 5 min. each before the appropriate secondary antibody was applied for 40 min at room temperature. A further 4 washes of PBS + 0.04 % Tween was applied to remove unbound antibody before protein visualisation.

2.2.6 Protein visualisation

Proteins were visualised by chemiluminescence using an ECL detection kit (SuperSignal West Pico or SuperSignal West Femto, Pierce) according to the manufacturer's instructions. Membranes were overlaid with clear acetate sheets before being exposed to X-ray film (Agfa Healthcare). Films were subsequently developed using a SRX-101A Film Processor (Konica-Minolta).

2.2.7 Antibodies used in this work

HRP-conjugated secondary antibodies are indicated with an asterisk (*).

Antibody	Species	Conc.	Source
Anti-GFP	Sheep	1:1000	Hardwick lab

Anti-tubulin (TAT1)	Mouse	1:1000	Gift from Keith Gull
Anti-Mph1	Sheep T	1:1000	Hardwick lab
Anti-FLAG M2	Mouse	1:1000	Sigma-Aldrich
Anti-Mad2	Sheep	1:1000	Hardwick lab
Anti-sheep, HRP conjugated*	Donkey	1:5000	Jackson Immuno-Research
Anti-mouse, HRP conjugated*	Donkey	1:5000	GE Healthcare
Anti-rabbit, HRP conjugated*	Sheep	1;5000	GE Healthcare

2.3 Yeast methods

2.3.1 Anhydrotetracycline

Addition of anhydroxytetracycline (aTc) to yeast medium at a final concentration of 10 µM enables binding of rTetR to *tetO* sequences. A concentrated (1000x) stock of 10 mM was prepared in DMSO and filter-sterilised prior to storage at -20 ºC.

2.3.2 Wide-field epi-fluorescence microscopy

All fluorescence microscopy experiments **except those for FRAP** were performed using a Zeiss Axiovert 200M inverted epi-fluorescent microscope (Carl Zeiss Ltd.) equipped with a 100x 1.49 N.A. objective lens and a CoolSnap CCD camera (Photometrics). Images were acquired and analysed using Slidebook 5.5 software (Intelligent Imaging Innovations Inc.). Acquisition settings were as follows: 300 ms exposure (FITC & CY3), 2x binning, Z-series over 3 µm range in 0.5 µm steps (7 planes). Maximum projection images were created using Slidebook. Cell culture conditions for FRAP, tethering and synthetic signalling assays are described in their own sections in this chapter.

2.3.3 Fluorescence recovery after photobleaching (FRAP)

All FRAP experiments were performed using a spinning disk confocal microscope comprising of a Nikon TE2000 inverted microscope with a Nikon 100x/1.45 NA Plan Apo objective, attached to a modified Yokogawa CSU-10 unit (Visitech) and an Andor iXon+ Du888 EMCCD camera, controlled by Metamorph software (Molecular Devices). The microscope was fitted with a temperature controlled chamber which was set at 25 ºC for all experiments. Typical acquisition settings were as follows: 100 ms exposure, 2x binning, Z-series over 3 µm range in 0.5 µm steps (7 planes).

Cells for FRAP were grown and prepared as follows. Exponentially growing cells were obtained by growth in liquid PMG medium (no aTc, with thiamine) at 30 ºC with shaking for 6-8 hours before diluting down in PMG medium (with aTc, no thiamine) for 12-20 hours until an OD_{600} of 0.5 was reached. Cells were washed in clear PMG medium (Section 2.5.2) (no aTc, no thiamine) before mounting onto lectin-coated 35 mm glass-bottomed dishes (Part no.: P35G-1.5-

20-C, MatTek) using the procedure below. Mounting of cells unto glass-bottom dishes in this way greatly reduces cell stress and allows them to be imaged for much longer periods of time.

20 µl of 1 mg/ml filter-sterilised lectin solution (Part no.: L1395-5MG, Sigma-Aldrich) was spread unto a 35 mm glass-bottomed dish using a sterilised bent glass pasteur pipette and incubated for 10 min. at 25 °C. To prevent scratches to the glass (coverslip) bottom, dishes were kept in a clean petri-dish throughout the mounting procedure. Excess lectin solution was then gently removed using five washes of 1 ml sterile water and two washes of 1 ml clear PMG medium (no aTc, no thiamine). **It is imperative that all washes be done gently by slowly pipetting liquid unto one side of the glass bottom whilst simultaneously aspirating from the opposite side**; excessively harsh washing reduces both the strength and uniformity of cell adhesion across the coverslip. Following washing approx. 0.2 OD_{600} units of cells (1 ml of OD_{600} = 0.5 cells equals 0.5 OD_{600} units) were gently added to the glass bottom and allowed to adhere for 20 min. at 25 °C. Dishes were left undisturbed throughout this time. Unbound cells were then gently removed using five washes of clear PMG (no aTc, no thiamine) before 400 µl of clear PMG (no aTc, no thiamine) was added. Cells were imaged immediately in a temperature controlled chamber pre-heated to 25 °C. Image and mathematical analysis of FRAP was performed as follows using ImagePro Premiere (MediaCybernetics) and Excel (Microsoft).

FRAP is modelled on the dissociation of irreversibly bleached molecules. As such the rise in post-bleach fluorescence due to the exchange of such molecules with the soluble pool of fluorescent molecules can be modelled using the following equation (assuming that recovery can be described by a single exponential):

$$\frac{dI}{dt} = -kI$$

where I is the amount of irreversibly bleached molecules, t is time and k is the dissociation constant. Note that this model assumes that the supply of fluorescent molecules in the soluble pool is infinite. Solving the above equation and re-arranging gives:

$$e^{-kt} = \frac{I(t)}{I_0}$$

where I_0 is the amount of irreversibly bleached molecules immediately post-bleach (at t_0). $I(t)$ can be expressed as $F_\infty - F(t)$, where F_∞ is the fluorescence at infinity (maximum recovery) and $F(t)$ is the fluorescence at a particular time point t. I_0 can be expressed as $F_\infty - F(0)$, where $F(0)$ is the fluorescence immediately following photobleaching. Thus the above equation can be expressed as:

$$e^{-kt} = \frac{F_\infty - F(t)}{F_\infty - F_0} \qquad (1)$$

To calculate the dissociation constant k, equation (1) can be rearranged to give:

$$kt = -\ln\left(\frac{F_\infty - F(t)}{F_\infty - F_0}\right)$$

k is obtained by plotting the expression on the right against time and determining the gradient of the line of best fit given by the equation $Y = kX$. Once k has been determined, it can then be substituted into equation (1) to calculate the half-life ($t_{½}$), which is defined as $[(F_\infty - F(t))/(F_\infty - F(t)]/2$. This gives $t_{½}$ as:

$$t_{1/2} = \frac{\ln(2)}{k}$$

Note that all measured fluorescence is corrected for (i) background noise and (ii) photobleaching damage before being used to calculate the FRAP parameters described above.

2.3.4 Tethering assay

To visualise tethered checkpoint proteins tagged with fluorescent proteins, exponentially growing cells were obtained by growth in liquid PMG medium (no aTc, no thiamine) at 30 ºC with shaking for 6-8 hours before diluting down in PMG medium (with aTc, no thiamine) for 12-20 hours until an OD_{600} of 0.3 was reached. Cells were harvested (1701 x *g*, 2 min 30 s) before washing in 1 ml of clear PMG medium (Section 2.5.2). Following washing cells were pelleted (1701 x *g*, 2 min 30 s) before resuspension in clear PMG medium and mounting on a slide. Cells were imaged immediately.

2.3.5 Synthetic arrest assay

For strains containing Mph1 kinase fragments driven by the *nmt* promoter, exponentially growing cells were obtained by growth in liquid PMG medium (no aTc, with thiamine) at 30 ºC with shaking for 6-12 hours to load cells with thiamine. Cell were then harvested (1701 x *g*, 2 min 30 s) before being washed twice with 50 ml PMG (no aTc, no thiamine) and then split into two PMG cultures, one with thiamine and one without. Both cultures contained aTc and were grown at 30 ºC with shaking for 12-20 hours, with samples taken for microscopy at regular intervals. Cells were imaged immediately.

2.4 Reaction kits

All kits were used in accordance with the manufacturer's instructions **unless otherwise stated**.

Product Name	Manufacturer	Catalogue Number
Gel Extraction Kit	Fermentas	K0691
Miniprep Kit	Fermentas	K0503
Qiaquick PCR Purification Kit	Qiagen	28104
QuikChange® II Site-Directed Mutagenesis Kit	Stratagene	200524
QuikChange® Lightning Site-Directed Mutagenesis Kit	Stratagene	210515
Gateway® LR Clonase® II Enzyme mix	Invitrogen	11791-100

Gateway® BP Clonase® II Enzyme mix	Invitrogen	11789-020

2.5 Yeast Media

Recipes are given for liquid media. For solid media, 2% (w/v) agar was added. All media were sterilised by autoclaving.

2.5.1 Yeast Extract Supplemented (YES)

Note: YES contains thiamine which represses the *nmt* promoter.

Component	Final conc.
Yeast extract	0.5 % (w/v)
D-glucose, anhydrous	0.5 % (w/v)
Supplements mix	1x

2.5.2 Pombe minimal medium (PMG)/clear PMG medium

PMG does not contain thiamine and thus allows for expression of *nmt* promoter driven genes, though filter-sterilised thiamine can optionally be added to a final concentration of 15 μM from a 10 mg/ml (2000x) stock to repress expression.

For clear PMG medium, the same recipe was used except that D-glucose was omitted prior to autoclaving. Following autoclaving, filter-sterilised glucose was added to a final concentration of 2 % (w/v). Clear PMG medium greatly reduces the autofluorescence seen when imaging GFP-tagged constructs as it lacks the yellow colour that results from the caramelisation of glucose during the autoclaving process.

Component	Final conc.
Phtalic acid	14.7 mM
Di-sodium hydrogen orthophosphate, anhydrous	15.5 mM
L-glutamic acid, monosodium salt	25.4 mM
D-glucose, anhydrous	2 % (w/v)
Vitamins mix	*1x*
Minerals mix	*1x*
Supplements mix	*1x*

2.5.3 Supplements mix (20x)

Adenine and leucine were added at double the concentration of the other amino acids – this is necessary for maximum growth rate of *ade-* and *leu-* strains. The following mix was dissolved with gentle heating and filter-sterilised before use.

Component	Mass
Adenine	1.6 g
Arginine	0.8 g
Histindine	0.8 g
Leucine	1.6 g
Uracil	0.8 g
Lysine	0.8 g
Distilled water	*to 500 ml*

2.5.4 Minerals mix (1000x)

The following mix was dissolved with gentle heating and filter-sterilised before use.

Component	Final conc.
Boric acid	80.9 mM
MnSO4	23.7 mM
$ZnSO_4$. 7 H_2O	13.9 mM
$FeCl_3$. 6 H_2O	7 mM
Molybdic acid	2.47 mM
KI	6.02 mM
$CuSO_4$. 5 H_2O	1.6 mM
Citric acid	47.6 mM

2.5.5 Vitamins mix (1000x)

The following mix was dissolved with gentle heating and filter-sterilised before use.

Component	Final conc.
Biotin	10 mg/l
Pantothenic acid	1 g/l
Nicotinic acid	10 g/l
Inositol	10 g/l

2.6 List of primers used in this work

No.	Name	Sequence (5′–3′)	Comments	Source
IY01	iy_mCherry_F.4	CTTAAATGTGAAAGTGGGTCCCGGATCCCCGGGTTAATTAA	To PCR mCherry for joining to rtTA by overlap extension PCR.	This work.
IY02	iy_mCherry_R.2	AGTCATTAATCTTGTACAGCTCGTCCATGCC	To PCR mCherry for joining to rtTA by overlap extension PCR.	This work.
IY03	iy_rtTA_F	GATCGCTAGCATGTCTAGATTAGATAAAAGT		This work.
IY04	iy_rtTA_R.3	GGACCCACTTTCACATTTAAGT		This work.
IY06	M1STAAF.2	TTGATGGCGAATCCGCTGCTATGAAATTGGTTG	Mutagenic primer to create Mad1C2A.	This work.
IY07	M1STAAR.2	CAACCAATTTCATAGCAGCGGATTCGCCATCAA	Mutagenic primer to create Mad1C2A.	This work.
IY10	iy_rtTA_seq_F	TCACTAGAGAACGCGTTATATG	Sequencing primer.	This work.
IY15	iy_rtTA_NLS_F	GATCGCTAGCATGCCTAAAAAAAAACGTAAAGTTTCTAGATTAGATAAAAGTAAAG		This work.
IY16	iy_rtTA_NLS_R	GATCATTAATGGACCCACTTTCACATTTAAGT		This work.
IY29	iy_mCherry_seq_F	CCACAACGAGGACTACACCATC	Sequencing primer.	This work.
IY49	iy_Adh1_seq_F	TCTCATTGGTCTTCCGCTCCG	Sequencing primer.	This work.
IY50	iy_ccdB_seq_F	GTCTGCAGGTCGACCATAGTG	Sequencing primer.	This work.
IY51	iy_pLYS1U_seq_F	GAGTCAGTGAGCGAGGAAGC	Sequencing primer.	This work.
IY55	iy_[KM]nmt1 F1	TCATCAATTGAATAAGTTGA	Sequencing primer.	This work.
IY56	iy_Adh_F.2	GATCGAGGTACCGCATGCCCTACAACAACTAAG		This work.
IY58	iy_ccdB_R.2	GATCGACTCGAGCCACTTTGTACAAGAAAGCTGAA		This work.

contd. next page

No.	Name	Sequence (5′–3′)	Comments	Source
IY59	iy_pLYS1U_F.2	GATCGACTCGAGGGCGCGCCACTTCTAAATAA		This work.
IY60	iy_pLYS1U_R.2	GATCGAGGTACCATGCAAGCTTGGCGTAATCAT		This work.
IY61	iy_pADH_mcs_F	CTCGAGTCGTTCCAGATTACGCTGCTC	Phosphorylated primer.	This work.
IY62	iy_pADH_mcs_R	GCTAGCAATTCTCTTGCTTAAAGAAAA	Phosphorylated primer.	This work.
IY64	iy_Mph1_FL_attB_R	GGGGACCACTTTGTACAAGAAAGCTGGGTCCTATTCTGGCATTTTTCGTAA		
IY74	ADHterm-F	CTCTTATTGACCACACCTCTACC	Sequencing primer.	
IY76	lys1-Rev	GTGATGTGTCTGGGAAAGGCAGAG	Sequencing primer.	
IY121	iy_Mph1_303_attB_F	GGGGACAAGTTTGTACAAAAAAGCAGGCTTCAAGCGTCAGCAGGACGTTG		

2.7 List of plasmids used in this work

Name	Description	Source
pIY01	*pDUAL-P_{nmt81}-2xFLAG-rtTA-mCherry-Gateway®* Purpose: Inducible expression (P_{nmt81}) Gateway-compatible TetON tethering vector with mCherry tag. Backbone: *pDUAL-HFF81C*. Marker: ampicillin. Construction described in Section 2.9.1.	This work.
pIY02	*pDUAL-P_{nmt81}-2xFLAG-rtTA-Gateway®* Purpose: Inducible expression (P_{nmt81}) Gateway-compatible TetON tethering vector without mCherry tag. Backbone: *pDUAL-HFF81C*. Marker: ampicillin. Construction described in Section 2.9.2.	This work.
pIY03	*pLYS1U-P_{adh15}-NLS-2xFLAG-rtTA-mCherry-Gateway®* Purpose: Constitutive high expression (P_{adh15}) Gateway-compatible TetON tethering vector with mCherry tag and SV40 NLS. Backbone: *pLYS1U*. Marker: ampicillin. Construction described in Section 2.9.3.	This work.
pIY10	*pLYS1U-P_{adh15}-NLS-2xFLAG-rtTA-mCherry-Spc7$_{1-666}$-9TE* Purpose: Tethering Spc7$_{1-666}$-9TE. Backbone: *pLYS1U*. Marker: ampicillin. Derived from pIY03.	This work.
	pDONR201-mph1$_{D1-302}$	This work.
	pDONR201-spc7$_{1-666}$-9TE	This work.
	pDONR201-spc7$_{1-666}$-9TA (?)	This work.
	pDONR201- mad1$_{D1-313}$	This work.
	pDONR201- mad1$_{D1-148}$	This work.
	pDONR201- mad1$_{D1-439}$	This work.

2.8 List of fission yeast strains used in this work

Strain	Genotype	Source
IY83	*P_{nmt81}-rTetR-mCherry-mad1$_{D1-313}$:leu1, tetO:kanR, mad1D::ura4*	This work
IY84	*P_{nmt81}-rTetR-mCherry-mad1$_{D1-148}$:leu1, tetO:kanR, mad1D::ura4*	This work
IY85	*P_{nmt81}-rTetR-mCherry-mad1$_{D1-439}$:leu1, tetO:kanR, mad1D::ura4*	This work
	mad1D::ura4	Hardwick lab
	mad1-GFP:his3	Hardwick lab
	mad2D::ura4	Hardwick lab
IY09	*mad1-C8A-GFP*	This work
IY11	*mad1-M6A-GFP*	This work
IY46	*mad1-C2A-GFP*	This work
IY48	*P_{nmt81}-rtTA-mCherry-mad1$_{D1-148}$:leu1, tetO:kanR, mad2-mCherry:natR*	This work
IY49	*P_{nmt81}-rTetR-mCherry-mad1$_{D1-148}$:leu1, tetO:kanR, fta3-tdT:natR*	This work
IY128	*lys1::P_{adh15}-rTetR-mCherry-spc7$_{1-666}$-9TE:ura4, tetO:kanR, bub3-GFP*	This work
IY130	*lys1::P_{adh15}-rTetR-mCherry-spc7$_{1-666}$-9TE:ura4, tetO:kanR, mad3-GFP*	This work
IY131	*lys1::P_{adh15}-rTetR-mCherry-spc7$_{1-666}$-9TE:ura4, tetO:kanR, bub1-GFP*	This work
IY146	*lys1::P_{adh15}-rTetR-mCherry-spc7$_{1-666}$-9TE:ura4, tetO:kanR, bub1-GFP*	This work
IY184	*lys1::P_{adh15}-rTetR-mCherry-spc7$_{1-666}$-9TE:ura4, tetO:kanR, mph1D:natR, bub1-GFP*	This work
IY185	*lys1::P_{adh15}-rTetR-mCherry-spc7$_{1-666}$-9TE:ura4, tetO:kanR, mph1D:natR, mad3-GFP*	This work
IY188	*lys1::P_{adh15}-rTetR-mCherry-spc7$_{1-666}$-9TE:ura4, tetO:kanR, mph1D:natR, bub3-GFP*	This work
IY191	*lys1::P_{adh15}-rTetR-mCherry-spc7$_{1-666}$-9TE:ura4, tetO:kanR, mad3-GFP, bub3D::ura4*	This work

contd. next page

Strain	Genotype	Source
IY192	*lys1::P_{adh15}-rTetR-mCherry-spc7$_{1-666}$-9TE:ura4, tetO:kanR, bub1-GFP, bub3D::ura4*	This work
IY195	*lys1::P_{adh15}-rTetR-mCherry-spc7$_{1-666}$-9TE:ura4, tetO:kanR, P_{nmt81}-rTetR-mph1$_{D1-302}$:leu1, mad2-GFP*	This work
IY230	*lys1::P_{adh15}-rTetR-mCherry-spc7$_{1-666}$-9TE:ura4, tetO:kanR, P_{nmt81}-rTetR-mph1$_{D1-302}$:leu1, mad2-GFP*	This work
IY221	*lys1::P_{adh15}-rTetR-mCherry-spc7$_{1-666}$-9TE:ura4, P_{nmt81}-rTetR-mph1$_{D1-302}$:leu1, mad2-GFP*	This work
IY227	*lys1::P_{adh15}-rTetR-mCherry-spc7$_{1-666}$-9TE:ura4, tetO:kanR, P_{nmt81}-rTetR-mph1$_{D1-302}$:leu1, mad1D::ura4, mad2-GFP*	This work
IY235	*lys1::P_{adh15}-rTetR-mCherry-spc7$_{1-666}$-9TE:ura4, tetO:kanR, P_{nmt81}-rTetR-mph1$_{D1-302}$:leu1, mad3-GFP*	This work
IY239	*lys1::P_{adh15}-rTetR-mCherry-spc7$_{1-666}$-9TE:ura4, tetO:kanR, P_{nmt81}-rTetR-mph1$_{D1-302}$:leu1, mad2-GFP, pcp1-mCherry:kanR*	This work
IY241	*lys1::P_{adh15}-rTetR-mCherry-spc7$_{1-666}$-9TE:ura4, P_{nmt81}-rTetR-mph1$_{D1-302}$:leu1, mad1D:ura4::adh21-rTetR-mad1$_{D1-148}$:natR, tetO:kanR, mad2-GFP*	This work
IY242	*lys1::P_{adh15}-rTetR-mCherry-spc7$_{1-666}$-9TE:ura4, tetO:kanR, P_{nmt81}-rTetR-mph1$_{D1-302}$:leu1, mad2-GFP, fta3-tdT:natR*	This work
IY245	*lys1::P_{adh15}-rTetR-mCherry-spc7$_{1-666}$-9TE:ura4, tetO:kanR, mad3D::ura4, mad3-G146V-NLS-GFP*	This work
IY246	*lys1::P_{adh15}-rTetR-mCherry-spc7$_{1-666}$-9TE:ura4, tetO:kanR, mad3D::ura4, mad3-NLS-GFP*	This work
IY247	*lys1::P_{adh15}-rTetR-mCherry-spc7$_{1-666}$-9TE:ura4, tetO:kanR, mad3D::ura4, mad3-H144V-NLS-GFP*	This work

2.9 Plasmid construction

2.9.1 *pIY01 (pDUAL-P_{nmt81}-2xFLAG-rTetR-mCherry-Gateway®)*

The *rTetR* gene (encoding rTetR) was amplified from pAK2 (gift from Alexander Kagansky) using primers 3 and 4 and joined to a mCherry fragment amplified out from pFA6a-mCherry-natR using primers 1 and 2 by overlap extension PCR. After purification this combined *rTetR-mCherry* fragment was digested with NheI and AseI and ligated to pHFF81C (gift from Ken Sawin) digested with NheI and NdeI. The resulting plasmid was sequenced using primers 10 and 29. This plasmid is Gateway® cloning compatible.

2.9.2 *pIY02 (pDUAL-P_{nmt81}-2xFLAG-rTetR-Gateway®)*

The *rTetR* gene (encoding rTetR) was amplified from pAK2 (gift from Alexander Kagansky) using primers 3 and 16. After purification this *rtTA* fragment was digested with NheI and AseI and ligated to pHFF81C (gift from Ken Sawin) digested with NheI and NdeI. The resulting plasmid was sequenced using primers 10. This plasmid is Gateway® cloning compatible.

2.9.3 *pIY03 (pLYS1U-P_{adh15}-NLS-2xFLAG-rTetR-Gateway®)*

The construction of pIY03 is described in Fig. 2.1. This plasmid is Gateway® cloning compatible.

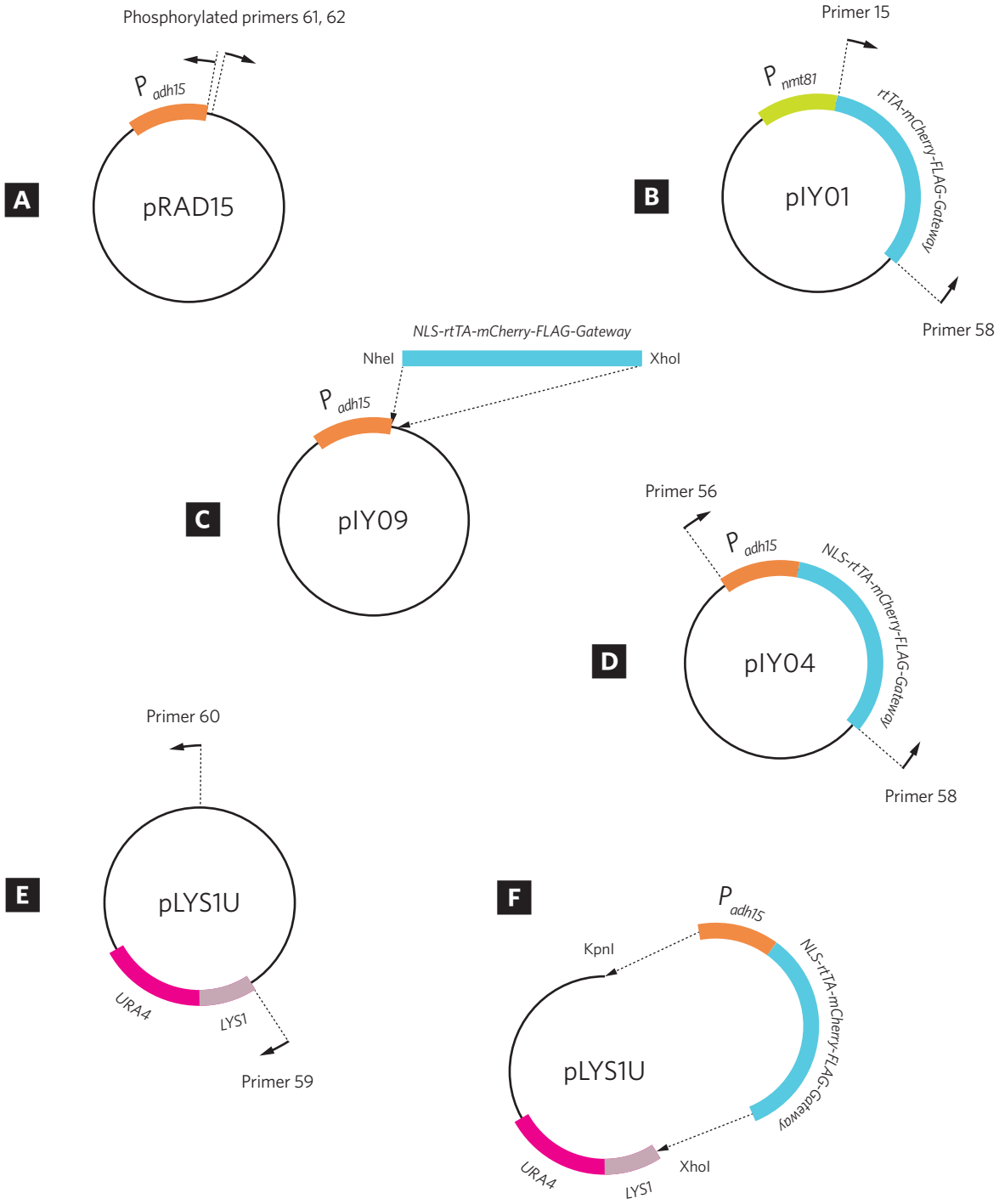

Fig. 2.1 – Engineering an improved tethering vector, pIY03. (A) pRAD15 was amplified using phosphorylated primers 61 & 62 before DpnI digestion and ligation to form pIY09. This re-created the pRAD15 vector with new NheI and XhoI restriction sites which were then used to insert a PCR fragment comprising of *NLS-rtTA-mCherry-FLAG-Gateway*® **(C)** (amplified using primers 15 and 58 from pIY01 **(B)**). pIY09 was then used as a template to PCR amplify out P_{adh15}*-NLS-rtTA-mCherry-2xFLAG-Gateway*® using primers 56 and 58 **(D)**, which was subsequently joined to a PCR fragment containing the pLYS1U backbone (primers 59 and 60) **(E)** using KpnI and XhoI to form pIY03 **(F)**. This new construct was verified by sequencing using primers 49, 50 and 51 and is Gateway® recombination compatible.

CHAPTER 3

Phosphorylation of a C-terminal Mad1 fragment is sufficient for C-Mad2 recruitment

3.1 Introduction: the usefulness of ectopic tethering systems

When studying complex signalling pathways with defined triggers such as the spindle checkpoint, a simple yet powerful approach is to separate the trigger from the rest of the signalling pathway; this often reveals important insights into how the signal is generated and propagated in both space and time. As detailed in Chapter 1, many studies of the spindle checkpoint have sought to adopt this approach and temporally separate the origin of the checkpoint signal at the kinetochores from the rest of the signalling pathway.

In human-derived cells, constitutive tethering of Mad1 to the kinetochores by fusing it with the outer kinetochore component Mis12 (part of the conserved KNL1-Mis12-Ndc80 complex) was found to constitutively localise Mad2 to the kinetochores and activate the spindle checkpoint, even after proper bi-orientation was achieved (Kuijt et al., 2014; Maldonado and Kapoor, 2011). A similar experimental setup was adopted in *S. pombe* by Ito and colleagues when Ndc80 was used as an anchor with which Mph1 kinase was constitutively tethered to kinetochores (Heinrich et al., 2012; Ito et al., 2012). This produced constitutive kinetochore localisation of Bub1 and activation of the spindle checkpoint. Although Mad1 and Mph1 normally localise to the kinetochores when the spindle checkpoint is activated, by artificially forcing the interaction these two studies have turned the kinetochores into a constitutive checkpoint signal (MCC) generator that may temporally uncouple the checkpoint trigger at the kinetochores from the rest of the checkpoint signalling pathway.

Although both of these kinetochore tethering studies yielded interesting insights into spindle checkpoint signalling, their experimental approach suffers from a serious drawback in that the fusion of kinetochore and spindle checkpoint components risks unintentionally activating the spindle checkpoint by disrupting microtubule-kinetochore interactions or by perturbing kinetochore structure itself. Maldonado and colleagues attempted to discount these possibilities by showing that their mCherry-Mis12-Mad1 construct does not affect the localisation of various spindle checkpoint and kinetochore components (Bub1, CENP-E, RZZ components &etc.) and that it is capable of supporting normal chromosome segregation when the Mad1 in the construct was replaced by a Mad1 mutant unable to bind Mad2 (Maldonado and Kapoor, 2011). However, Ito and colleagues only demonstrated that their kinetochore tethered Ndc80-Mph1 fusion generates a checkpoint-dependent arrest that is Mad2 dependent and thus presumably does not inactivate checkpoint function; no evidence ruling out checkpoint activation through disruption of kinetochore-microtubule interaction or kinetochore structure was presented (Ito et al., 2012).

An alternative method of uncoupling spindle checkpoint signalling from its kinetochore trigger is to spatially separate the site of checkpoint signalling away from the kinetochore; our lab was the first to demonstrate the usefulness of this approach by ectopically tethering the Bub1 scaffold protein to *S. pombe* telomeres; this proved sufficient to recruit the downstream partners of Bub1: Bub3 and Mad3 (Rischitor et al., 2007). A similar approach proved useful in the study of the DNA damage pathway in human-derived cells; by tethering LacI-tagged fusions of DNA damage signalling components to a chromosome arm containing LacO repeats, Bonilla and colleagues were able to spatially separate the assembly of DNA damage signalling components from the double-strand break (DSB) sites that normally serve as the trigger of the pathway (Bonilla et al., 2008).

Artificially moving the spindle checkpoint components away from the kinetochore in the way described above allows a key question of spindle checkpoint assembly to be addressed: is a high local concentration of spindle checkpoint components sufficient for checkpoint signalling? If true, then it would be expected that artificially concentrating basal spindle checkpoint components such as Mad1, Bub1, Spc7 and Mph1 at an ectopic site away from the kinetochores should be sufficient to drive kinetochore-independent assembly of MCC. If successful, this approach can be expected to produce an informative reductionist picture of the minimal requirements for spindle checkpoint signalling, both in terms of the checkpoint proteins as well as any PTMs that may also be required.

With this goal in mind, this chapter will describe how an ectopic tethering system was developed in *S. pombe* and how the system proved to be capable of artificially re-creating one of the key steps in the activation of the spindle checkpoint: the Mad1-dependent recruitment of Mad2.

3.2 Designing an ectopic tethering system in *S. pombe*

To create an effective ectopic tethering system in *S. pombe*, the proven tetracycline-controlled transcriptional activation system was adapted for use in *S. pombe*. The original tetracycline-controlled transactivator system (Gossen and Bujard, 1992) was based on a tetracycline repressor (TetR) protein derived from *E. coli* that is capable of binding to both the antibiotic tetracycline as well as a *cis*-acting 19 bp tet operator sequence (*tetO*). When TetR is fused with an activation domain, such as the virion protein 16 of herpes simplex virus (VP16), the resulting transcriptional transactivator (tTA) fusion protein is capable of driving transcription when it is bound to *tetO* sites placed near a minimal promoter of the target gene. Two versions of this system exists. Under the original system, now commonly referred to as TetOFF, the tTA fusion protein is bound to *tetO* sites and thus activates transcription in the absence of tetracycline. In the TetON system, point mutations in the TetR protein produces a reverse transcriptional transactivator (rtTA) fusion that binds to *tetO* sites only in the presence of tetracycline.

The ectopic tethering system used in this work is based on the TetON system and is comprised of two parts. The first part is the ectopic location to which tethered checkpoint proteins will be targeted, which is defined by an array consisting of 112 tandem copies (5.6 kb) of *tetO* sequence integrated at the *arg3* locus on chromosome I (2273765-2275516) (Fig. 3.1A). The location for this array was chosen to ensure that there was sufficient spatial separation between it and the centromere (3753687-3789421) as well other chromosomal features that might perturb ectopic spindle checkpoint signalling, such as telomeres. The array is marked with the G418 drug resistance (*kanR*) gene for selection.

The second part of the system is the protein to be tethered, which is expressed from a tethering vector (pIY01) based on the pDUAL plasmid (Matsuyama et al., 2004). Construction details can be found in (Section 2.9.1). The checkpoint protein to be tethered is cloned into pIY01 using Gateway® recombination, which fuses it to an N-terminal reverse TetR (rTetR) protein that enables regulated binding to the *tetO* array and (optionally) a fluorescent tag such as mCherry or GFP to enable visualisation of the tethered checkpoint protein. A double FLAG tag, also N-terminal to the tethered protein, provides a biochemical handle for co-immunoprecipitation of tethered proteins as well as a mean of detection by immunoblot. Expression of the whole construct is driven by a weak inducible **n**o **m**essage in **t**hiamine (*nmt81*) promoter (Basi et al., 1993; Maundrell, 1993).

Once the checkpoint protein to be tethered is expressed in a yeast strain containing the *tetO* array, localisation of the tethered protein is achieved through the addition of a tetracycline derivative, anhydrotetracycline (aTc) (Section 2.3.1) to the medium. Interaction between the tethered protein and fluorescently tagged downstream partners can then be visualised as co-localising fluorescent foci. Unlike the original TetOFF system, which responds to both tetracycline and its derivatives such as doxycycline and anhydrotetracycline, the TetON system only responds to the latter. Although costlier than doxycycline, anhydrotetracycline is the preferred derivative due to its lower working concentration (10 µM final).

3.3 Using ectopic tethering to examine Mad1-Mad2 interaction

As a checkpoint scaffold, the main function of Mad1 is to bind stably associated Mad2 (C-Mad2) and thus provide a template for the conversion of dynamically cycling O-Mad2 to C-Mad2 (De Antoni et al., 2005). As described in Chapter 1, *S. pombe* Mad1 is a 689 amino acid protein that can be approximately divided into five coiled coil domains. How these coiled coils contribute to the ability of Mad1 to bind Mad2 or its ability to stimulate Mad2:Mad2 dimerisation remains unclear. The Mad2 binding site on Mad1 consists of a small (~20 a/a) C-terminal stretch that lies near coiled coil 4 (Fig. 3.1B). Crystallography data from the hsMad1:hsMad2 complex suggests that the C-terminus of Mad1 folds-back onto Mad1 close to the Mad2 binding site, and this fold-back has been hypothesised to be important for the ability of Mad1 to bind Mad2 or to induce Mad2:Mad2 dimerisation (Musacchio et al., 2002). Heinrich and colleagues attempted to test this directly by mutating or deleting C-terminal portions of Mad1 that were predicted to interfere

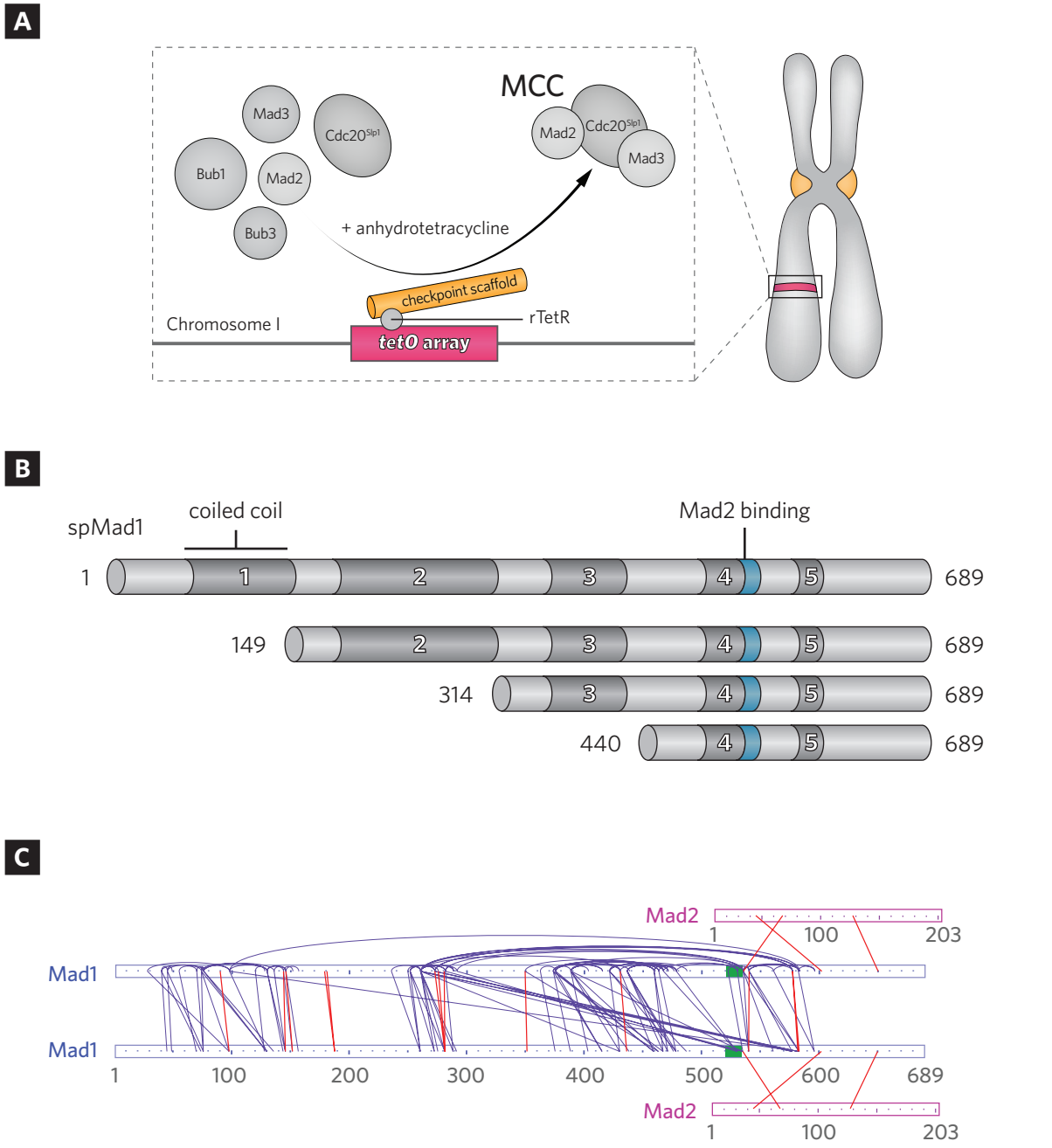

Fig. 3.1 – Ectopic tethering of Mad1 fragments. (A) Schematic of ectopic tethering system for synthetic spindle checkpoint signalling from chromosome arm. **(B)** Schematic of *S. pombe* Mad1 showing coiled coil structure and Mad2 binding site, along with N-terminal truncations based on these coiled coil domains. **(C)** Cross-linking map of *S. pombe* Mad1:C-Mad2 tetrametric complex. Purple lines denote intra- or inter-molecular cross-links. Red lines denote inter-molecular cross-links. Note long range cross-link between N and C terminus of Mad1 suggesting fold back of Mad1. Cross-linking co-immunoprecipitation performed by Sjaak van der Sar (alumni, Hardwick lab; reproduced with permission).

with its folding-back, and it was found that neither of the mutants tested exhibited perturbed Mad1-C-Mad2 or C-Mad2-O-Mad2 interaction (Heinrich et al., 2014).

This chapter sets out to examine the role of Mad1 coiled coils in both Mad1-C-Mad2 and C-Mad2-O-Mad2 complex formation in two ways. First, the coiled coils of Mad1 will be truncated from the N-terminus and the resulting Mad1 fragments will be ectopically tethered to a chromosome arm; the ability of these fragments to form Mad1-C-Mad2 complexes will be tested *in vivo* by assaying for Mad2-GFP recruitment. If Mad1-C-Mad2 complexes are visualised, then the ability of these complexes to support C-Mad2-O-Mad2 complex formation will be tested by measuring Mad2 turnover by FRAP. Second, mass spectrometry data from previous work in our lab was used to generate a series of Mad1 phospho-mutants; these will be used to examine if phosphorylation of Mad1 plays a role in regulating its interactions with Mad2 in *S. pombe*.

3.4 Mad1 coiled coils 1-3 not required for stably associated Mad2 binding

To examine whether the N-terminal coiled-coils of Mad1 are required for its ability to bind Mad2 *in vivo*, a series of N-terminal truncations of Mad1 was made (Fig. 3.1B). A GFP-tagged fragment of Mad1 with its first N-terminal coiled coil (coiled coil 1) truncated proved capable of localising to the ectopic array and forming distinct GFP foci in interphase cells (Fig. 3.2A). These GFP foci do not co-localise with an Fta3-tdT kinetochore marker, demonstrating that the GFP foci observed are not the result of Mad1 localising to kinetochores. Fta3 serves as a kinetochore marker by virtue of being a component of the Mis6 centromeric complex that associates with the kinetochore throughout the cell cycle (Liu et al., 2005).

As the cells shown in Fig. 3.2A are taken from asynchronous cultures, a small proportion of the population (~10-15 %) can be expected to be mitotic; in these cells Mad1-GFP foci are observed at both kinetochores as well as the ectopic array (data not shown). It should be noted that removal of coiled coil 1 from Mad1 also removes the ability of Mad1, and hence Mad2, to localise to the nuclear periphery during interphase (Lee et al., 2008). This explains why cells shown in Fig. 3.2A do not exhibit a distinctive 'Mad2-GFP ring' that is formed by Mad2-GFP-Mad1 complexes localised around the nuclear periphery during interphase. The loss of this Mad2-GFP ring pattern is desirable for technical reasons as GFP foci formed by tethered Mad2-GFP-Mad1 complexes near the nuclear periphery are often partially obscured by the Mad2-GFP ring.

Strikingly, the removal of coiled coils 2 and 3 from Mad1 does not impair its ability to recruit Mad2 (Fig. 3.2B). As Mad1 normally exists as a dimer, it may have been possible for tethered molecules of Mad1 to recruit Mad2 to the array by heterodimerising with endogenous molecules of Mad1; to exclude this possibility, the strains presented in Fig. 3.2B were made in a *mad1D* background. When interpreting these results it should be noted that, as detailed in Chapter 1, Mad2 exists in two structurally distinct forms: a stably associated C-Mad2 form that is bound to Mad1 and a dynamically O-Mad2 form that is free to bind Cdc20. Thus, while the images

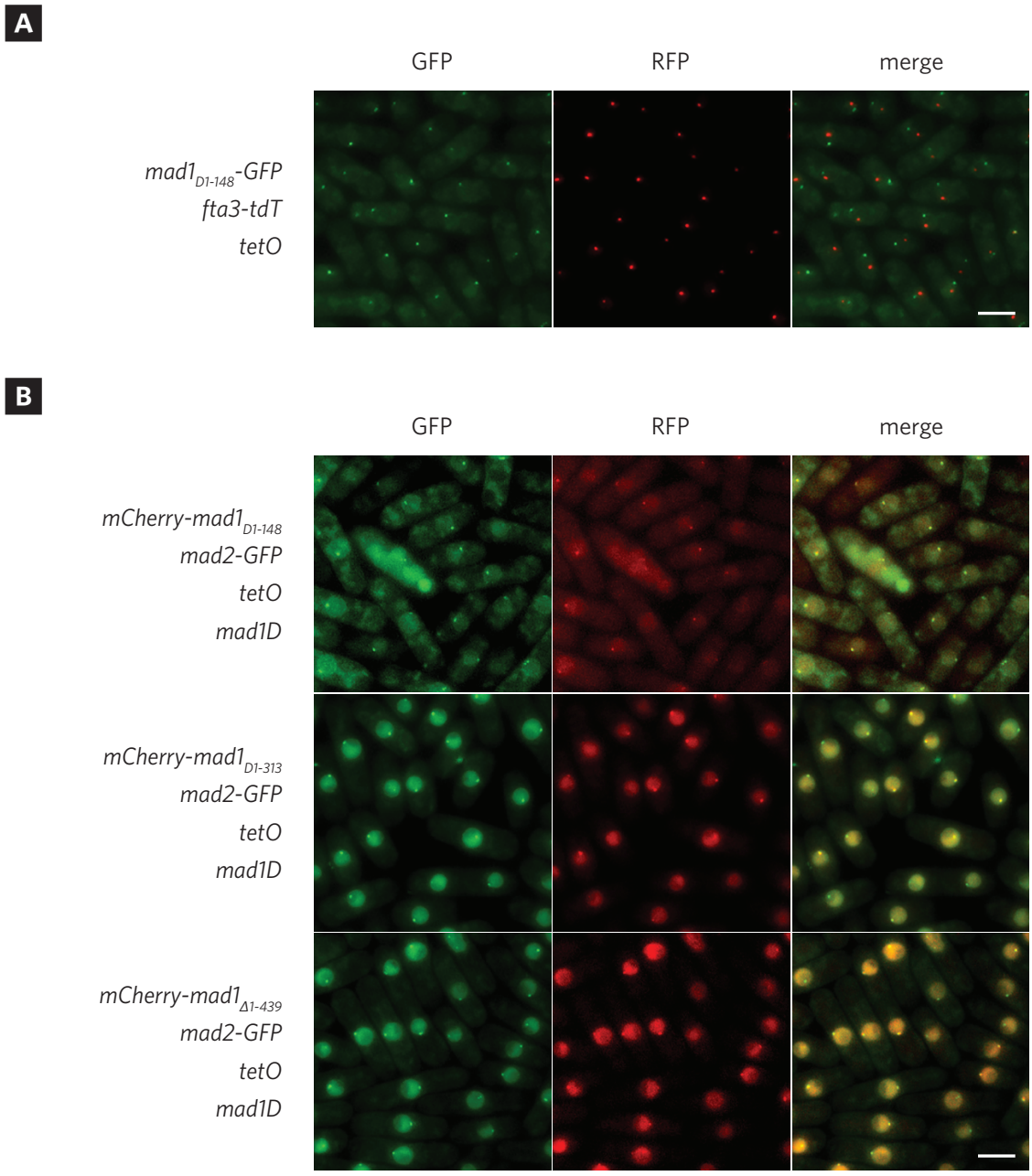

Fig. 3.2 – N-terminal coiled coils of Mad1 are dispensable for C-Mad2 recruitment. (A) Ectopically tethered Mad1$_{\Delta 1\text{-}148}$-GFP fragment does not localise to kinetochores. A Mad1$_{\Delta 1\text{-}148}$ fragment lacking the first N-terminal coiled coil was GFP-tagged and tethered to a *tetO* array on a chromosome arm (green). fta3-tdT: kinetochore marker (red). (B) Ectopically tethered Mad1 fragments capable of recruiting C-Mad2. Mad2-GFP forms co-localising foci in interphasic cells expressing ectopically tethered Mad1 fragments tagged with mCherry. Scale-bar represents 5 microns.

presented here demonstrate that the first three N-terminal coiled coils of Mad1 are dispensable for its ability to ectopically recruit the stably associated form of Mad2 (C-Mad2), FRAP experiments would be required before the impact of these coiled coils on the ability of Mad1 to recruit dynamic O-Mad2 can be assessed. This forms the subject of the subsequent section (Section 3.5).

More importantly, tethering of these Mad1 truncations was not sufficient to activate the spindle checkpoint, as evidenced from the morphology and viability of the strains imaged after the induction of *nmt* promoter driving Mad1 expression. This agrees with other studies where Mad1 tethering to chromosome arms was found to be unable to activate the checkpoint, and suggests that the co-localisation of other checkpoint components is required for checkpoint activation.

3.5 Ectopically recruited Mad2 is more dynamic than tethered Mad1$_{\Delta 1\text{-}148}$

To determine if the N-terminal coiled coils of Mad1 are required for its ability to recruit dynamically cycling Mad2 (O-Mad2), the dynamics of ectopically tethered Mad1$_{\Delta 1\text{-}148}$ and that of Mad2 being recruited by this fragment of Mad1 were measured by FRAP. It was necessary to first determine the dynamics of tethered Mad1 before Mad2 dynamics could be considered because although kinetochore-bound Mad1 is known to be highly stable, this could not be assumed to be the case for ectopically tethered Mad1, which may be isolated from kinetochore-specific factors that may affect its dynamics, such as phosphorylation by kinetochore-bound Mph1 kinase. Unfortunately, full-length Mad1 proved technically impossible to FRAP reliably due to low signal to noise ratios and the difficulty associated with trying to identifying Mad2-GFP foci that were not at least partly obscured by the ring of Mad2-GFP around the nuclear periphery (see above). Nevertheless, ectopically tethered Mad1$_{\Delta 1\text{-}148}$-GFP was found to have a low rate of turnover and recovery (Fig. 3.3B, half-time: 125 ± 33s, recovery = 43 ± 12 %, n = 5) compared to the Mad2-GFP recruited by Mad1$_{\Delta 1\text{-}148}$ (Fig. 3.3C, half-time: 87 ± 33s, recovery = 88 ± 20 %, n = 6), suggesting that Mad1$_{\Delta 1\text{-}148}$ is more stable associated at the ectopic site than Mad2, as expected.

Published Mad1 and Mad2 dynamics vary considerably depending on the experimental setup and interpretation applied. For Mad1, *in vivo* data from higher eukaryotes including *Drosophila*, PtK2 and HeLa cells present a wide range of recovery levels for Mad1 (10 – 45 %) at unattached kinetochores, with more recent studies suggesting that vertebrate Mad1 may be more dynamic than previously envisaged (Défachelles et al., 2015; Howell et al., 2004; Matson and Stukenberg, 2014; Shah et al., 2004). The differences in methodology between these higher eukaryotic studies and the present work limit the meaningfulness of direct comparisons of FRAP parameters; indeed, the level of variation within the higher eukaryotic data limits even the meaningfulness of direct comparisons within these model systems. More importantly, the recovery level of tethered Mad1$_{\Delta 1\text{-}148}$ obtained here (43 ± 12 %) agrees with unpublished data from our lab of full length Mad1 dynamics measured at *S. pombe* kinetochores in strains arrested using

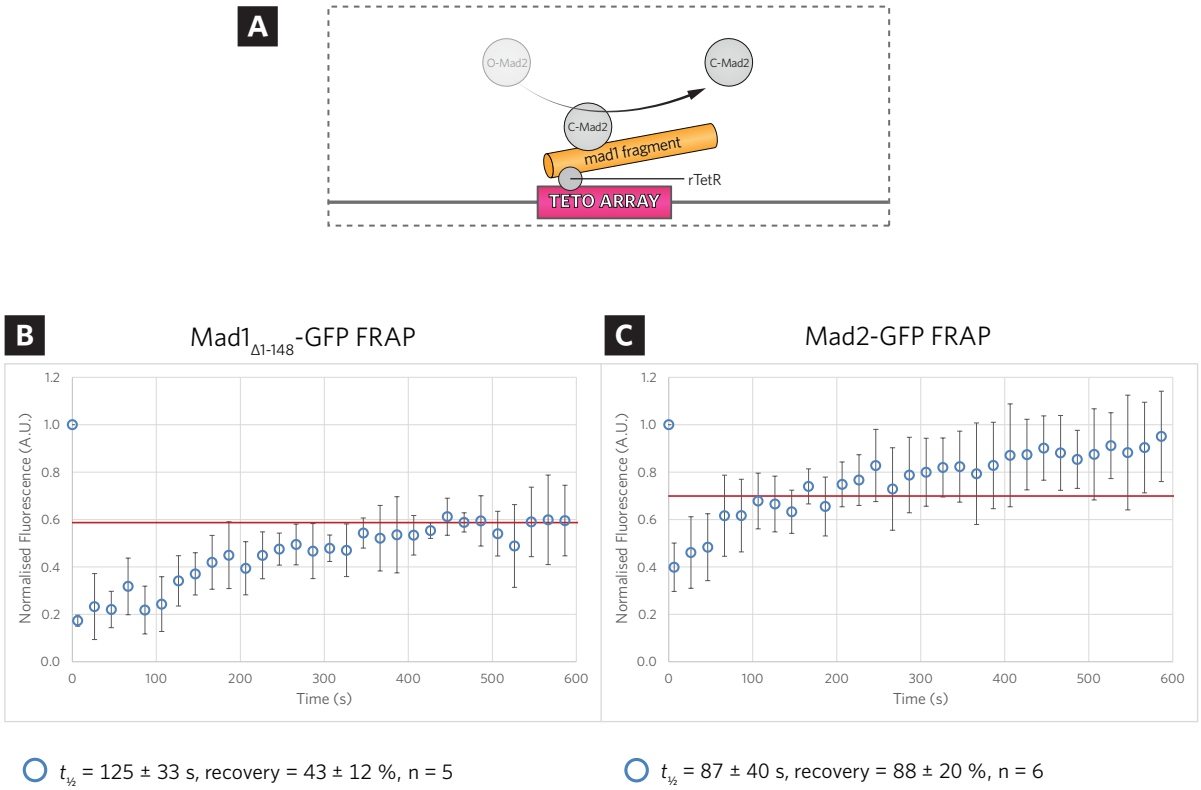

Fig. 3.3 – C-Mad2 more dynamic than tethered Mad1$_{\Delta 1\text{-}148}$ at ectopic array. (A) Schematic of Mad2 cycling on tethered Mad1$_{\Delta 1\text{-}148}$. **(B)** FRAP of Mad1$_{\Delta 1\text{-}148}$-GFP. GFP foci formed by Mad1$_{\Delta 1\text{-}148}$ tethered to ectopic array was photobleached with a laser, and images captured at the specified intervals throughout the recovery period. The % fluorescence recovery and half-times shown are the mean of the indicated number of experiments. Error bars indicate standard deviation. The red line indicates the 50 % post-bleach recovery level. **(C)** FRAP of Mad2-GFP recruited by tethered Mad1$_{\Delta 1\text{-}148}$. GFP foci formed by Mad2-GFP recruited by tethered Mad1$_{\Delta 1\text{-}148}$-mCherry was subjected to FRAP as described for **(B)** above. For full FRAP methods, see Section 2.3.3.

the cold-sensitive *nda3* mutation (recovery = 54 ± 13 %; Karen May, personal communication, cited with permission).

Regarding the half-life of Mad1, several of the above studies argue that Mad1 exhibits a bi-phasic recovery with an initially fast recovery phase (half-time: 12 – 18 s) followed by a much slower recovery phase (half-time: 15 – 145 min.). Whether Mad1 does in fact exhibit a bi-phasic recovery in all the examples cited in these studies is debatable; careful examination of the recovery profiles presented by Matson and Stukenberg (Fig. 2D, control curve; Matson and Stukenberg, 2014) and Howell et al. (Fig. 3; Howell et al., 2004) shows that, during the period after Mad1 recovery reaches its plateau, there is negligible recovery and thus measurements made during this period are arguably meaningless. This would however explain some of the unusually long Mad1 half-times reported by these studies (up to 145 min.). Nevertheless, these studies together present a picture where a relatively small pool of Mad1 turns over rapidly whilst the bulk of Mad1 remains stably associated with the unattached kinetochores.

Contrary to these studies, the $Mad1_{\Delta 1\text{-}148}$ recovery profile presented here is not indicative of a bi-phasic recovery, as $Mad1_{\Delta 1\text{-}148}$-GFP levels reach their peak in a gradual manner. This difference in recovery profile and half-time may be due to (i) the truncation of first N-terminal coiled coil of Mad1, (ii) the absence of kinetochore-specific post-translational modifications on ectopically tethered $Mad1_{\Delta 1\text{-}148}$, or (iii) methodological differences. These possibilities form important questions for the future. The first possibility will be addressed by using an improved tethering vector, described later in Chapter 4, which should improve the signal to noise ratio of tethered full-length Mad1, whilst the second question will be addressed analysis of Mad1 phosphomutants in the following section (Section 3.6). It should be noted here before this data can be usefully interpreted it will be essential to measure tetR turnover rates at the ectopic array; without correcting for this turnover it will be impossible to know what proportion of the observed GFP dynamics are attributable to modifications of Mad1, and what portion is attributable simply to tetR turnover.

It is perhaps for these same reasons that the half-time of Mad2 recruited by tethered $Mad1_{\Delta 1\text{-}148}$ (Fig. 3.2C, half-time: 87 s) differs from the published vertebrate data (half-time: 1.7 – 26 s) (Vink et al., 2006). Published Mad2 recovery levels from both *in vitro* and *in vivo* studies agree that because the Mad1-C-Mad2 interaction is highly stable and thus photobleached Mad2 molecules in this Mad1-bound pool do not recover during the course of a typical FRAP experiment, approximately half of the Mad2 population can be expected to recover in experimental setups where Mad1 is immobilised and soluble Mad2 is provided either by transient transfection or direct injection (Howell et al., 2000; Shah et al., 2004). In contrast, when the Mad2 present in the Mad1-C-Mad2 complex is allowed to exchange, higher Mad2 recovery rates close to 100 % were observed (Howell et al., 2004). The same would be expected if a certain proportion of the Mad1 population were to turn over, and the high Mad2 recovery rate (88 %) obtained is likely a direct result of the higher than expected turnover of $Mad1_{\Delta 1\text{-}148}$ described earlier.

3.6 Phosphorylation of Mad1 C-terminus crucial for C-Mad2 binding

To determine if phosphorylation of Mad1 played a role in regulating Mad2 interactions in *S. pombe*, two set of alanine (non-phosphorylatable) substitutions were made in Mad1 based on mass spectrometry data. These were named according to the number of alanine substitutions that they contained and the approximate location of these mutations: *mad1-M6A*, which contains six substitutions in the middle region of Mad1, and *mad-C8A*, which contains eight substitutions near the C-terminus of Mad1. A summary of these mutations is shown in Fig. 3.4A. Both of these mutant strains were also C-terminally tagged with GFP to enable them to be used with microscopic and biochemical assays.

To assess if these substitutions affect spindle checkpoint function, *mad1-C6A-GFP* and *mad1-C8A-GFP* mutants were first subjected to the microtubule depolymerising drug benomyl. As shown in Fig. 3.4B, the *mad1-C8A-GFP* mutant exhibits a strong sensitivity to benomyl, suggesting that it may be checkpoint deficient, whilst the *mad1-M6A-GFP* mutant appeared unaffected by benomyl. To determine if the benomyl sensitivity of the *mad1-C8A-GFP* mutant corresponded to a specific checkpoint defect, the ability of *mad1-C8A-GFP* to bind C-Mad2 was tested. Strikingly, the ability of the *mad1-C8A-GFP* mutant to co-immunoprecipitate with Mad2 is greatly diminished compared to Mad1-GFP, whilst the *mad1-M6A-GFP* mutant is undiminished in its Mad2 binding ability (Fig. 3.4C). It should be noted here that only the stably associated form of Mad2 (C-Mad2) is detectable by co-immunoprecipitation; the interaction between O-Mad2 and the Mad1-C-Mad2 complex is likely too weak to be preserved during the co-immunoprecipitation process. Taken together, these results suggest that phosphorylation of Mad1 along its C-terminus is likely essential for its ability to form the stable Mad1-C-Mad2 scaffold and presumably its ability to activate the spindle checkpoint.

These results form the basis of ongoing work. The strong benomyl sensitivity exhibited by the *mad1-C8A-GFP* mutant combined with its inability to co-immunoprecipitate Mad2 point to a checkpoint activation defect that will be tested by assessing its ability to arrest in the cold-sensitive microtubule-depolymerising *nda3* background. Ectopic tethering of mad1-C8A and assaying of its ability to ectopically recruit Mad2 will provide important *in vivo* confirmation of the loss of Mad2 binding ability described above. In addition, the creation of a phosphomimetic *mad1-C8E-GFP* mutant that may exhibit stronger/constitutive Mad2 binding should provide further confirmation of the importance of these sites.

It is unlikely that all eight residues mutated in the *mad1-C8A-GFP* mutant contribute equally to the observed phenotype, and thus a new mutant containing only two of these two substitutions, *mad1-C2A-GFP*, has been created in an attempt to narrow down the most important residues. The *mad1-C2A-GFP* mutant does not exhibit sensitivity to benomyl (Fig. 3.4B), and is yet diminished in its ability to co-immunoprecipitate with Mad2 (Fig. 3.4C), albeit not to the same extent as the *mad1-C8A-GFP* mutant.

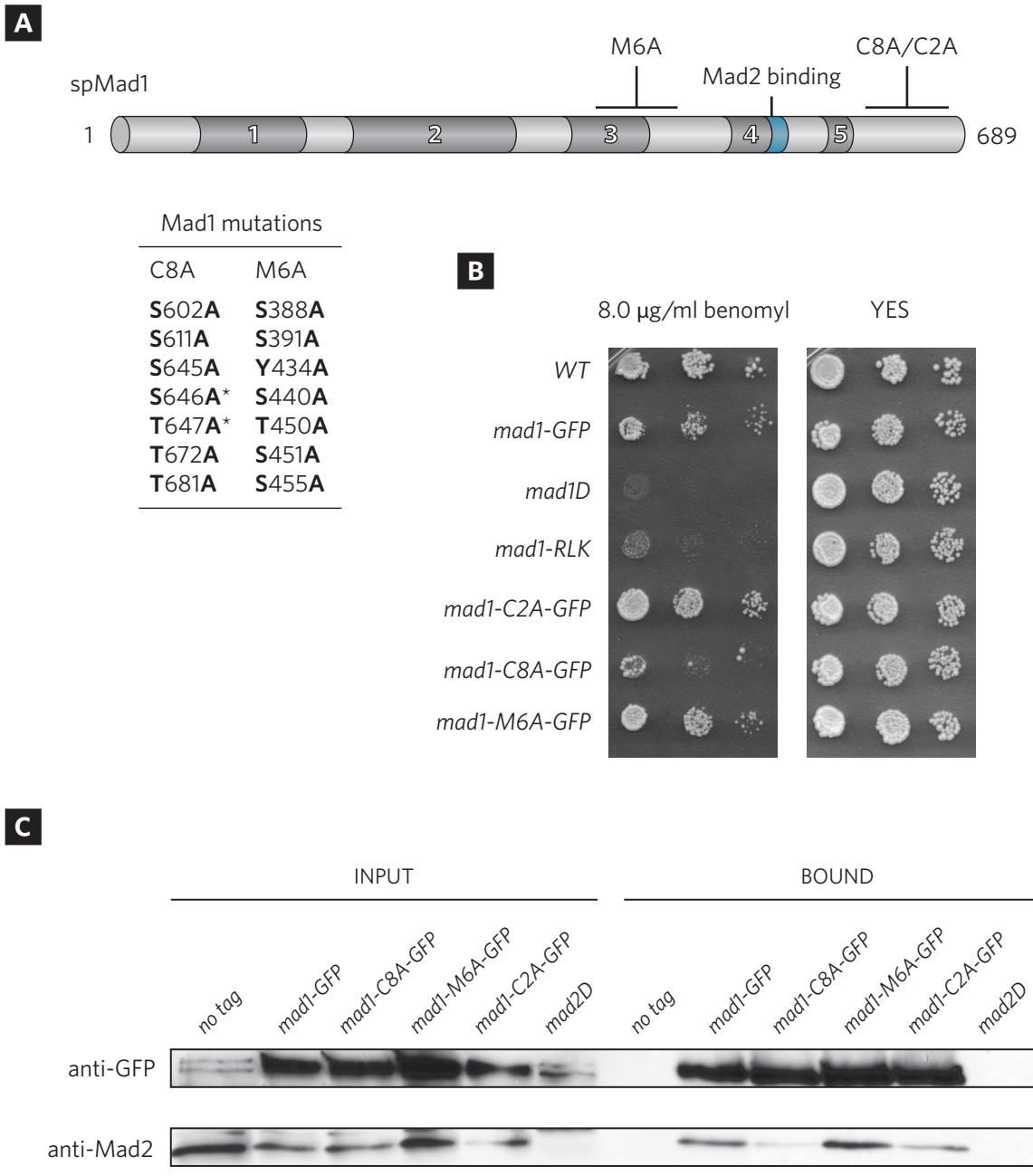

Fig. 3.4 – Phosphorylation of Mad1 C-terminus crucial for C-Mad2 binding. (A) List of predicted Mad1 phosphorylation sites mutated to alanine **(A)** and their relative positions on Mad1. All mutants were C-terminally tagged with GFP. Note that *mad1-C2A-GFP* is a subset of *mad1-C8A-GFP*, with the relevant residues indicated with an asterisk (*). **(B)** Mad1 C-terminal phosphomutants (*mad1-C8A-GFP* and *mad1-C2A-GFP*) exhibit benomyl sensitivity indicative of spindle checkpoint defect. Serial dilutions of each strain was plated on 8.0 µg/ml benomyl and YES plates as indicated. **(C)** *mad1-C8A-GFP* and *mad1-C2A-GFP* defective in C-Mad2 binding. Extracts from asynchronous cultures of the indicated strains were co-immunoprecipitated using anti-GFP.

The reduced ability of the *mad1-C2A-GFP* mutant to bind stably associated Mad2 without exhibiting any obvious benomyl sensitivity can be understood in light of the work of Heinrich and colleagues (Heinrich et al., 2012) showing that at least in *S. pombe*, Mad2 is a highly abundant checkpoint component that can still mediate a robust checkpoint response even when its levels are reduced by up to 35 %. Moreover, benomyl sensitivity is a crude assay of spindle checkpoint activity that does not always detect subtle checkpoint defects. Thus, the absence of benomyl sensitivity shown by the *mad1-M6A-GFP* mutant, or even indeed its inability to co-immunoprecipitate with Mad2 does not preclude the presence of a subtle checkpoint defect; such a defect may be mediated by reduced, but not abolished, ability to recruit dynamically cycling Mad2. To detect such subtle checkpoint defects, the ability of the *mad1-M6A-GFP* and *mad1-C2A-GFP* mutant to arrest in a *nuf2-3* background will be tested. *nuf2-3* is a temperature-sensitive allele of the gene encoding the conserved centromeric protein Nuf2 (Nabetani et al., 2001); upon shifting to the restrictive temperature, *nuf2-3* strains arrest in a checkpoint-dependent manner with the spindle intact. Compared to the cold-sensitive *nda3-KM311* allele in which microtubules are completed depolymerised upon shifting to the restrictive temperature, the *nuf2-3* allele often allows identification of more subtle checkpoint defects. Should a subtle checkpoint phenotype be detected in these strains, any potential defects in Mad2 cycling dynamics will be assessed by FRAP of tethered mad1-M6A-GFP/mad1-C2A-GFP.

3.7 Conclusions and perspectives

This chapter demonstrated the usefulness of an *in vivo* ectopic tethering assay as a way of complementing biochemical approaches in the investigation of complex interactions within the spindle checkpoint. This is most easily appreciated when one considers the problems associated with alternative *in vivo* approaches to addressing the central question of this chapter i.e. the function of the N-terminal coiled coils of Mad1. One such approach would have been to replace endogenous Mad1 with N-terminally truncated fragments and then assay for C-Mad2 binding using a Mad2-GFP reporter. While seemingly obvious, this approach is fraught with technical risks. Truncation of the first coiled coil of Mad1 would abolish its nuclear periphery localisation, meaning that Mad1-C-Mad2-GFP complexes would only be expected to be observable during a checkpoint-induced metaphase arrest, when they would presumably appear as GFP foci on the kinetochores. Although checkpoint arrest could be achieved using a variety of mutant backgrounds such as *nda3*, if truncation of any of the coiled coils of Mad1 were to inactivate the checkpoint, then it be impossible to determine whether the loss of Mad1 coiled coils disrupted Mad2 interaction, or indeed if this was the cause of checkpoint inactivation. By contrast, ectopically tethered Mad1 truncations allow its interactions with Mad2 to be easily visualised completely independently of the ability to these truncation to support checkpoint function. Moreover, investigating the effects of Mad1 truncations on Mad2 cycling dynamics without ectopically tethering Mad1 would have required performing FRAP on Mad1-C-Mad2 complexes

at unattached kinetochores, which is technically challenging due to the propensity of kinetochores to move during imaging.

In summary, this chapter has shown that a minimal fragment of Mad1 lacking all but the last two coiled coil domains is sufficient to recruit stably associated C-Mad2, and that this binding is likely dependent on the phosphorylation of key sites along the C-terminus of Mad1. Whether the N-terminal coiled coils of Mad1 or the phosphorylation of its C-terminus are required for the recruitment of dynamically cycling Mad2 remains important work for the future. More importantly, the ectopic tethering of Mad1 here has reproduced previous findings that ectopic localisation of Mad1 away from the kinetochores is by itself is insufficient to activate the checkpoint (Maldonado and Kapoor, 2011), and that the combinatorial action of Mad1 and Bub1 scaffolds is likely required for checkpoint activation. This will be tested in the following chapter. Finally, the work presented thus far has shown that, on a technical level, the ectopically tethering system has scope for improvement and expansion to enable more complex and interesting tethering experiments to be done. These improvements are described at the beginning of the following chapter.

CHAPTER 4

Phosphomimetic Spc7$_{1-666}$-9TE is sufficient to recruit Bub1, Bub3 and Mad3 in a manner comparable to that at endogenous kinetochores

4.1 Introduction

The preceding chapter described the usefulness of a simple ectopic tethering system in studying one of the most well characterised interactions in the spindle checkpoint, that between Mad1 and Mad2. More importantly, it identified aspects of the system that could be improved upon; in this chapter the ectopic tethering construct is re-engineered to determine if the tethering system can be expanded upon to faithfully reproduce a much more complex set of interactions in the checkpoint signalling pathway, that between the core kinetochore protein Spc7 and its downstream partners, Bub3, Bub1 and Mad3. More importantly, whether ectopic recruitment of these checkpoint component is sufficient to ectopically generate MCC will be tested.

4.2 Interplay between Bub3, Bub1, Mad3/BUBR1 and Spc7/KNL1

As demonstrated in Chapter 3, the ectopic tethering assay provides a simple and highly flexible way of investigating interactions between the Spc7-Bub3-Bub1 complex and Mad3. Moreover, an ectopic MCC generator will almost certainly require the recruitment of Mad3 to the array via some arrangement of Spc7/Bub1/Bub3 – would this be sufficient to generate a strong enough checkpoint signal to trigger metaphase arrest, or will co-tethering with Mad1/Mad2, as described in the preceding chapter, also be required?

Thus, this chapter sets out to determine the following:

1. Whether Spc7 can be exploited in a tethering system to recruit the Bub1 scaffold protein in a Bub3-dependent manner;
2. If the above is true, then whether the recruitment of Bub1 and Bub3 is also sufficient to recruit Mad3, a critical component of the MCC;
3. Whether Mph1 kinase activity be required for any of the above interactions;
4. If Mad3 recruitment to the tether was observed, whether it would exhibit the dynamic cycling behaviour that is observed at endogenous kinetochores and which is likely essential for its ability to form MCC;
5. Finally, whether tethered Spc7 would be sufficient for checkpoint arrest.

4.3 Selecting the right fragment of Spc7 to tether

In order to address the question of whether Spc7 could be used to recruit Bub1 in a Bub3-dependent manner, the fragment of Spc7 to be tethered must contain two important features. First, it must incorporate the nine threonine (T) to glutamic acid (E) substitutions along the

MELT motifs that mimic phosphorylation by Mph1 required for Bub1 binding. This is because the phosphorylation of Spc7 along its MELT motifs required co-localised Mph1 (Shepperd et al., 2012). Second, it is important that the tethered Spc7 fragment is unable to localise to kinetochores, so as not to leave it in a 'tug-of-war' with conflicting localisation signals targeting it to both the *tetO* array and the kinetochores. This would likely partition the intracellular pool of tether-able Spc7 into at least three pools (kinetochore-bound, array-bound and unbound), thus making it difficult to attribute any observed phenotypes to the ectopic array.

With these requirements in mind, an N-terminal fragment of Spc7, $Spc7_{1\text{-}666}$-9TE, was used as the tethered fragment of Spc7 (Fig. 4.1A). This fragment has previous been shown to be capable of co-immunoprecipitating with Bub1 in yeast extracts (Shepperd et al., 2012). As the figure shows, this mutant of Spc7 contains the key phosphomimetic MELT motifs whilst lacking the C-terminal kinetochore localisation domain, thus making it an ideal Spc7 fragment for ectopic tethering. However, initial attempts to tether $Spc7_{1\text{-}666}$-9TE using the same tethering construct used previously in Chapter 3 (pIY01) resulted in low levels of Spc7 expression that were difficult to detect by fluorescence microscopy, making it impossible to reliably assay for ectopic Bub1-GFP and Bub3-GFP recruitment (data not shown). Together with the technical limitations encountered in Chapter 3 when examining Mad1-Mad2 interactions, it became clear that improvements to the tethering assay would first be required before Spc7-Bub3-Bub1-Mad3 interactions could be studied.

4.4 Re-engineering the tethering construct

Work done using the ectopic tethering assay described in Chapter 3 identified four aspects of the tethering system with scope for improvement.

First, the inducible *nmt81* promoter driving the expression of the tethered protein produced variable levels of expression between individual cells, and while this was not problematic when addressing simple questions such as whether Mad1 fragments could interact with stably-associated Mad2, it did present a problem when cycling dynamics were investigated using FRAP assays that are highly sensitive to cell-to-cell variability in fluorescence levels.

Second, whilst the *nmt81* promoter provided sufficient levels of Mad1 expression for the visualisation of both Mad1 itself at the ectopic array (via the mCherry tag) as well as its recruitment of Mad2-GFP, it cannot be assumed that this level of expression would be sufficient for other tethered proteins, such as Spc7, to recruit their downstream signalling partners.

Third, the tethering construct produced fusion proteins that lacked an artificial NLS, thus relying on the presence and function of endogenous NLS sequences on the tethered protein. Although the truncations of the Mad1 protein described thus far have not caused deficiencies in the nuclear localisation of Mad1, the same assumption cannot reliably be made of other checkpoint proteins.

Lastly, the number of tether-able checkpoint proteins that can be expressed at any given time was limited to one, given that the tethering construct relied on the pDUAL plasmid backbone for integration into the yeast genome at the *LEU1* locus. Whilst this is not a limitation of the system *per se*, additional loci from which tether-able constructs could be expressed would be required before multiple checkpoint components could be tethered together simultaneously.

These four limitations were overcome by almost completely re-engineering the tethering constructs to generate pIY03 (pLYS1U-Padh15-NLS-2xFLAG-rtTA-mCherry-Gateway®). This plasmid makes use of the pLYS1U plasmid backbone (Matsuyama et al., 2008) and has the following advantages compared to pIY01:

1. Constitutive, stable protein expression, provided by the P_{adh15} promoter cloned from plasmid pRAD15 (gift from Y. Watanabe). A comparison of the relative expression levels of this promoter with an *nmt41* promoter can be found in Figure 4.1B);
2. An artificial NLS derived from SV40;
3. Integration into the *S. pombe* genome at the *LYS1* locus, thus freeing up the *LEU1* locus for the integration of another tethering construct. This allows for the combined tethering of multiple checkpoint components.

A detailed description of re-engineered tethering construct, pIY03, can be found in Chapter 2. Once s*pc7$_{1\text{-}666}$-9TE* was cloned into pIY03 by Gateway®-mediated recombination, testing showed that unlike previous attempts using pIY01, the resulting fusion protein could be successfully targeted to the ectopic array, forming bright RFP foci that do not co-localise with an Fta3-GFP kinetochore marker (Fig. 4.1C).

4.5 Ectopically tethered Spc7$_{1\text{-}666}$-9TE is sufficient to recruit a stably associated form of Mad3 independently of Mph1 kinase

Having created a functional Spc7$_{1\text{-}666}$-9TE tether, it was decided to first examine the effect that tethered Spc7$_{1\text{-}666}$-9TE would have on the cell-cycle dependent localisation of Bub1 and Bub3. Ectopically tethered Spc7$_{1\text{-}666}$-9TE was found to be sufficient to recruit both C-terminally GFP-tagged Bub1 and Bub3 fusions (expressed under their own promoters) to the ectopic array in interphase cells (Fig. 4.2A). The activity of endogenous Mph1 kinase activity is not required for this ectopic recruitment, as *mph1Δ spc7$_{1\text{-}666}$-9TE* strains continue to exhibit co-localising Spc7$_{1\text{-}666}$-9TE and Bub1-GFP/Bub3-GFP foci (Fig. 4.2B). This confirms previous findings that phosphorylation of the MELTs of Spc7 is the sole requirement for Bub3-Bub1 recruitment. Importantly, tethered Spc7$_{1\text{-}666}$-9TE was also found to be sufficient to ectopically recruit Mad3-GFP in an *mph1Δ* background (Fig. 4.2B), showing that phosphorylation of Bub3 and Bub1 is not required for Mad3 recruitment to unattached kinetochores. However, although Mad3 can be recruited by ectopically tethered Spc7$_{1\text{-}666}$-9TE, this strain does not exhibit the morphological changes or the decrease in viability associated with prolonged activation of the spindle checkpoint

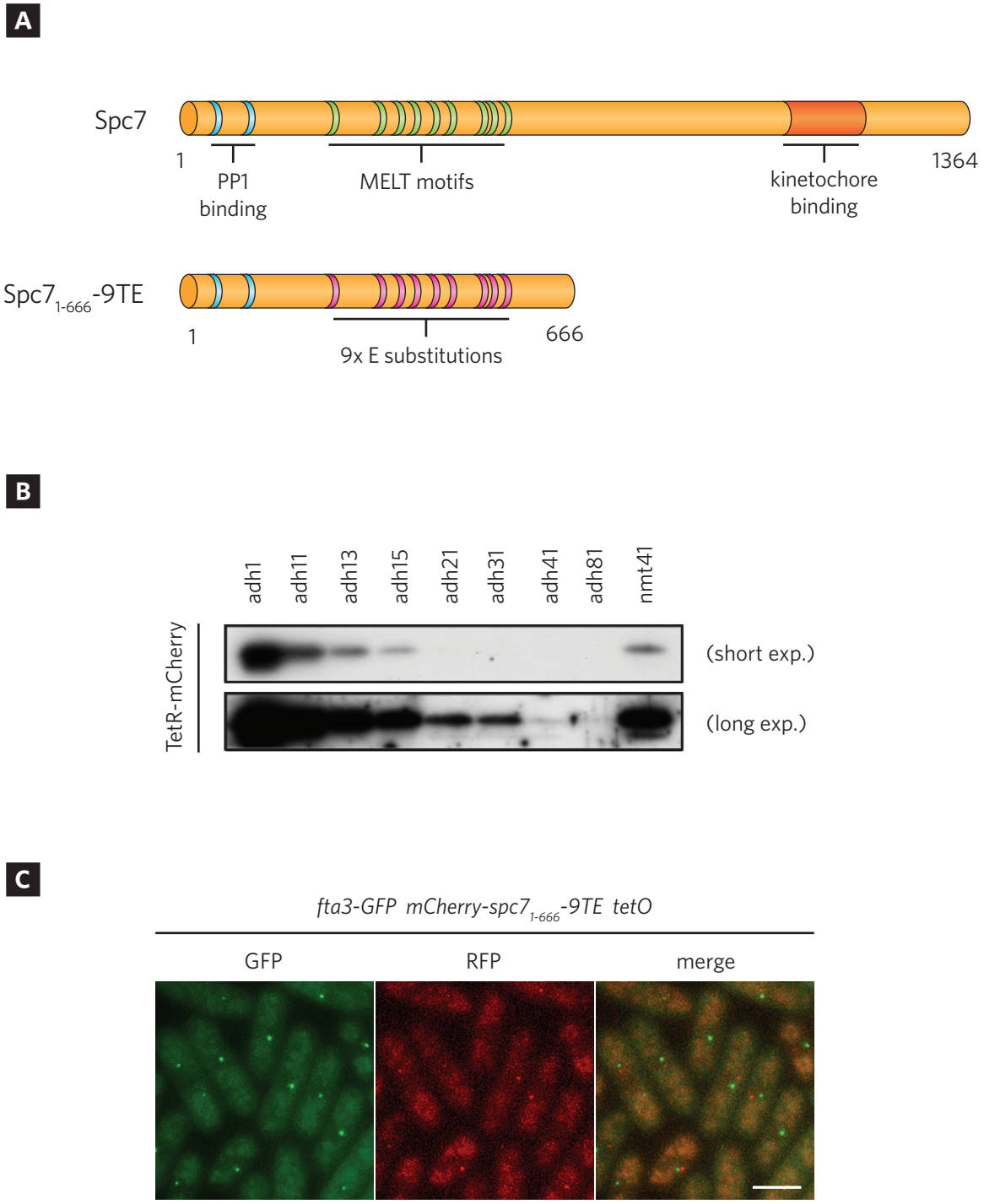

Fig. 4.1 – Spc7$_{1\text{-}666}$-9TE as an ectopic anchor for Bub3, Bub3 and Mad3. (A) Schematic of Spc7$_{1\text{-}666}$-9TE showing its nine phosphomimetic (E) substitutions and its truncation of the C-terminal kinetochore localisation domain. **(B)** Expression levels of the P$_{adh}$ series of constutitive promoters compared to inducible intermediate strength P_{nmt41} promoter. **(C)** Ectopically tethered Spc7$_{1\text{-}666}$-9TE does not localise to kinetochores. Tethered Spc7$_{1\text{-}666}$-9TE-mCherry (red) does not co-localise with a GFP-tagged kinetochore marker, Fta3. Scale bar represents 5 microns. Diagrams not to scale.

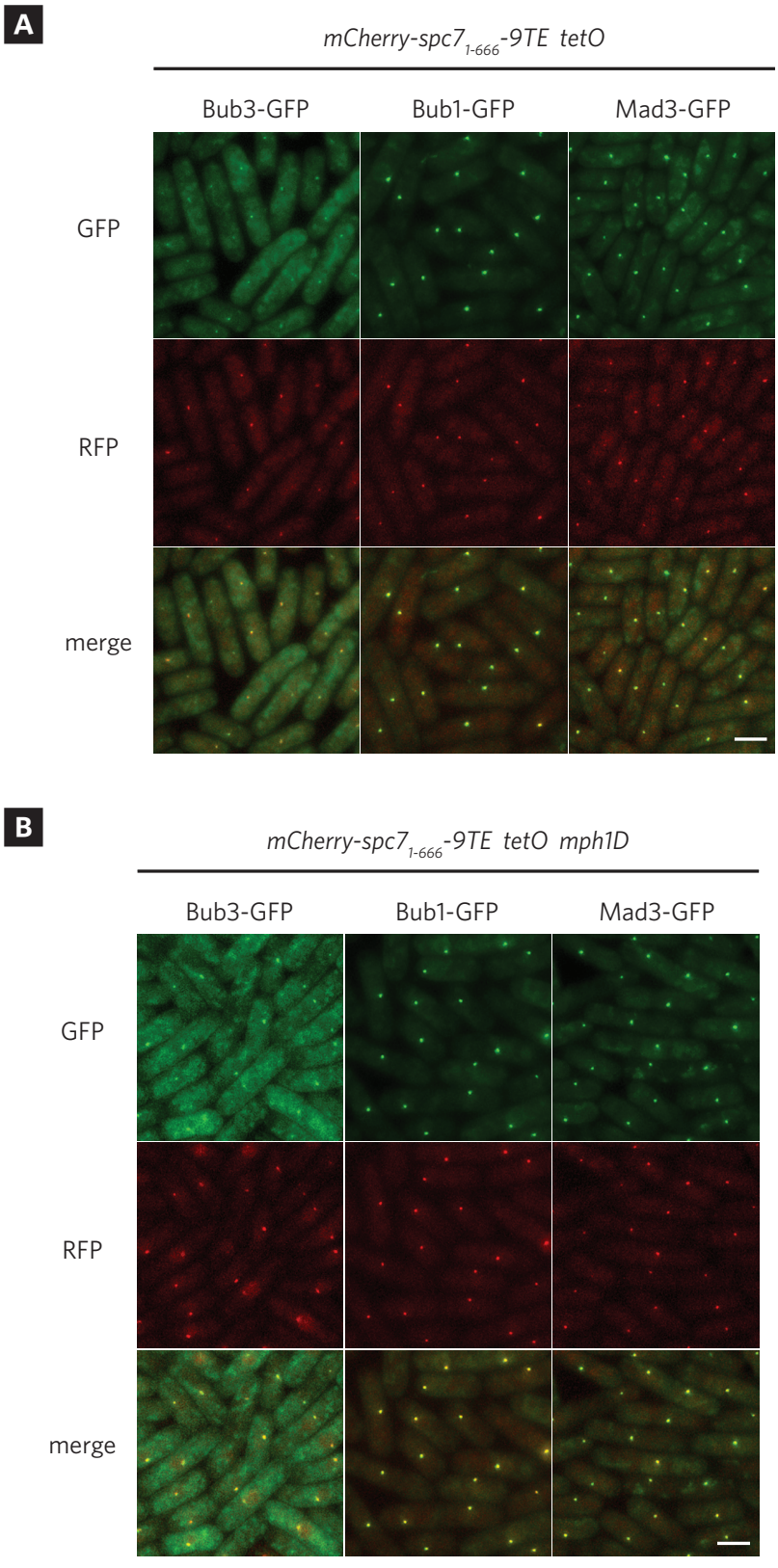

Fig. 4.2 – Ectopically tethered Spc7$_{1\text{-}666}$-9TE is sufficient to recruit Bub3, Bub1 and Mad3 independently of Mph1 kinase. (A) Tethered Spc7$_{1\text{-}666}$-9TE (red) forms co-localising ectopic foci in interphase cells with Bub3-GFP, Bub1-GFP and Mad3-GFP (green). **(B)** Co-localisation between tethered Spc7$_{1\text{-}666}$-9TE (red) and Bub3-GFP, Bub1-GFP and Mad3-GFP persists in strains with an *mph1Δ* background. Scale bar represents 5 microns.

(not shown), showing that the Spc7$_{1-666}$-9TE-Bub3-Bub1-Mad3 complex is not sufficient to activate the spindle checkpoint by itself.

4.6 Ectopically tethered Spc7$_{1-666}$-9TE recruits Mad3 in a manner similar to that at unattached kinetochores

The inability of ectopically tethered Spc7$_{1-666}$-9TE to generate a checkpoint arrest in spite of being capable of Mad3 recruitment suggested two possibilities: (i) co-localisation of at least one other spindle checkpoint component, perhaps Mad2, is required for active signalling, or (ii) the mechanism of Mad3 recruitment at the ectopic array, and hence its ability to form active MCC, is different from that at unattached kinetochores. For example, if ectopic recruitment of Mad3 occurred via an unknown Bub1-independent pathway, perhaps by direct interaction with tethered Spc7$_{1-666}$-9TE, or if ectopically recruited Mad3 exhibited very different dynamics to that at unattached kinetochores, then it may well be dysfunctional in its ability to form MCC. To determine if this was the case, the dependencies between Mad3, Bub3 and Bub1 were first examined. Ectopic co-localisation of Mad3 with tethered Spc7$_{1-666}$-9TE was lost upon deletion of either Bub1 or Bub3 (Fig. 4.3), demonstrating that the ectopic recruitment of Mad3 occurs in the same Bub1-Bub3 dependent manner as at the kinetochores.

It was then decided to examine the dynamics of Bub1 and Mad3 at the ectopic array. Bub1 and Mad3 exhibit very different dynamics at unattached kinetochores that are reflective of their different roles within the spindle checkpoint; whereas Bub1 is a stably associated component, hence its role as a scaffold protein, Mad3 cycles very dynamically on unattached kinetochores (Howell et al., 2004; Rischitor et al., 2007). Thus if ectopically recruited Bub1 and Mad3 exhibit very different dynamics to that at unattached kinetochores, then once again this may adversely affect their ability to generate active MCC at the *tetO* array. To determine if this was the case, FRAP was used to measure the dynamics of both Bub1-GFP and Mad3-GFP at the *tetO* array (Fig. 4.4B). Analysis of the recovery profiles (for methodology see Section 2.3.3) showed that Bub1-GFP exhibited a recovery of 44 ± 16 % (n = 10), and that this was achieved with a half-time of 18 ± 5 s (n = 10). In comparison, Mad3-GFP exhibited a higher level of recovery (60 ± 26 %, n = 7) and a shorter half-time (11 ± 5 s, n = 7), indicating that it is more dynamic that Bub1.

The relative dynamics of Bub1 and Mad3 measured at the ectopic array strongly correlate with those measured at *S. pombe* kinetochores in cells arrested using the cold-sensitive *nda3* mutation in combination with the anti-microtubule drug carbendazim (CBZ) (Bub1: recovery = 39 % ± 16 %, half-time = 31 ± 3 s; Mad3: recovery = 82 % ± 9 %, half-time = 17 ± 4 s) (Fig. 4.4C) (Rischitor et al., 2007). These dynamics also correlate well with results from vertebrate FRAP studies of Bub1 and BUBR1. For Bub1, vertebrate dynamics vary somewhat depending on the experimental setup; one study using a cell line stably expressing YFP observed less than 20 % recovery (Shah et al., 2004), whilst a different study using a cell line transiently transfected N-terminally tagged GFP-Bub1 obtained a recovery of 56 % with a corresponding half-time of ~30 s. In this context, *S. pombe* Bub1 dynamics at both unattached kinetochores and at the ectopic array

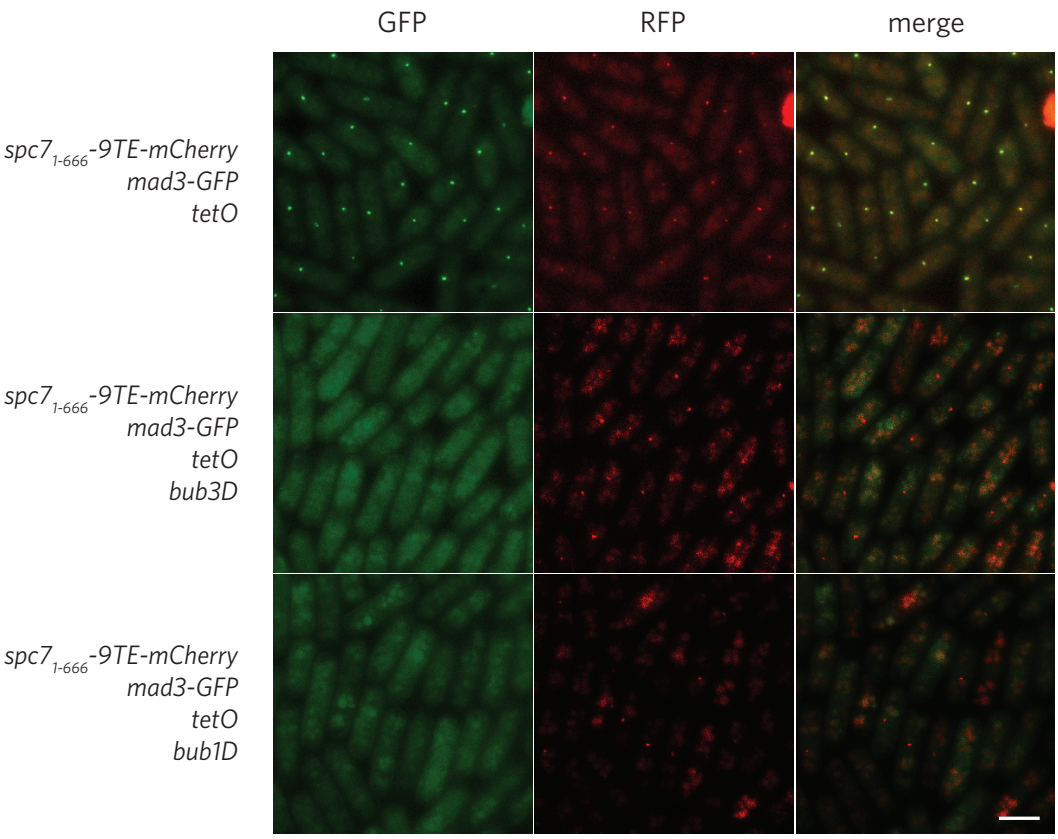

Fig. 4.3 – Ectopic recruitment of Mad3 by Spc7$_{1\text{-}666}$-9TE is Bub1 and Bub3 dependent.
For description see text. Scale bar represents 5 microns.

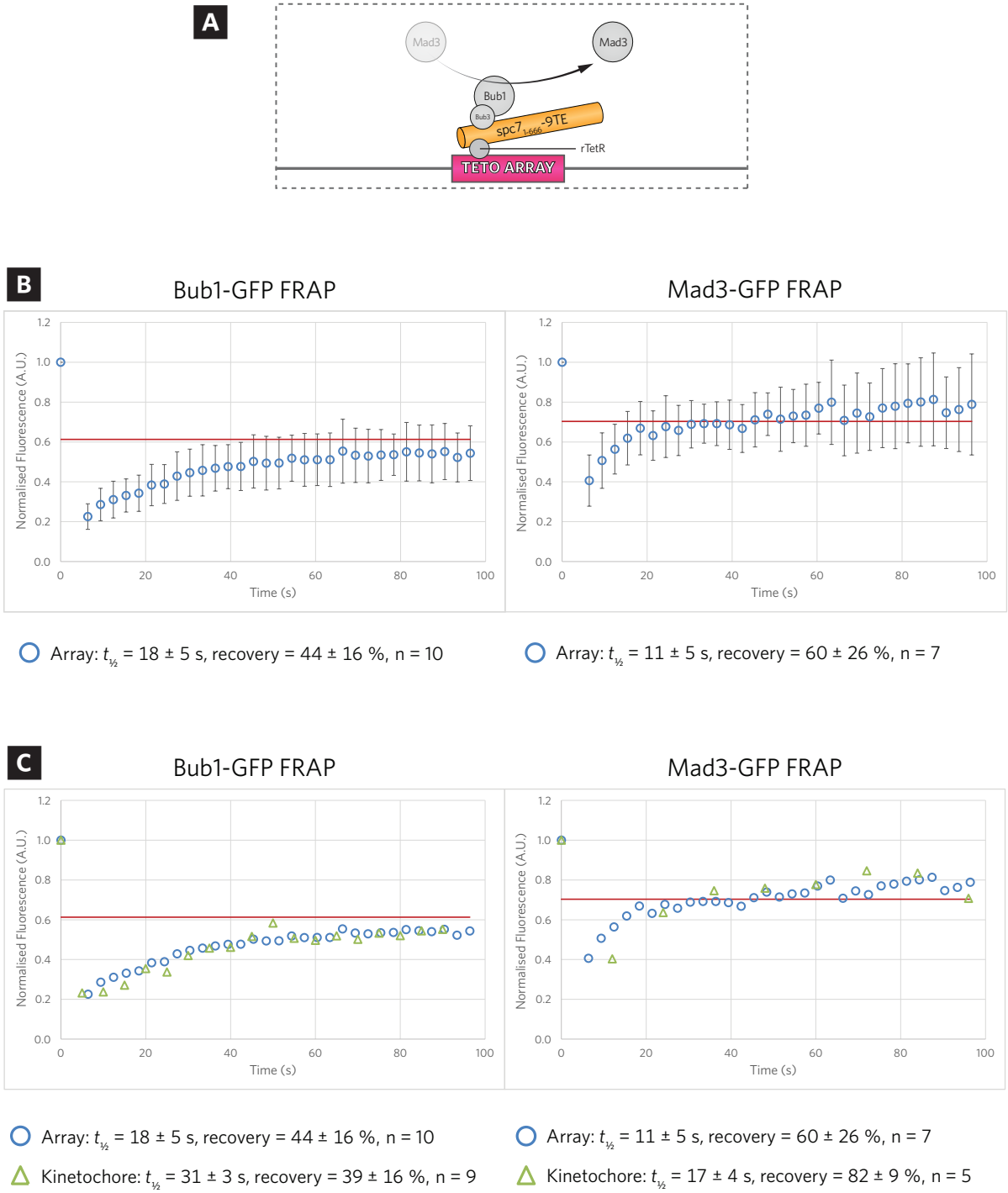

Fig. 4.4 – Bub1 and Mad3 dynamics at ectopic array mirrors those at unattached kinetochores.
(A) Schematic of Bub1 and Mad3 cycling on tethered Spc7$_{1\text{-}666}$-9TE. **(B)** FRAP of Bub1 and Mad3 recruited by ectopically tethered Spc7$_{1\text{-}666}$-9TE. Ectopic Mad3/Bub1-GFP foci formed by tethered Spc7$_{1\text{-}666}$-9TE were then photobleached with a laser, and images captured at the specified intervals throughout the recovery period. The % fluorescence recovery and half-times shown are the mean of the indicated number of experiments. Error bars indicate standard deviation. The red line indicates the 50 % post-bleach recovery level. **(C)** Comparison of Bub1 and Mad3 cycling dynamics at the ectopic array and at unattached kinetochores. Kinetochore dynamics were measured by Karen May and are reproduced with permission from (Rischitor *et al.*, 2007). For full FRAP methods, see Section 2.3.3.

would fall within the bounds of the current published vertebrate Bub1 data. More importantly, it is evident that *S. pombe* Mad3 dynamics agree with vertebrate BUBR1 data (Howell et al., 2004) showing that it is much more dynamic compared to Bub1.

From this FRAP data it was concluded that the ectopic *tetO* array is capable of re-capitulating the different range of protein dynamics exhibited by different checkpoint components at unattached kinetochores, thus simultaneously underscoring the potential usefulness of the ectopic tethering assay in studying individual checkpoint protein interactions whilst increasing the likelihood that the ultimate aim of this work, namely the synthetic generation of functional MCC from the ectopic array, can be realised.

4.7 The role of the Mad3 HIG motif in checkpoint signalling

The above data demonstrated that the ectopic array was capable of not only recruiting checkpoint components, but also recruiting them in a physiological (similar to unattached kinetochores) manner. This greatly increased the confidence with which the system could be used to study unknown interactions in the checkpoint signalling pathway, and it was decided to adapt the system to examine a thus unstudied question, that of how a structural HIG motif on Mad3 affects its ability to localise to unattached kinetochores.

The homologues of *S. pombe* Bub1 and Mad3 contain a well-known and highly-conserved GIG motif ($G_{137}I_{138}G_{139}$ in budding yeast Bub1) that is crucial for multiple key interactions in spindle checkpoint signalling. In budding yeast, a double mutation in the GIG motif of scMad3 renders scMad3 unable to interact with scCdc20 (Hardwick et al., 2000), while in humans mutations in the GIG motifs of both hsBUB1 (Bolanos-Garcia et al., 2009) and hsBUBR1 (Bolanos-Garcia et al., 2011) abolish their ability to bind hsKNL1. Note that, in all of these examples, expression of the GIG mutants remains at WT levels, ruling out simple mis-folding as the reason for the observed losses of interaction. Structural details of how mutations in the GIG motif may cause loss of interaction emerged from the analysis of a crystallised hsBUBR1 and hsKNL1 complex which revealed that double and triple mutations of the hsBUBR1 GIG motif are predicted to disrupt the TPR domains making up the hsKNL1 interaction surface (Bolanos-Garcia et al., 2011).

These results point to an important, undefined role in the GIG-like $H_{144}I_{145}G_{146}$ motif of *S. pombe* Mad3. To investigate this, two HIG point mutants were created (H144V and G146V) and their ability to localise to tethered $Spc7_{1\text{-}666}$-9TE was examined. The $Mad3_{H144V}$-GFP mutant was found to be capable of localising to tethered $Spc7_{1\text{-}666}$-9TE, whilst the localisation of the $Mad3_{G146V}$-GFP mutant is completely abolished (Fig. 4.5B), suggesting that it is unable to interact with Bub1 or Bub3, or both. Preliminary data (Fig. 4.5C) shows that $Mad3_{G146V}$-GFP does not co-immunoprecipitate with Bub3, suggesting that its failure to localise to tethered $Spc7_{1\text{-}666}$-9TE may be due to an inability to bind Bub3, although this may be an indirect effect caused by loss of Bub1

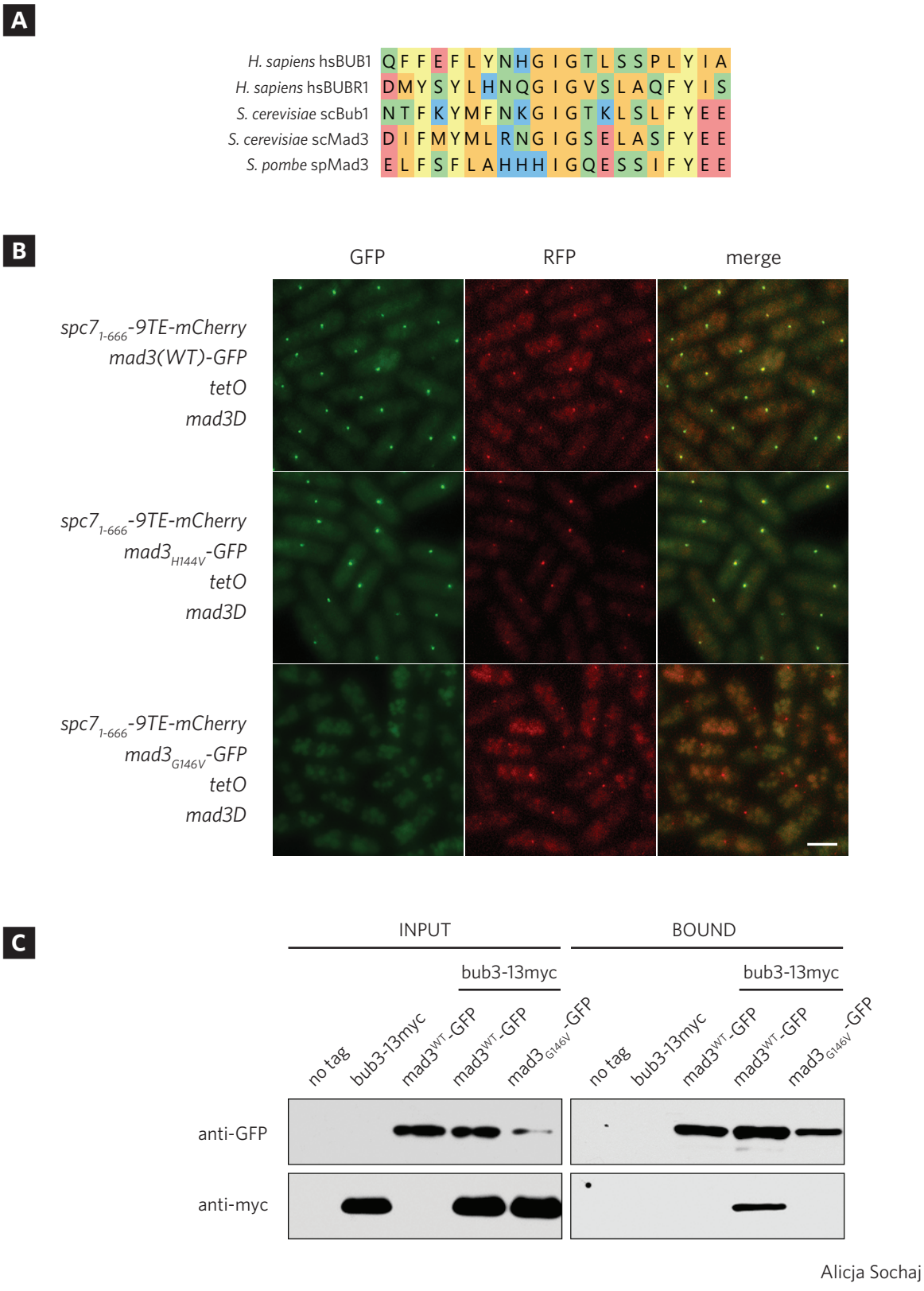

Fig. 4.5 – The role of the Mad3 HIG motif in checkpoint signalling. (A) Alignment of human and yeast Bub1 and BubR1/Mad3 proteins showing the homology of the $H_{144}I_{145}G_{146}$ motif in spMad3 to the GIG motif. **(B)** The ability of $Mad3_{H144V}$-GFP to localise to ectopically recruited Spc71-666-9TE is unimpaired compared to WT Mad3, whereas that of $Mad3_{G146V}$ is completely abolished. **(C)** The ability of Mad3 to co-immunoprecipitate with Bub3 is impaired in the $Mad3_{G146V}$ mutant. Co-immunoprecipitation performed by Alicja Sochaj.

binding. To test this, current work in the lab is focussed on tethering the $Mad3_{G146V}$ mutant and assaying its ability to bind Bub1 and Bub3.

4.8 Ectopically co-tethered Mad1 and $Spc7_{1-666}$-9TE insufficient to generate checkpoint arrest

Having verified the dependencies and dynamics of Mad3 recruitment to the ectopic array, it became apparent that the inability of tethered $Spc7_{1-666}$-9TE to generate a checkpoint arrest was likely due to the absence of other checkpoint components at the ectopic array, with the most likely candidate being Mad2. As mentioned in Chapter 1 and Chapter 3, a myriad of works have over the years demonstrated in both mammalian and *S. pombe* systems that ectopic tethering of Mad1 or C-Mad2 to kinetochores by fusing them to outer kinetochore proteins (Ndc80, Mis12) is sufficient for constitutive spindle checkpoint activation (Kuijt et al., 2014; Maldonado and Kapoor, 2011). However, like the ectopic recruitment of Mad3 by $Spc7_{1-666}$-9TE demonstrated in this work, the ectopic tethering of Mad1 to chromosome arms (Maldonado and Kapoor, 2011) was by itself insufficient to activate the spindle checkpoint.

These findings made it plausible that co-localisation of Mad3 and C-Mad2 at the ectopic array through co-tethering of $Spc7_{1-666}$-9TE and Mad1 would be sufficient to generate a synthetic checkpoint arrest by forming MCC at the array. Surprisingly however, when this was tested cells continued to cycle normally without exhibiting signs of checkpoint arrest (data not shown), suggesting that co-recruited C-Mad2 and Mad3 on the ectopic array was unable to form active MCC.

This could be because:

1. Although the *tetO* array is acting to bring Mad1 and $Spc7_{1-666}$-9TE molecules close together, it may be restricting the conformational freedom with which these proteins are able to interact with one another and thus inhibiting critical interactions that would occur at unattached kinetochores required for MCC formation; the same may be true of ectopically recruited C-Mad2 and Mad3;
2. The fragment of Spc7 being tethered, $Spc7_{1-666}$-9TE, retains its N-terminal protein phosphatase ($PP1^{Dis2}$) binding site and may therefore be suppressing any MCC being generated at the ectopic array; In mammalian cells, there is evidence suggesting that hsPP1 binding to KNL1 is inversely proportional to localised Aurora B activity (Liu et al., 2010), and thus the absence of Ark1 at the ectopic array may be producing a level of localised $PP1^{Dis2}$ activity sufficient to overwhelm ectopic signalling;
3. Another checkpoint component remains missing from the ectopic tether.

If the absence of ectopic checkpoint assembly is indeed due to the absence of another checkpoint component, the likely candidate is Mph1 kinase. As described in Chapter 1, Mph1 has multiple checkpoint protein substrates, including Mad1, and its localisation to unattached kinetochores is crucial for activation of the spindle checkpoint. Indeed, tethering of Mph1 kinase to kinetochores

is sufficient for checkpoint dependent cell arrest (Heinrich et al., 2012; Ito et al., 2012). Thus, the subsequent chapter will explore whether tethered Mph1 kinase will be sufficient for ectopic signalling.

4.9 Summary and perspectives

This chapter achieved two broad goals. First, it demonstrated that the simple tethering system used to examine Mad1-Mad2 interaction in Chapter 2 could be improved to faithfully re-create a much more complex set of checkpoint interactions, namely that between Bub3, Bub1 and Mad3. This makes the system a useful *in vivo* assay for examining checkpoint protein interactions beyond the ones presented here: ongoing work in the lab include using the tethering assay for investigate Bub1 dimerisation and the effect of point mutations in Bub1 on its ability to bind Mad3. Second, the work presented here represents a step forward in the generation of ectopic MCC; the closeness with which the behaviour of ectopically recruited components resembles that at the kinetochores increases the likelihood that, with the addition of other checkpoint components such as Mph1 kinase, complete MCC assembly can be achieved at the ectopic site. This forms the subject of the following chapter.

CHAPTER 5

Co-localisation of Spc7$_{1-666}$-9TE and Mph1$_{\Delta 1-302}$ kinase is sufficient to ectopically activate the spindle checkpoint away from kinetochores

5.1 Introduction

The previous chapter described how, contrary to expectations, the co-targeting of key MCC components Mad2 and Mad3 to the ectopic array was insufficient to generate a synthetic checkpoint arrest. This chapter examines whether this is due to the absence of key phosphorylation events at the ectopic array due to a lack of localised checkpoint kinase activity. Specifically, it will determine whether the co-targeting of Mph1 kinase and Spc7$_{1-666}$-9TE to the ectopic array is sufficient to generate a synthetic checkpoint arrest, possibly through a phosphorylation-dependent interaction between the Spc7$_{1-666}$-9TE-Bub3-Bub1-Mad3 and Mad1-C-Mad2 scaffolds.

5.2 Co-tethered Mph1$_{\Delta 1-303}$ and Spc7$_{1-666}$-9TE are sufficient to generate a *tetO* array dependent metaphase arrest

As detailed in Chapter 1, the checkpoint kinase Mps1/Mph1 is the most upstream component in the spindle checkpoint signalling pathway alongside Ark1 (Heinrich et al., 2012). Importantly, Mph1/Mps1 targets the basal checkpoint scaffold components such as Spc7, Bub3, Bub1 and Mad1, and in *S. cerevisiae* the co-localisation and activity of Mps1 is essential for both the Spc105-mediated recruitment of Bub1, as well the subsequent ability of Bub1 to recruit Mad1 and form a functional signalling scaffold (London and Biggins, 2014a). Whether this model of checkpoint scaffold assembly extends to *S. pombe* remains unknown, but if so then tethered Mph1 at the ectopic array would likely be essential for the ability of Spc7$_{1-666}$-9TE to generate a synthetic checkpoint arrest.

To test this directly, it was decided to co-tether a fragment of Mph1 to the ectopic array together with Spc7$_{1-666}$-9TE. It was determined that the fragment of Mph1 to be tethered should have the following features:

1. *Inducible expression*. Should co-targeting of Mph1 and Spc7$_{1-666}$-9TE be sufficient to activate the checkpoint, cells may eventually leak through the constitutive metaphase arrest and septate without having satisfied the checkpoint. This would produce the 'cut' phenotype that is characteristic of fission yeast: undivided nuclei are either cleaved by septa formation or are asymmetrically distributed to the daughter cells. In either case, cell death shortly follows. To prevent this from making the combined Mph1/Spc7$_{1-666}$-9TE strain inviable, Mph1 expression must be inducible.

2. *Expression levels similar to WT*. Overexpression of Mph1 results in constitutive spindle checkpoint activation, possibly through the hyper-phosphorylation of Mad1, and this drives Mad1 to kinetochores (Chapter 1). To minimise the possibility of checkpoint activation by Mph1 overexpression rather than its localised effects on tethered Spc7$_{1\text{-}666}$-9TE, the levels of tether-able Mph1 should be kept as close to endogenous as possible.
3. *Kinetochore localisation deficient*. To simplify the interpretation of Mph1 tethering experiments, it is advantageous to remove the ability of tether-able Mph1 to localise to endogenous kinetochores; this will allow any effects on checkpoint signalling to attributable solely to tethered Mph1 at the ectopic site (in the absence of endogenous Mph1).

After initial experimentation with a number of N-terminal Mph1 truncations and expression constructs failed to produce a mutant with these features (data not shown), it was decided to incorporate an Mph1$_{\Delta1\text{-}302}$ fragment into a modified *nmt81*-driven tethering vector (pIY02). This fragment of Mph1 had been characterised by Heinrich and colleagues as being deficient in kinetochore localisation but capable of catalysing checkpoint activation when forcibly localised to kinetochores (Heinrich et al., 2012). Immunoblotting of Mph1$_{\Delta1\text{-}302}$ expressed from pIY02 showed that the abundance of rTetR-mph1$_{\Delta1\text{-}302}$ was comparable to wild-type Mph1 (Fig. 5.1C). Importantly, this level of expression is significantly below that which is required for checkpoint arrest (Fig. 5.1C, *P$_{nmt41}$-Mph1*, lanes 12-13).

It was then tested whether co-tethering Mph1$_{\Delta1\text{-}302}$ with Spc7$_{1\text{-}666}$-9TE would be sufficient to activate the spindle checkpoint. To do this a strain that combined constitutive expressed rTetR-mCherry-Spc7$_{1\text{-}666}$-9TE and inducibly expressed rTetR-Mph1$_{\Delta1\text{-}302}$ with a Mad2-GFP reporter was analysed as described in Fig. 5.1B. In control cells (*rtTA-mph1$_{\Delta1\text{-}302}$* OFF), rTetR-mCherry-Spc7$_{1\text{-}666}$-9TE could be observed as singular red foci at the ectopic array, whilst Mad2-GFP forms a green ring along the nuclear periphery (Fig. 5.2A). By contrast, in cells where rTetR-Mph1$_{\Delta1\text{-}302}$ expression had been induced for 14 hours, Mad2-GFP had de-localised from the nuclear periphery and could be observed forming two distinct foci at opposite poles of the nucleus (Fig. 5.2A). rTetR-mCherry-Spc7$_{1\text{-}666}$-9TE did not co-localise with these Mad2-GFP foci. The proportion of cells exhibiting this phenotype increased in later time points. Concomitant with Mad2-GFP foci formation, cells began to display morphological changes consistent with the 'cut' phenotype, namely the formation of septa through undivided nuclei and the appearance of aneuploid daughter cells (Fig. 5.2A).

These observations are indicative of an initial metaphase arrest followed by septation. In both *S. pombe* (Saitoh et al., 2005) and vertebrates (Howell et al., 2000, 2001), Mad2 migrates from the nuclear periphery to the SPBs in late metaphase, forming two distinct foci consistent with that described above. These foci disappear in late anaphase, again consistent with the observations above when cells begin to leak through the prolonged metaphase arrest with 'cut' characteristics (Fig. 5.2A). These phenotypes are not observed in a strain in which only rTetR-

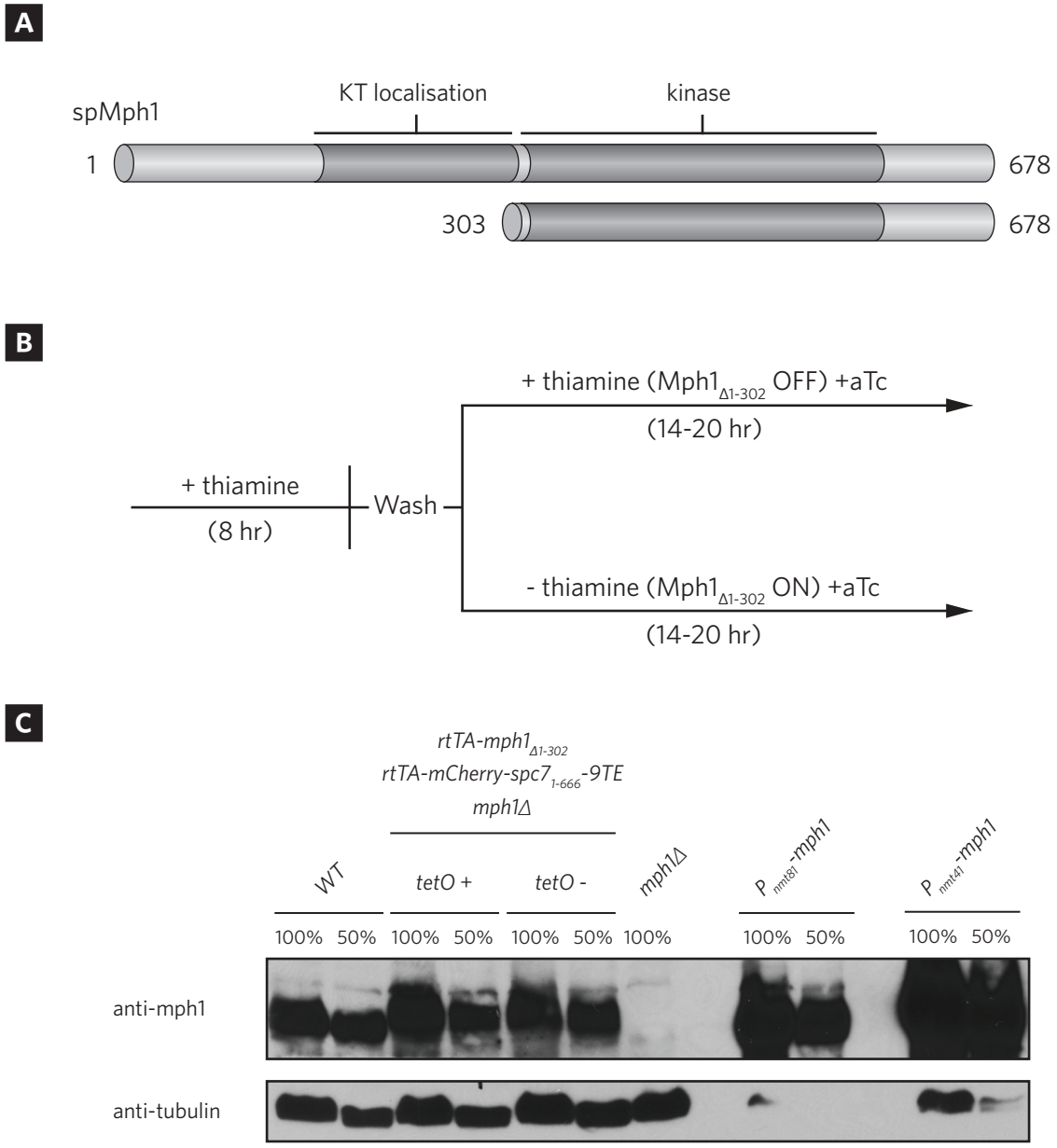

Fig. 5.1 – Ectopic tethering of a Mph1 fragment that is unable to localise to kinetochores. (A) Kinetochore localisation of Mph1 is dependent on its N-terminus. Schematic of spMph1 kinase showing the $Mph1_{\Delta1\text{-}302}$ truncation used in (Heinrich *et al.*, 2012) to identify the N-terminal kinetochore localisation domain. **(B)** Schematic of inducible $Mph1_{\Delta1\text{-}302}$ time-course experiment. Cells are loaded with thiamine for 8 hours before being split into two parallel cultures, one with $Mph1_{\Delta1\text{-}302}$ expression induced and the other with $Mph1_{\Delta1\text{-}302}$ expression repressed. **(C)** Expression of tether-able $Mph1_{D1\text{-}302}$ (rTetR-$Mph1_{\Delta1\text{-}302}$) similar to WT Mph1 levels. Cells were grown as shown in **(B)** and harvested after 16 hours of growth in the absence of thiamine. Note the high degree of Mph1 overexpression required for checkpoint arrest (P_{nmt41}-Mph1, lanes 12-13) as described in (Ito *et al.*, 2012).

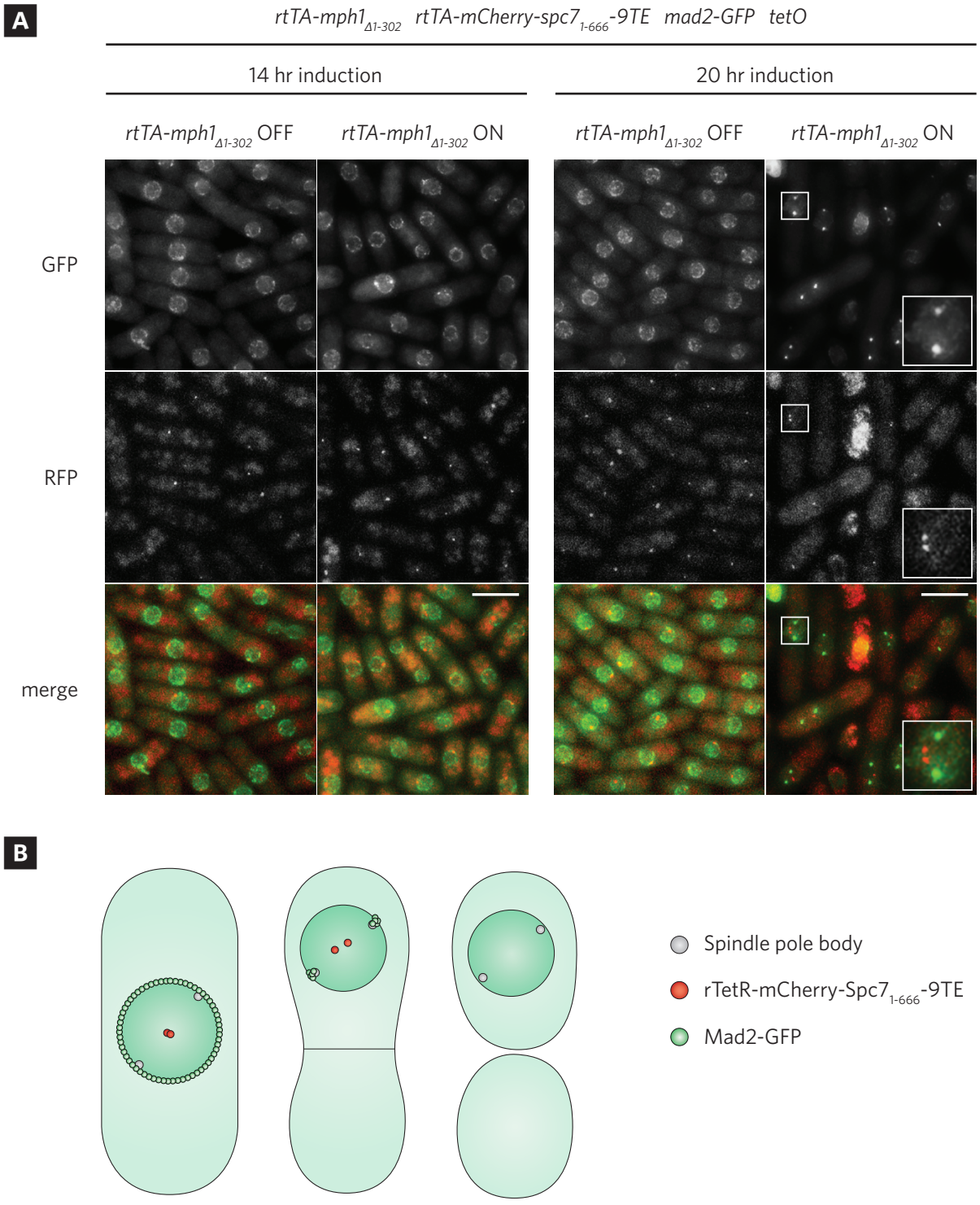

Fig. 5.2 – Co-tethered Mph1$_{\Delta 1\text{-}302}$ and Spc7$_{1\text{-}666}$-9TE sufficient to generate a metaphase arrest. (A) Co-tethered Mph1$_{\Delta 1\text{-}302}$ and Spc7$_{1\text{-}666}$-9TE induces cellular changes consistent with sustained metaphase arrest. Cells were grown as described in Fig. 5.1B and representatives samples taken after 14 and 20 hours of *rtTA-mph1*$_{\Delta 1\text{-}302}$ induction are shown. **(B)** Schematic of morphological changes shown in (A). (From left to right): unarrested interphase cell with Mad2-GFP at the nuclear periphery and rTetR-mCherry-Spc7$_{1\text{-}666}$-9TE localised at the ectopic array; arrested cell showing Mad2-GFP at SPBs, a sign of late metaphase/early anaphase, and rTetR-mCherry-Spc7$_{1\text{-}666}$-9TE signal separation as sister chromatids come under tension; prolonged metaphase arrest leads to septation without nuclear division ('cut'), resulting in either two aneuploid daughters or septation through the nucleus and cell death. Scale bar represents 5 microns.

Mph1$_{\Delta 1\text{-}302}$ is tethered (Fig. 5.3A), indicating that phosphorylation of Spc7$_{1\text{-}666}$-9TE-recruited checkpoint components (Bub3, Bub1 and Mad3) by Mph1$_{\Delta 1\text{-}302}$ is required for this metaphase arrest. It is possible that this metaphase arrest requires phosphorylation of other checkpoint components recruited by the Spc7$_{1\text{-}666}$-9TE-Bub3-Bub1-Mad3 complex. These phenotypes are likewise not observed when rTetR-mCherry-Spc7$_{1\text{-}666}$-9TE and rTetR-Mph1$_{\Delta 1\text{-}302}$ are expressed in the absence of the *tetO* array (Fig. 5.2B), demonstrating that the enrichment of Spc7$_{1\text{-}666}$-9TE and Mph1$_{\Delta 1\text{-}302}$ at a single location is crucial for the generation of the observed metaphase arrest.

To confirm that the Mad2-GFP foci observed were truly localised at the SPBs rather than at kinetochores that have been pulled close to the SPBs by the spindle, rTetR-Mph1$_{\Delta 1\text{-}302}$ was co-tethered with rTetR-mCherry-Spc7$_{1\text{-}666}$-9TE in strains expressing an SPB marker, Pcp1-mCherry, or a kinetochore marker, Fta3-tdT. Pcp1 (**P**ole target of **C**almodulin in **P**ombe), a pericentrin-like protein, serves as a SPB marker by virtue of being a constitutive component of SPBs (Flory et al., 2002). In metaphase arrested (*rtTA-mph1$_{\Delta 1\text{-}302}$* ON) cells, Mad2-GFP co-localisation was observed with Pcp1-mCherry (Fig. 5.4A), but not Fta3-tdT (Fig. 5.4B), confirming the SPB localisation of the Mad2-GFP foci above. In addition, the absence of Mad2-GFP at kinetochores serves as further evidence that this metaphase arrest is distinct from that observed upon simple Mph1 overexpression, in which Mad1-C-Mad2 can be observed localising to kinetochores (Ito et al., 2012).

5.3 Spc7$_{1\text{-}666}$-9TE and Mph1$_{\Delta 1\text{-}302}$ induced metaphase arrest is spindle checkpoint-dependent

To determine if the tethering-induced metaphase arrest was spindle checkpoint-dependent, rTetR-Mph1$_{\Delta 1\text{-}302}$ was co-tethered with rTetR-mCherry-Spc7$_{1\text{-}666}$-9TE in strains lacking Mad1. This strain failed to arrest upon induction of *rtTA-Mph1$_{\Delta 1\text{-}302}$* (Fig. 5.5A). Furthermore, preliminary work shows that the same phenotype is observed in a strain lacking Mad3 (not shown). Together, these results suggest that (i) the tethering-induced metaphase arrest is mediated by the spindle checkpoint, and (ii) the arrest requires a combination of the Mad1-C-Mad2 and Spc7$_{1\text{-}666}$-9TE-Bub3-Bub1-Mad3 scaffolds. A key question is where these two checkpoint scaffolds interact to generate the checkpoint signal. One possible model is that one or more constituents of the tethered Spc7$_{1\text{-}666}$-9TE-Bub3-Bub1-Mad3 scaffold is phosphorylated by co-tethered Mph1$_{\Delta 1\text{-}302}$, thus initiating a checkpoint signal that is then propagated away from the ectopic array.

To test this model, Mad3-GFP localisation was followed in a strain in which rTetR-mCherry-Spc7$_{1\text{-}666}$-9TE and rTetR-Mph1$_{\Delta 1\text{-}302}$ were co-tethered. In control cells (*rtTA-Mph1$_{\Delta 1\text{-}302}$* OFF), Mad3-GFP can be observed as a single focus that co-localises with tethered rTetR-mCherry-Spc7$_{1\text{-}666}$-9TE (Fig. 5.5B). However, 14 hours after *rtTA-mph1$_{\Delta 1\text{-}302}$* induction, Mad3-GFP can be observed forming two additional foci at the SPBs, suggesting that Mad3 had migrated from the ectopic array to the SPBs. Consistent with this, the intensity of Mad3-GFP foci

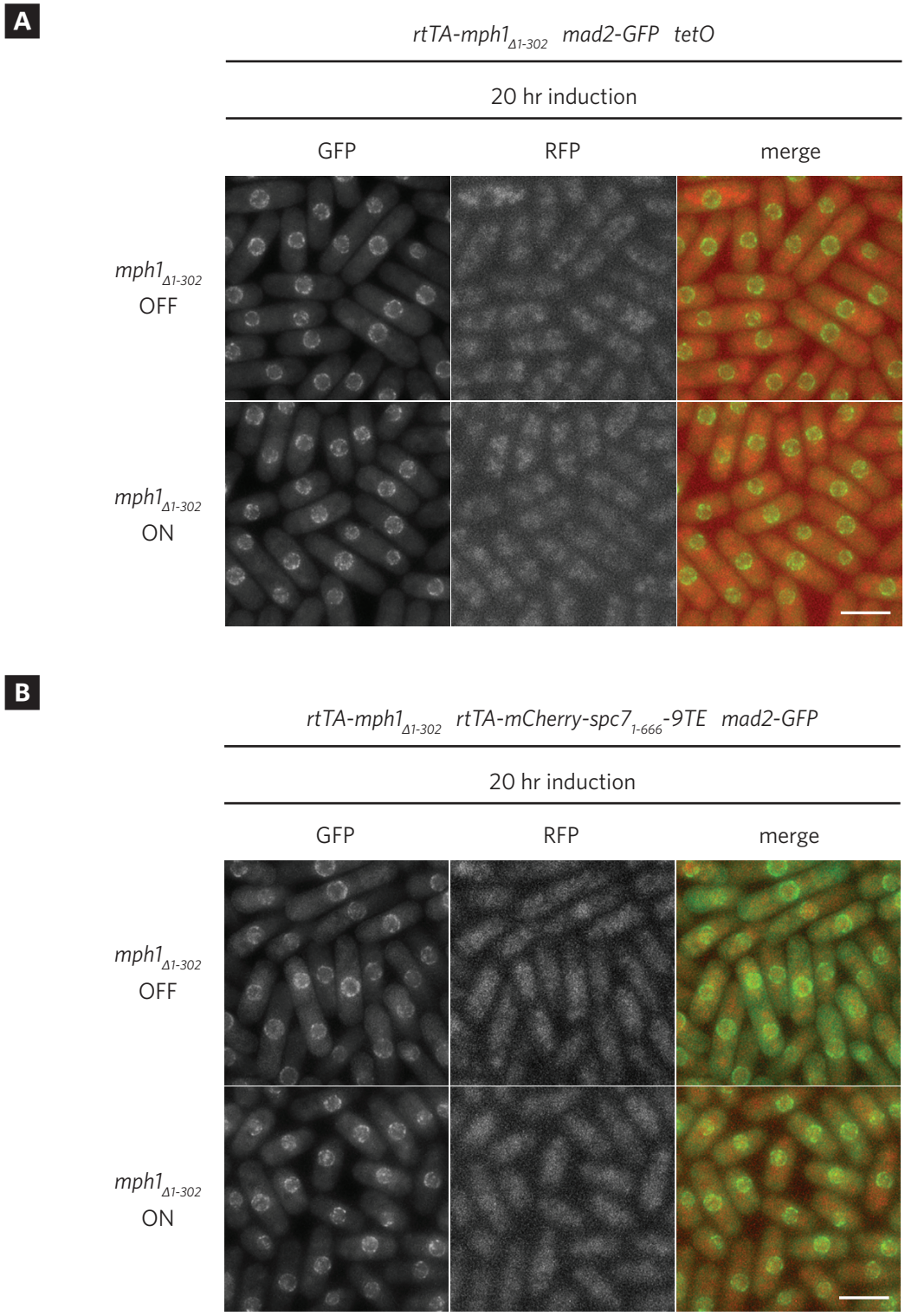

Fig. 5.3 – Tethering induced metaphase arrest requires both tethered Mph1$_{\Delta 1\text{-}302}$ and Spc7$_{1\text{-}666}$-9TE. (A) Tethered Mph1$_{\Delta 1\text{-}302}$ is insufficient to induce metaphase arrest. Cells were grown as described in Fig. 5.1B and representative samples taken after 20 hours of *rtTA-mph1*$_{\Delta 1\text{-}302}$ induction are shown. **(B)** Spc7$_{1\text{-}666}$-9TE and Mph1$_{\Delta 1\text{-}302}$ are insufficient to induce metaphase arrest when de-localised from ectopic tether site. Cells were grown as described in Fig. 5.1B and representative samples taken after 20 hours of *rtTA-mph1*$_{\Delta 1\text{-}302}$ induction are shown. Note that in the absence of the *tetO* array, rTetR-mCherry-Spc7$_{1\text{-}666}$-9TE can no longer be visualised as distinct foci. Scale-bar represents 5 microns.

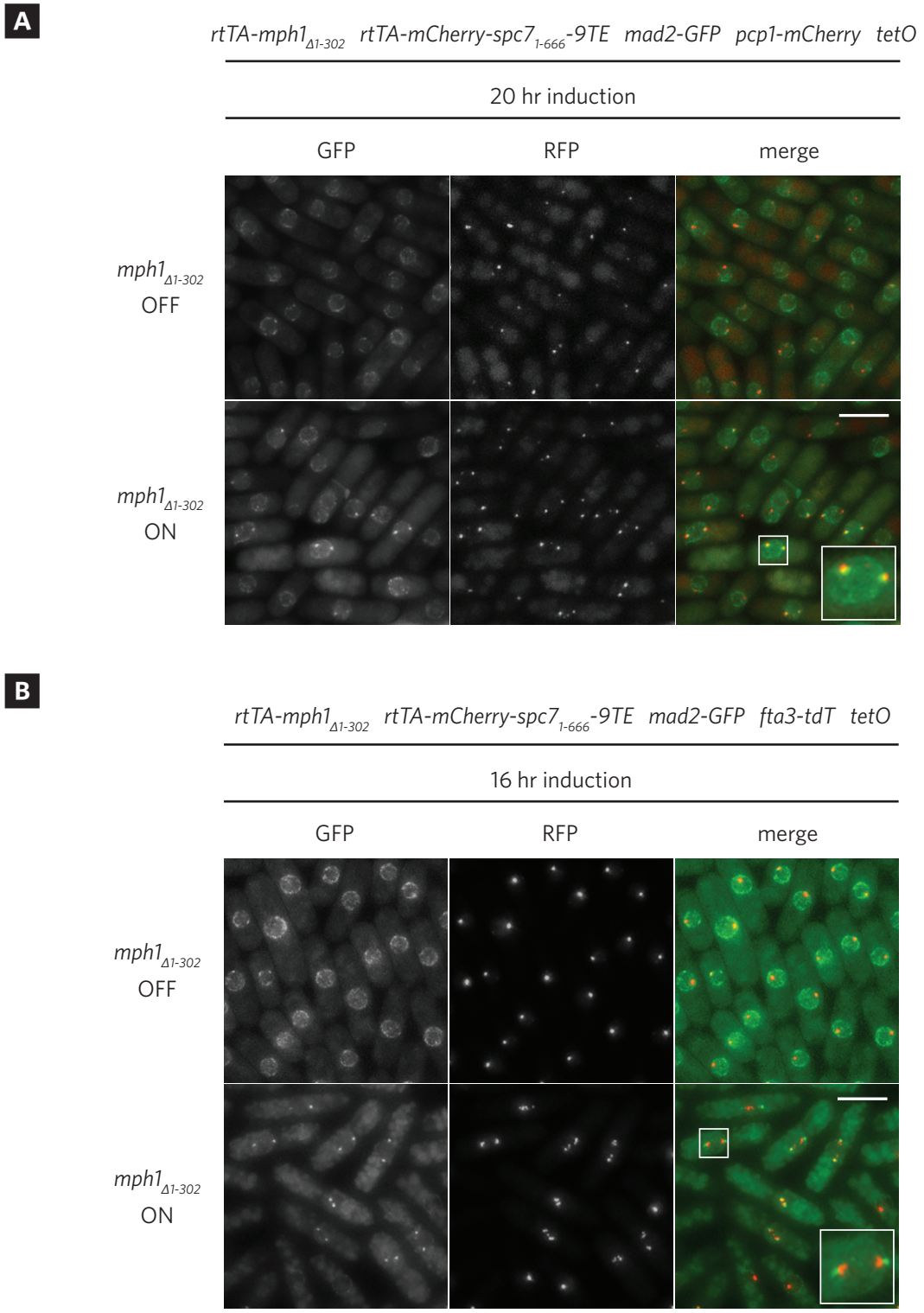

Fig. 5.4 – Mad2 localises to SPBs during tethering induced metaphase arrest. (A) Mad2-GFP co-localises with SPB marker Pcp1-mCherry during tethering induced metaphase arrest. Cells were grown as described in Fig. 5.1B and representative samples taken after 20 hours of *rtTA-mph1*$_{\Delta 1\text{-}302}$ induction are shown. **(B)** Mad2-GFP does not co-localise with KT marker fta3-tdT during tethering induced metaphase arrest. Cells were grown as described in Fig. 5.1B and representative samples taken after 16 hours of *rtTA-mph1*$_{\Delta 1\text{-}302}$ induction are shown. Note that in interphasic (non-arrested) cells, clustering of kinetochores causes the formation of singular fta3-tdT foci. In contrast, cells leaking through prolonged metaphase arrest exhibit multiple fta3-tdT foci indicative of sister chromatids separating under tension. Scale bar represents 5 microns.

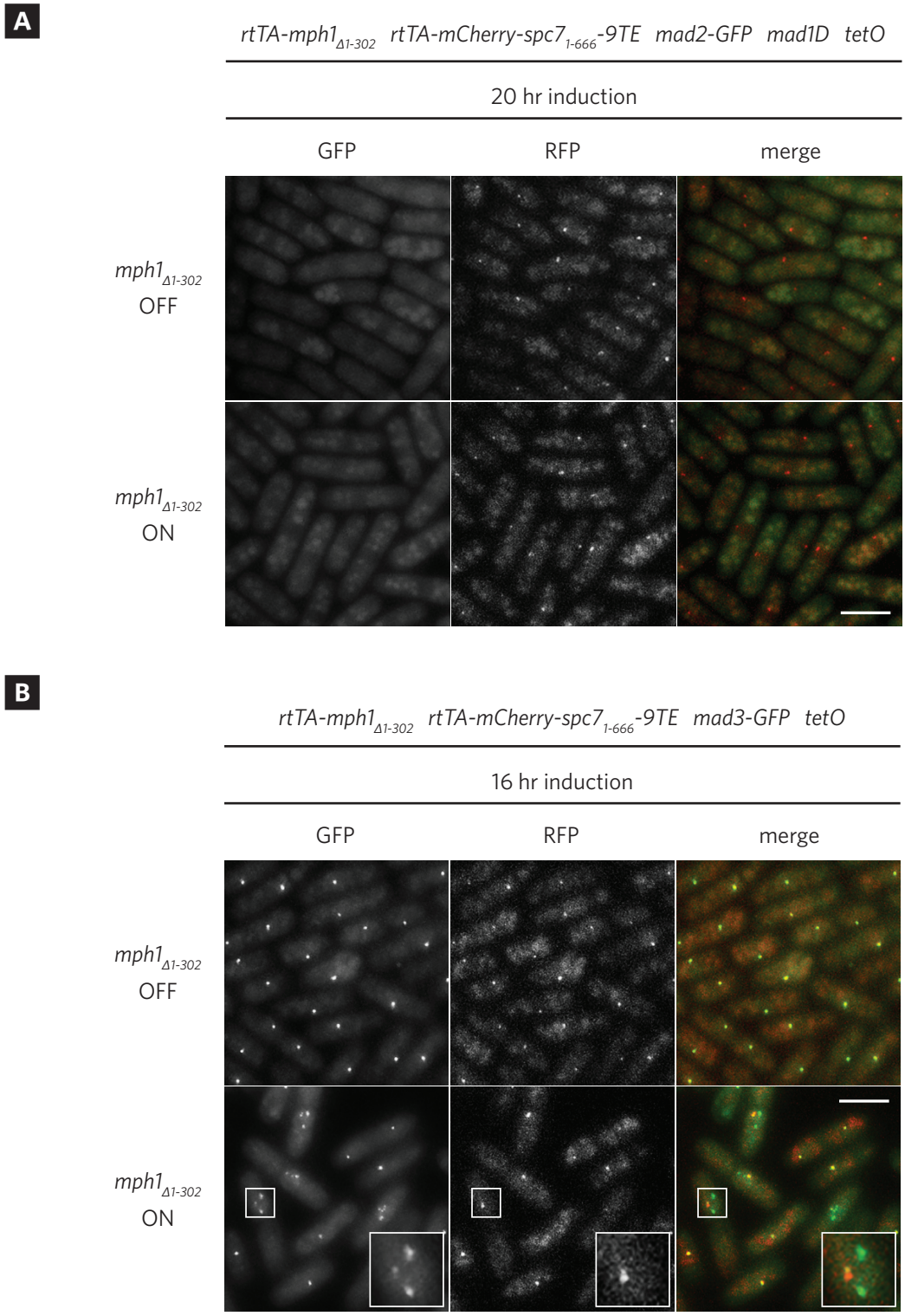

Fig. 5.5 – Tethering induced metaphase arrest is spindle checkpoint dependent. (A) Tethering-induced metaphase arrest is dependent on Mad1. Cells were grown as described in Fig. 5.1B and representative samples taken after 20 hours of *rtTA-mph1*$_{\Delta 1\text{-}302}$ induction are shown. Deletion of checkpoint component Mad1 rescues tethering-induced metaphase arrest. **(B)** Mad3 migrates from ectopic tether site to SPBs during tethering-induced metaphase arrest. Cells were grown as described in Fig. 5.1B and representative samples taken after 16 hours of *rtTA-mph1*$_{\Delta 1\text{-}302}$ induction are shown. Scale-bar represents 5 microns.

remaining at the ectopic array is diminished compared to that in cells where Mad3-GFP had not yet begun migrating to the SPBs. Together, these observations are supportive of the above model of checkpoint initiation at the ectopic array followed by propagation elsewhere in the nucleoplasm.

5.4 Summary and perspectives

5.4.1 Concentration of checkpoint components key for signalling activation

As described in Chapter 3, various studies have tested whether individual spindle checkpoint components tethered at non-centromeric locations are sufficient to activate the checkpoint. Although unsuccessful in checkpoint activation, these studies have paved the way to addressing what is arguably the most central question of spindle checkpoint signalling: do the kinetochores serve only to enrich for checkpoint components, or do they possess other features required for checkpoint activation? The results presented in this chapter argue in favour of the former. Together with Ark1/Aurora B, Spc7/KNL1 and Mph1/Mps1 are both recognised as the most upstream components of the checkpoint signalling pathway. By demonstrating that the combined targeting of Spc7 and Mph1 fragments is sufficient to activate the checkpoint away from the kinetochores, the results here emphasise the importance of enrichment and post-translational modification for checkpoint activation. These are central concepts common to all signalling pathways both biological and synthetic, and by underscoring their importance here these results serve as a reminder of why the study of the spindle checkpoint is important not only for its own sake, but also for furthering our understanding of signalling pathways in general.

5.4.2 Mapping the synthetic signalling pathway

Nevertheless, important questions about the tethering induced checkpoint signal remain. First and foremost, the signalling pathway remains incomplete. When cells enter a normal checkpoint arrest, Mad2 moves from the nuclear periphery first to the kinetochores in metaphase and from there to the SPBs in late metaphase/early anaphase. During a tethering-induced checkpoint arrest, however, Mad2 disappears from the nuclear periphery and later re-appears at the SPBs without ever appearing at the ectopic array. This stands in contrast to the localisation pattern of Mad3, which forms clear foci at the ectopic array during interphase before re-locating to the SPBs during a tethering-induced arrest. These observations raise two important questions. First, where is soluble O-Mad2 activated to form C-Mad2 that is then capable of binding Slp1? In a normal checkpoint arrest this occurs via Mad1 binding at the unattached kinetochores, but as noted above Mad2 does not appear to co-localise with kinetochore markers (Fig. 5.4B), and nor does it seem to co-localise with the ectopic array. Second, once the Mad2-C-Slp1 complex is formed, where does it interact with Mad3 to form MCC?

There are two possible models that address these questions. First, Mad2 may be activated via transient Mad1 binding to the tethered $Spc7_{1\text{-}666}$-9TE-Bub3-Bub1-Mad3 complex, similar to the model in *S. cerevisiae* in which Mps1-phosphorylated Bub1 forms a stable complex with Mad1 (London and Biggins, 2014a). The transient nature of this interaction would then explain why it

has thus far escaped detection by snapshot imaging. If so, a switch to time-lapse imaging (currently ongoing) will provide the temporal resolution required to resolve this issue. However, such a transient interaction between Mad2-C-Mad1 and the tethered Spc7 complex would run contrary to the canonical Mad2-template model, which would predict that a pool of stably associated Mad1-C-Mad2 is required at the ectopic array before it could potentially catalyse Mad2-C-Slp1^{Cdc20} formation. It is important to note here that, at least in *S. pombe*, endogenous Mad1 levels can be reduced by up to 70 % without significant impairment of the checkpoint response (Heinrich et al., 2013). This means that only a relatively small pool of Mad1-C-Mad2 complexes would need to present at the ectopic array in order to support Mad2 activation and checkpoint function. As mentioned above, improvements to imaging will likely be required before this possibility can be ruled out. Immuno-fluorescence imaging using anti-Mad1 and/or anti-Mad2 antibodies may also prove useful in determining the localisation of these upstream checkpoint components during the early stages of synthetic checkpoint arrest.

An alternative model is that Mad1 in *S. pombe* does not form a stable association with the Spc7-Bub3-Bub1-Mad3 complex. Instead, Mad2 can be activated away from the kinetochores, where it can then interact with nucleoplasmic Mad3 and Slp1^{Cdc20} to form MCC. This model is consistent with several lines of evidence. First, it has long been known that checkpoint components are capable of assembling MCC away from the unattached kinetochores where they are usually enriched. When the majority of checkpoint components (including Mad1 and Mad2) are evicted from *S. pombe* kinetochores by deletion of *bub3* (Vanoosthuyse et al., 2009; Windecker et al., 2009), or from human-derived kinetochores by Hec1 knock-down (Martin-Lluesma et al., 2002), the checkpoint remains surprisingly functional. These studies imply that Mad2 and Mad3 is capable of being activated at location(s) other than unattached kinetochores.

As described previously in Chapter 1, the NPC is a prime candidate for this location. In human-derived cells, Mad1 interaction with the nuclear basket protein Tpr (*S. pombe*: Nup211; *S. cerevisiae*: Mlp1) during interphase enables it to activate Mad2 and drive MCC formation in the same manner as Mad1-kinetochore interaction (Rodriguez-Bravo et al., 2014). How BUBR1 and Cdc20 interact with C-Mad2 and form MCC in this NPC-driven signalling pathway is unclear, but given that the KNL1-Bub3-Bub1-BUBR1 complex has not been observed to localise to NPCs, these interactions will almost certainly be different from kinetochore-driven signalling. Specifically, it suggests that Mad2 and BUBR1/Mad3 co-localisation is not a requirement for MCC generation and that, as may be the case for the tethering-induced signalling described above, NPC-activated C-Mad2 is capable of nucleoplasmic interaction with Cdc20/Slp1 and Mad3 to form MCC.

The data presented thus far is consistent with the following model for tethering-induced checkpoint signalling. Tethered Spc7$_{1\text{-}666}$-9TE recruits the Bub3-Bub1 complex, which in turn promotes the recruitment of dynamically cycling Mad3. Phosphorylation of these checkpoint components by tethered Mph1$_{\Delta 1\text{-}302}$ then enables Mad3 to efficiently bind Cdc20^{Slp1} and Mad2,

either diffusely in the nucleoplasm or possibly at or near the SPBs (see following section). This forms a pool of MCC generated independently of kinetochores.

5.4.3 The role of the SPBs in tethering-induced checkpoint signalling

In order to fully explore the above model, ongoing work aims to track the localisation of Slp1-GFP during a tethering-induced arrest: would Slp1-GFP localise to the SPBs in late metaphase, as with Mad2 and Mad3 described above? If so, what is the signalling function of this localisation, if any? The role of SPBs in spindle checkpoint signalling is poorly understood. Although Mad1 and Mad2 have been observed migrating from kinetochores to SPBs along spindle fibres in both *S. pombe* (Saitoh et al., 2005) and higher eukaryotes (Défachelles et al., 2015), this dynein-dependent migration is thought to be part of a silencing mechanism unique to higher eukaryotes (Chapter 1), and its role in yeast remains unknown. Thus even if Slp1-GFP was observed to co-localise with Mad2 and Mad3 at the SPBs during a synthetic arrest, this does not necessarily imply that the SPBs act as a kinetochore-independent site of MCC assembly.

To determine if the accumulation of Mad2 and Mad3 at the SPBs described in this chapter serves an active role in tethering-induced signalling or is a merely a passive by-product of metaphase arrest, current work is examining if disrupting the spindle transport apparatus upon which Mad2 depends for its SPB localisation will affect the ability of cells to arrest. Specifically, the spindles will be depolymerised through use of the *nda3-KM311* mutation, whilst deletion of dynein will abolish motor-dependent spindle transport.

Furthermore, determining the location of APC/C will likely provide useful information on the role of SPBs in signalling; if the SPBs truly function as a site of MCC assembly in a tethering-induced checkpoint arrest, then it may also serve as a site of MCC-APC/C interaction. The APC/C has been documented to localise to unattached kinetochores in a checkpoint-dependent manner (Gillett et al., 2004), and although the function of this localisation remains unclear, speculation points to MCC-driven APC/C inhibition at the unattached kinetochores. Thus if APC/C interaction was observed at the SPBs, this would provide at least limited evidence for the idea that the APC/C is actively recruited to sites of MCC generation, whether it be kinetochores or SPBs.

CHAPTER 6

Final discussion

As stated in Chapter 1, the main goal of this work was to determine whether the role of the kinetochores within the spindle checkpoint signalling pathway is limited to concentrating checkpoint components. By using an artificial, non-kinetochore binding platform to concentrate selected checkpoint components, and then by demonstrating that this can generate a checkpoint signal, this work suggests that the kinetochores serve as a 'component concentrator' in the context of spindle checkpoint signalling.

As described in the preceding chapter, other groups have succeeded in either generating a checkpoint signal through tethering signalling components to the kinetochore, or in tethering signalling components to non-kinetochores locations without a resultant checkpoint, but not both. Thus these approaches have left unanswered the central question of the role of the kinetochores. This work represents the first time that a spindle checkpoint signal capable of robust metaphase arrest has been generated by concentrating checkpoint components at a location other than the kinetochores, and it is here that the novelty and the value of this work lies.

Further work is needed to realise the full potential of the *tetO*-based 'checkpoint generator' developed in this work. In particular, the *tetO*-based ectopic checkpoint generator has three drawbacks in its current configuration that limits its potential. First, sometimes tetR-fused molecules localise to the tetO array in absence of anhydrotetracycline; this 'leakiness' in the system limits the inducibility of checkpoint protein tethering and forces the user to use the inducible expression of tether-able Mph1 as a means of controlling checkpoint signal generation.

Second, there is currently no way to regulate the number and stoichiometry of checkpoint proteins being targeted to the *tetO* array, *viz*. for every molecule of Spc7 recruited to the array, how many molecules of Mph1 are recruited? How many molecules of Spc7 and Mph1 are typically present at the array? The ability to measure, and in future experimentally manipulate these parameters can be expected to yield data useful for producing a more quantitative model of ectopic checkpoint signalling. This in turn will be informative for the building of even more minimalistic ectopic 'checkpoint generators'.

The third and final drawback is that it is currently difficult to obtain a comprehensive list of downstream checkpoint components that are being recruited by ectopically tethered Spc7 and Mph1, e.g. is Slp1 recruited to the array? Related to this point, it is unknown what PTMs may be associated with the checkpoint components that are recruited to the array.

To overcome many of these technical limitations the current *tetO* array will be replaced by a mixed *tetO*/*lacO* array that will be synthesised in a 1:1 ratio on an artificial chromosome arm. Under this scheme, one checkpoint component (e.g. Spc7) will be targeted to the array by fusion

with lacI, while a second component will be targeted by fusion with tetR (e.g. Mph1). This mixed array will thus be able to ensure that ectopically recruited checkpoint components are present in a strict 1:1 stoichiometry. Furthermore, it is envisaged that the new array will be synthesised with flanking loxP sites that, after checkpoint components are recruited to the array, will enable the entire array to be excised through the introduction of Cre recombinase. The excised array with bound checkpoint components can then be analysed through mass spectrometry to reveal the identity of the bound components. Building such a long stretch of repetitive sequence (mixed *tetO* and *lacO* repeats) using conventional cloning will be an extremely difficult if not impossible task, and thus the synthesis of this mixed array will be outsourced to a third-party, such as the newly established Edinburgh Genome Foundry.

Bibliography

De Antoni, A., Pearson, C.G., Cimini, D., Canman, J.C., Sala, V., Nezi, L., Mapelli, M., Sironi, L., Faretta, M., Salmon, E.D., et al. (2005). The Mad1/Mad2 complex as a template for Mad2 activation in the spindle assembly checkpoint. Curr. Biol. *15*, 214–225.

Basi, G., Schmid, E., and Maundrell, K. (1993). TATA box mutations in the Schizosaccharomyces pombe nmt1 promoter affect transcription efficiency but not the transcription start point or thiamine repressibility. Gene *123*, 131–136.

Bolanos-Garcia, V.M., Kiyomitsu, T., D'Arcy, S., Chirgadze, D.Y., Grossmann, J.G., Matak-Vinkovic, D., Venkitaraman, A.R., Yanagida, M., Robinson, C. V., and Blundell, T.L. (2009). The Crystal Structure of the N-Terminal Region of BUB1 Provides Insight into the Mechanism of BUB1 Recruitment to Kinetochores. Structure *17*, 105–116.

Bolanos-Garcia, V.M., Lischetti, T., Matak-Vinković, D., Cota, E., Simpson, P.J., Chirgadze, D.Y., Spring, D.R., Robinson, C. V., Nilsson, J., and Blundell, T.L. (2011). Structure of a Blinkin-BUBR1 complex reveals an interaction crucial for kinetochore-mitotic checkpoint regulation via an unanticipated binding site. Structure *19*, 1691–1700.

Bonilla, C.Y., Melo, J.A., and Toczyski, D.P. (2008). Colocalization of Sensors Is Sufficient to Activate the DNA Damage Checkpoint in the Absence of Damage. Mol. Cell *30*, 267–276.

Brady, D.M., and Hardwick, K.G. (2000). Complex formation between Mad1p, Bub1p and Bub3p is crucial for spindle checkpoint function. Curr. Biol. *10*, 675–678.

Chao, W.C.H., Kulkarni, K., Zhang, Z., Kong, E.H., and Barford, D. (2012). Structure of the mitotic checkpoint complex. Nature *484*, 208–213.

Dasso, M., and Newport, J.W. (1990). Completion of DNA replication is monitored by a feedback system that controls the initiation of mitosis in vitro: Studies in Xenopus. Cell *61*, 811–823.

Défachelles, L., Raich, N., Terracol, R., Baudin, X., Williams, B., Goldberg, M., and Karess, R.E. (2015). RZZ and Mad1 dynamics in Drosophila mitosis. Chromosom. Res. *23*, 333–342.

DeLuca, K.F., Lens, S.M. a, and DeLuca, J.G. (2011). Temporal changes in Hec1 phosphorylation control kinetochore-microtubule attachment stability during mitosis. J. Cell Sci. *124*, 622–634.

Desai, A., Rybina, S., Müller-Reichert, T., Shevchenko, A., Shevchenko, A., Hyman, A., and Oegema, K. (2003). KNL-1 directs assembly of the microtubule-binding interface of the kinetochore in C. elegans. Genes Dev. *17*, 2421–2435.

Essex, A., Dammermann, A., Lewellyn, L., Oegema, K., and Desai, A. (2008). Systematic Analysis in C. elegans Reveals that the Spindle Checkpoint Is Comprised of Two Largely Independent Branches. Mol. Biol. Cell E08–E10 – 1047–E08 – 10–1047.

Fang, G. (2002). Checkpoint protein BubR1 acts synergistically with Mad2 to inhibit anaphase-promoting complex. Mol. Biol. Cell *13*, 755–766.

Fang, G., Yu, H., and Kirschner, M.W. (1998). The checkpoint protein MAD2 and the mitotic regulator CDC20 form a ternary complex with the anaphase-promoting complex to control anaphase initiation. Genes Dev. *12*, 1871–1883.

Flory, M.R., Morphew, M., Joseph, J.D., Means, A.R., and Davis, T.N. (2002). Pcp1p, an Spc110p-related calmodulin target at the centrosome of the fission yeast Schizosaccharomyces pombe. Cell Growth Differ. *13*, 47–58.

Gassmann, R., Holland, A.J., Varma, D., Wan, X., Çivril, F., Cleveland, D.W., Oegema, K., Salmon, E.D.,

and Desai, A. (2010). Removal of Spindly from microtubule-attached kinetochores controls spindle checkpoint silencing in human cells. Genes Dev. *24*, 957–971.

Gillett, E.S., Espelin, C.W., and Sorger, P.K. (2004). Spindle checkpoint proteins and chromosome-microtubule attachment in budding yeast. J. Cell Biol. *164*, 535–546.

Gossen, M., and Bujard, H. (1992). Tight control of gene expression in mammalian cells by tetracycline-responsive promoters. Proc. Natl. Acad. Sci. U. S. A. *89*, 5547–5551.

Habu, T., Kim, S.H., Weinstein, J., and Matsumoto, T. (2002). Identification of a MAD2-binding protein, CMT2, and its role in mitosis. EMBO J. *21*, 6419–6428.

Hardwick, K.G., Weiss, E., Luca, F.C., Winey, M., and Murray, a W. (1996). Activation of the budding yeast spindle assembly checkpoint without mitotic spindle disruption. Science *273*, 953–956.

Hardwick, K.G., Johnston, R.C., Smith, D.L., and Murray, A.W. (2000). MAD3 encodes a novel component of the spindle checkpoint which interacts with Bub3p, Cdc20p, and Mad2p. J. Cell Biol. *148*, 871–882.

He, X., Jones, M.H., Winey, M., and Sazer, S. (1998). Mph1, a member of the Mps1-like family of dual specificity protein kinases, is required for the spindle checkpoint in S. pombe. J. Cell Sci. *111 (Pt 1*, 1635–1647.

Heinrich, S., Windecker, H., Hustedt, N., and Hauf, S. (2012). Mph1 kinetochore localization is crucial and upstream in the hierarchy of spindle assembly checkpoint protein recruitment to kinetochores. J. Cell Sci. *626*, 4720–4727.

Heinrich, S., Geissen, E.-M., Kamenz, J., Trautmann, S., Widmer, C., Drewe, P., Knop, M., Radde, N., Hasenauer, J., and Hauf, S. (2013). Determinants of robustness in spindle assembly checkpoint signalling. Nat. Cell Biol. *15*, 1328–1339.

Heinrich, S., Sewart, K., Windecker, H., Langegger, M., Schmidt, N., Hustedt, N., and Hauf, S. (2014). Mad1 contribution to spindle assembly checkpoint signalling goes beyond presenting Mad2 at kinetochores. EMBO Rep. *15*, 291–298.

Herzog, F., Primorac, I., Dube, P., Lenart, P., Sander, B., Mechtler, K., Stark, H., and Peters, J.-M. (2009). Structure of the anaphase-promoting complex/cyclosome interacting with a mitotic checkpoint complex. Science *323*, 1477–1481.

Hewitt, L., Tighe, A., Santaguida, S., White, A.M., Jones, C.D., Musacchio, A., Green, S., and Taylor, S.S. (2010). Sustained Mps1 activity is required in mitosis to recruit O-Mad2 to the Mad1-C-Mad2 core complex. J. Cell Biol. *190*, 25–34.

Hiruma, Y., Sacristan, C., Pachis, S.T., Adamopoulos, a., Kuijt, T., Ubbink, M., von Castelmur, E., Perrakis, a., and Kops, G.J.P.L. (2015). Competition between MPS1 and microtubules at kinetochores regulates spindle checkpoint signaling. Science (80-.). *348*, 1264–1267.

Howell, B.J., Hoffman, D.B., Fang, G., Murray, a. W., and Salmon, E.D. (2000). Visualization of Mad2 dynamics at kinetochores, along spindle fibers, and at spindle poles in living cells. J. Cell Biol. *150*, 1233–1249.

Howell, B.J., McEwen, B.F., Canman, J.C., Hoffman, D.B., Farrar, E.M., Rieder, C.L., and Salmon, E.D. (2001). Cytoplasmic dynein/dynactin drives kinetochore protein transport to the spindle poles and has a role in mitotic spindle checkpoint inactivation. J. Cell Biol. *155*, 1159–1172.

Howell, B.J., Moree, B., Farrar, E.M., Stewart, S., Fang, G., and Salmon, E.D. (2004). Spindle checkpoint protein dynamics at kinetochores in living cells. Curr. Biol. *14*, 953–964.

Hoyt, M. a, Totis, L., and Roberts, B.T. (1991). S. cerevisiae genes required for cell cycle arrest in response to loss of microtubule function. Cell *66*, 507–517.

Hwang, L.H., Lau, L.F., Smith, D.L., Mistrot, C. a, Hardwick, K.G., Hwang, E.S., Amon, a, and Murray, a

W. (1998). Budding yeast Cdc20: a target of the spindle checkpoint. Science *279*, 1041–1044.

Ito, D., Saito, Y., and Matsumoto, T. (2012). Centromere-tethered Mps1 pombe homolog (Mph1) kinase is a sufficient marker for recruitment of the spindle checkpoint protein Bub1, but not Mad1. Proc. Natl. Acad. Sci. *109*, 209–214.

Ito, H., Fukuda, Y., and Murata, K. (1983). Transformation of intact yeast cells treated with alkali Transformation of Intact Yeast Cells Treated with Alkali Cations. J. Bacteriol. *153*, 166–168.

Izawa, D., and Pines, J. (2014). The mitotic checkpoint complex binds a second CDC20 to inhibit active APC/C. Nature.

Jelluma, N., Dansen, T.B., Sliedrecht, T., Kwiatkowski, N.P., and Kops, G.J.P.L. (2010). Release of Mps1 from kinetochores is crucial for timely anaphase onset. J. Cell Biol. *191*, 281–290.

Ji, Z., Gao, H., and Yu, H. (2015). Kinetochore attachment sensed by competitive Mps1 and microtubule binding to Ndc80C. Science (80-.). *348*, 1260–1264.

Kemmler, S., Stach, M., Knapp, M., Ortiz, J., Pfannstiel, J., Ruppert, T., and Lechner, J. (2009). Mimicking Ndc80 phosphorylation triggers spindle assembly checkpoint signalling. EMBO J. *28*, 1099–1110.

Kim, S., Sun, H., Tomchick, D.R., Yu, H., and Luo, X. (2012). Structure of human Mad1 C-terminal domain reveals its involvement in kinetochore targeting. Proc. Natl. Acad. Sci. *109*, 6549–6554.

Kim, S.H., Lin, D.P., Matsumoto, S., Kitazono, a, and Matsumoto, T. (1998). Fission yeast Slp1: an effector of the Mad2-dependent spindle checkpoint. Science *279*, 1045–1047.

King, E.M.J., van der Sar, S.J. a, and Hardwick, K.G. (2007). Mad3 KEN boxes mediate both Cdc20 and Mad3 turnover, and are critical for the spindle checkpoint. PLoS One *2*, e342.

Kiyomitsu, T., Obuse, C., and Yanagida, M. (2007). Human Blinkin/AF15q14 Is Required for Chromosome Alignment and the Mitotic Checkpoint through Direct Interaction with Bub1 and BubR1. Dev. Cell *13*, 663–676.

Kiyomitsu, T., Murakami, H., and Yanagida, M. (2011). Protein interaction domain mapping of human kinetochore protein Blinkin reveals a consensus motif for binding of spindle assembly checkpoint proteins Bub1 and BubR1. Mol. Cell. Biol. *31*, 998–1011.

Krenn, V., Wehenkel, A., Li, X., Santaguida, S., and Musacchio, A. (2012). Structural analysis reveals features of the spindle checkpoint kinase Bub1-kinetochore subunit Knl1 interaction. J. Cell Biol. *196*, 451–467.

Kuijt, T.E.F., Omerzu, M., Saurin, A.T., and Kops, G.J.P.L. (2014). Conditional targeting of MAD1 to kinetochores is sufficient to reactivate the spindle assembly checkpoint in metaphase. Chromosoma 471–480.

Lampson, M. a., and Cheeseman, I.M. (2011). Sensing centromere tension: Aurora B and the regulation of kinetochore function. Trends Cell Biol. *21*, 133–140.

Lee, M., and Nurse, P. (1988). Cell cycle control genes in fission yeast and mammalian cells. Trends Genet. *4*, 287–290.

Lee, S.H., Sterling, H., Burlingame, A., and McCormick, F. (2008). Tpr directly binds to Mad1 and Mad2 and is important for the Mad1-Mad2-mediated mitotic spindle checkpoint. Genes Dev. *22*, 2926–2931.

Li, R., and Murray, a. W. (1991). Feedback control of mitosis in budding yeast. Cell *66*, 519–531.

Liu, D., Vader, G., Vromans, M.J.M., Lampson, M. a, and Lens, S.M. a (2009). Sensing chromosome bi-orientation by spatial separation of aurora B kinase from kinetochore substrates. Science *323*, 1350–1353.

Liu, D., Vleugel, M., Backer, C.B., Hori, T., Fukagawa, T., Cheeseman, I.M., and Lampson, M. a. (2010). Regulated targeting of protein phosphatase 1 to the outer kinetochore by KNL1 opposes Aurora B kinase. J.

Cell Biol. *188*, 809–820.

Liu, X., McLeod, I., Anderson, S., Yates, J.R., and He, X. (2005). Molecular analysis of kinetochore architecture in fission yeast. EMBO J. *24*, 2919–2930.

London, N., and Biggins, S. (2014a). Mad1 kinetochore recruitment by Mps1-mediated phosphorylation of Bub1 signals the spindle checkpoint. Genes Dev. *28*, 140–152.

London, N., and Biggins, S. (2014b). Signalling dynamics in the spindle checkpoint response. Nat. Rev. Mol. Cell Biol. *15*, 736–748.

London, N., Ceto, S., Ranish, J. a., and Biggins, S. (2012). Phosphoregulation of Spc105 by Mps1 and PP1 regulates Bub1 localization to kinetochores. Curr. Biol. *22*, 900–906.

Lõoke, M., Kristjuhan, K., and Kristjuhan, A. (2011). Extraction of genomic DNA from yeasts for PCR-based applications. Biotechniques *50*, 325–328.

Lucchini, G., Muzi Falconi, M., Pizzagalli, a, Aguilera, a, Klein, H.L., and Plevani, P. (1990). Nucleotide sequence and characterization of temperature-sensitive pol1 mutants of Saccharomyces cerevisiae. Gene *90*, 99–104.

Luo, X., Tang, Z., Rizo, J., and Yu, H. (2002). The Mad2 spindle checkpoint protein undergoes similar major conformational changes upon binding to either Mad1 or Cdc20. Mol. Cell *9*, 59–71.

Maciejowski, J., George, K. a., Terret, M.E., Zhang, C., Shokat, K.M., and Jallepalli, P. V. (2010). Mps1 directs the assembly of Cdc20 inhibitory complexes during interphase and mitosis to control M phase timing and spindle checkpoint signaling. J. Cell Biol. *190*, 89–100.

Maldonado, M., and Kapoor, T.M. (2011). Constitutive Mad1 targeting to kinetochores uncouples checkpoint signalling from chromosome biorientation. Nat. Cell Biol. *13*, 475–482.

Mapelli, M., Massimiliano, L., Santaguida, S., and Musacchio, A. (2007). The Mad2 Conformational Dimer: Structure and Implications for the Spindle Assembly Checkpoint. Cell *131*, 730–743.

Martin-Lluesma, S., Stucke, V.M., and Nigg, E. a (2002). Role of Hec1 in spindle checkpoint signaling and kinetochore recruitment of Mad1/Mad2. Science *297*, 2267–2270.

Matson, D.R., and Stukenberg, P.T. (2014). CENP-I and Aurora B act as a molecular switch that ties RZZ/Mad1 recruitment to kinetochore attachment status. J. Cell Biol. *205*, 541–554.

Matsuyama, A., Shirai, A., Yashiroda, Y., Kamata, A., Horinouchi, S., and Yoshida, M. (2004). pDUAL, a multipurpose, multicopy vector capable of chromosomal integration in fission yeast. Yeast *21*, 1289–1305.

Matsuyama, A., Shirai, A., and Yoshida, M. (2008). A novel series of vectors for chromosomal integration in fission yeast. Biochem. Biophys. Res. Commun. *374*, 315–319.

Maundrell, K. (1993). Thiamine-repressible expression vectors pREP and pRIP for fission yeast. Gene *123*, 127–130.

McCarroll, R.M., and Fangman, W.L. (1988). Time of replication of yeast centromeres and telomeres. Cell *54*, 505–513.

Moyle, M.W., Kim, T., Hattersley, N., Espeut, J., Cheerambathur, D.K., Oegema, K., and Desai, A. (2014). A Bub1-Mad1 interaction targets the Mad1-Mad2 complex to unattached kinetochores to initiate the spindle checkpoint. J. Cell Biol. *204*, 647–657.

Murray, A.W., and Kirschner, M.W. (1989). Dominoes and clocks: the union of two views of the cell cycle. Science *246*, 614–621.

Musacchio, a., Sironi, L., Mapelli, M., Knapp, S., DeAntoni, a., and Jeang, K.-T. (2002). The Mad1-Mad2 complex: implications of a "safety belt" binding mechanism for the spindle checkpoint. Acta Crystallogr. Sect. A Found. Crystallogr. *58*, c223–c223.

Nabetani, a, Koujin, T., Tsutsumi, C., Haraguchi, T., and Hiraoka, Y. (2001). A conserved protein, Nuf2, is implicated in connecting the centromere to the spindle during chromosome segregation: a link between the kinetochore function and the spindle checkpoint. Chromosoma *110*, 322–334.

Nicklas, R.B., and Koch, C. a. (1969). Chromosome micromanipulation. 3. Spindle fiber tension and the reorientation of mal-oriented chromosomes. J. Cell Biol. *43*, 40–50.

Overlack, K., Primorac, I., Vleugel, M., Krenn, V., Maffini, S., Hoffmann, I., Kops, G.J.P.L., and Musacchio, A. (2015). A molecular basis for the differential roles of Bub1 and BubR1 in the spindle assembly checkpoint. Elife *4*, 1–24.

Primorac, I., and Musacchio, A. (2013). Panta rhei: The APC/C at steady state. J. Cell Biol. *201*, 177–189.

Primorac, I., Weir, J.R., Chiroli, E., Gross, F., Hoffmann, I., van Gerwen, S., Ciliberto, A., and Musacchio, A. (2013). Bub3 reads phosphorylated MELT repeats to promote spindle assembly checkpoint signaling. Elife *2013*, 1–20.

Rieder, C.L., Cole, R.W., Khodjakov, A., and Sluder, G. (1995). The checkpoint delaying anaphase in response to chromosome monoorientation is mediated by an inhibitory signal produced by unattached kinetochores. J. Cell Biol. *130*, 941–948.

Rischitor, P.E., May, K.M., and Hardwick, K.G. (2007). Bub1 is a fission yeast kinetochore scaffold protein, and is sufficient to recruit other spindle checkpoint proteins to ectopic sites on chromosomes. PLoS One *2*, e1342.

Rodriguez-Bravo, V., Maciejowski, J., Corona, J., Buch, H.K., Collin, P., Kanemaki, M.T., Shah, J. V., and Jallepalli, P. V. (2014). Nuclear pores protect genome integrity by assembling a premitotic and mad1-dependent anaphase inhibitor. Cell *156*, 1017–1031.

Saitoh, S., Ishii, K., Kobayashi, Y., and Takahashi, K. (2005). Spindle checkpoint signaling requires the mis6 kinetochore subcomplex, which interacts with mad2 and mitotic spindles. Mol. Biol. Cell *16*, 3666–3677.

Sczaniecka, M., Feoktistova, A., May, K.M., Chen, J.S., Blyth, J., Gould, K.L., and Hardwick, K.G. (2008). The spindle checkpoint functions of Mad3 and Mad2 depend on a Mad3 KEN box-mediated interaction with Cdc20-anaphase-promoting complex (APC/C). J. Biol. Chem. *283*, 23039–23047.

Seeley, T.W., Wang, L., and Zhen, J.Y. (1999). Phosphorylation of human MAD1 by the BUB1 kinase in vitro. Biochem. Biophys. Res. Commun. *257*, 589–595.

Shah, J. V., Botvinick, E., Bonday, Z., Furnari, F., Berns, M., and Cleveland, D.W. (2004). Dynamics of centromere and kinetochore proteins: Implications for checkpoint signaling and silencing. Curr. Biol. *14*, 942–952.

Shepperd, L. a., Meadows, J.C., Sochaj, A.M., Lancaster, T.C., Zou, J., Buttrick, G.J., Rappsilber, J., Hardwick, K.G., and Millar, J.B. a (2012). Phosphodependent recruitment of Bub1 and Bub3 to Spc7/KNL1 by Mph1 kinase maintains the spindle checkpoint. Curr. Biol. *22*, 891–899.

Sliedrecht, T., Zhang, C., Shokat, K.M., and Kops, G.J.P.L. (2010). Chemical Genetic Inhibition of Mps1 in Stable Human Cell Lines Reveals Novel Aspects of Mps1 Function in Mitosis. PLoS One *5*, e10251.

Tang, Z., Bharadwaj, R., Li, B., and Yu, H. (2001). Mad2-Independent Inhibition of APCCdc20 by the Mitotic Checkpoint Protein BubR1. Dev. Cell *1*, 227–237.

Tange, Y., and Niwa, O. (2008). Schizosaccharomyces pombe Bub3 is dispensable for mitotic arrest following perturbed spindle formation. Genetics *179*, 785–792.

Vanoosthuyse, V., Meadows, J.C., van der Sar, S.J. a, Millar, J.B. a, and Hardwick, K.G. (2009). Bub3p facilitates spindle checkpoint silencing in fission yeast. Mol. Biol. Cell *20*, 5096–5105.

Varma, D., and Salmon, E.D. (2012). The KMN protein network–chief conductors of the kinetochore orchestra. J. Cell Sci. *125*, 5927–5936.

Vigneron, S., Prieto, S., Bernis, C., Labbé, J.-C., Castro, A., and Lorca, T. (2004). Kinetochore localization of spindle checkpoint proteins: who controls whom? Mol. Biol. Cell *15*, 4584–4596.

Vink, M., Simonetta, M., Transidico, P., Ferrari, K., Mapelli, M., De Antoni, A., Massimiliano, L., Ciliberto, A., Faretta, M., Salmon, E.D., et al. (2006). In Vitro FRAP Identifies the Minimal Requirements for Mad2 Kinetochore Dynamics. Curr. Biol. *16*, 755–766.

Vleugel, M., Hoogendoorn, E., Snel, B., and Kops, G.J.P.L. (2012). Evolution and Function of the Mitotic Checkpoint. Dev. Cell *23*, 239–250.

Wassmann, K., Liberal, V., and Benezra, R. (2003). Mad2 phosphorylation regulates its association with Mad1 and the APC/C. EMBO J. *22*, 797–806.

Watanabe, Y. (2012). Geometry and force behind kinetochore orientation: lessons from meiosis. Nat. Rev. Mol. Cell Biol. *13*, 370–382.

Weinert, T., and Hartwell, L. (1988). The RAD9 gene controls the cell cycle response to DNA damage in Saccharomyces cerevisiae. Science (80-.). *241*, 317–322.

Westhorpe, F.G., Tighe, a., Lara-Gonzalez, P., and Taylor, S.S. (2011). p31comet-mediated extraction of Mad2 from the MCC promotes efficient mitotic exit. J. Cell Sci. *124*, 3905–3916.

Windecker, H., Langegger, M., Heinrich, S., and Hauf, S. (2009). Bub1 and Bub3 promote the conversion from monopolar to bipolar chromosome attachment independently of shugoshin. EMBO Rep. *10*, 1022–1028.

Xia, G., Luo, X., Habu, T., Rizo, J., Matsumoto, T., and Yu, H. (2004). Conformation-specific binding of p31(comet) antagonizes the function of Mad2 in the spindle checkpoint. EMBO J. *23*, 3133–3143.

Yamagishi, Y., Yang, C.-H., Tanno, Y., and Watanabe, Y. (2012). MPS1/Mph1 phosphorylates the kinetochore protein KNL1/Spc7 to recruit SAC components. Nat. Cell Biol. *14*, 746–752.

Yang, M., Li, B., Tomchick, D.R., Machius, M., Rizo, J., Yu, H., and Luo, X. (2007). p31comet Blocks Mad2 Activation through Structural Mimicry. Cell *131*, 744–755.

Zich, J., and Hardwick, K.G. (2010). Getting down to the phosphorylated “nuts and bolts” of spindle checkpoint signalling. Trends Biochem. Sci. *35*, 18–27.

Zich, J., Sochaj, A.M., Syred, H.M., Milne, L., Cook, A.G., Ohkura, H., Rappsilber, J., and Hardwick, K.G. (2012). Kinase activity of fission yeast Mph1 Is required for Mad2 and Mad3 to stably bind the anaphase promoting complex. Curr. Biol. *22*, 296–301.